

# TECHNICAL RESEARCH REPORT

Phase Analysis of Actuator Response for Sub-Optimal Bang-Bang and Velocity Cancellation Control of Base Isolated Structures

*by Mark Austin, Robert Sebastianelli*

**SEIL TR 2005-4  
(ISR TR 2005-105)**



*ISR develops, applies and teaches advanced methodologies of design and analysis to solve complex, hierarchical, heterogeneous and dynamic problems of engineering technology and systems for industry and government.*

*ISR is a permanent institute of the University of Maryland, within the Glenn L. Martin Institute of Technology/A. James Clark School of Engineering. It is a National Science Foundation Engineering Research Center.*

**Web site <http://www.isr.umd.edu>**

# Phase Analysis of Actuator Response for Sub-Optimal Bang-Bang and Velocity Cancellation Control of Base Isolated Structures

By Mark Austin<sup>1</sup> and Robert R. Sebastianelli<sup>2</sup>

**ABSTRACT:** Starting with simplified models of displacement response for a base isolated structure supplemented with sub-optimal bang-bang control, we formulate models of phase analysis of actuator force direction in relation to system displacements and velocities. For the case of steady state displacement response, we prove that the direction of actuator application can neither be perfectly in phase with displacements, nor perfectly in phase with velocities. In practice, however, the actuator force direction is “almost in phase” with velocities and “almost orthogonal” to sign changes in displacements. This observation suggests that a very simple velocity cancellation control might be effective in adding value to base isolation system responses. Numerical experiments are conducted to assess improvements in performance due to sub-optimal bang-bang control and velocity cancellation control, and to validate the extent to which the phase analysis predictions hold in linearly elastic and nonlinear time-domain settings.

**Keywords:** Phase Analysis, Base Isolation, Active Control, Structural Performance.

Last updated : September 16, 2005.

---

<sup>1</sup>Associate Professor, Department of Civil and Environmental Engineering, and Institute for Systems Research, University of Maryland, College Park, MD 20742, USA. E-mail: austin@isr.umd.edu

<sup>2</sup>Graduate Student, Department of Civil and Environmental Engineering, and Institute for Systems Research, University of Maryland, College Park, MD 20742, USA. E-mail: sebastn@isr.umd.edu

# Contents

<b>1</b>	<b>Problem Statement</b>	<b>1</b>
1.1	Scope and Objectives . . . . .	3
1.2	Equation of Motion . . . . .	4
1.3	Bang-Bang Control Law . . . . .	5
<b>2</b>	<b>Actuator Behavior for Simplified Models of System Response</b>	<b>8</b>
2.1	Steady State Response . . . . .	9
2.2	Free Vibration Response . . . . .	15
<b>3</b>	<b>Correlation Coefficients for Simplified Response</b>	<b>18</b>
<b>4</b>	<b>Numerical Experiments</b>	<b>24</b>
4.1	Actively Controlled Mass-Spring-Damper System . . . . .	25
4.2	Library of Ground Motions . . . . .	27
4.3	Scatter Diagram/Correlation Analysis . . . . .	34
4.4	Case Study 1. Linear Time-History Behavior . . . . .	36
4.5	Case Study 2. Nonlinear Time-History Response . . . . .	56
<b>5</b>	<b>Summary and Conclusions</b>	<b>76</b>

# Phase Analysis of Actuator Response for Sub-Optimal Bang-Bang and Velocity Cancellation Control of Base Isolated Structures

## 1 Problem Statement

The design of base isolated structures to resist earthquake loading, and protect structures and their contents from significant damage is one of the most challenging problems facing structural engineers. State-of-the-art practice is to interpose structural elements (e.g., rubber bearings) with low horizontal stiffness between the structure and foundation. Use of this design mechanism leads to structures having a fundamental frequency that is much lower than their fixed-base counterparts and, by design, also well separated from the most likely dominant frequencies of ground motion at a site. Performance improvements are measured in terms of reductions to maximum inter-story drifts and floor accelerations.

Unfortunately, the design of base isolated structures is complicated by: (1) The large uncertainty in predicting the spatial and temporal nature of future seismic events; (2) The limited ability of analytical models to properly describe the nonlinear response of structures under severe earthquake excitations, and (3) The need to design complex or irregular structural systems, supplemented with new types of isolation devices. Because designers may have no prior experience in such cases, design code provisions may not apply. Designers may be forced to return to first principles for engineering analysis, and may have difficulty in making quantitative decisions regarding the adequacy of a design, and in choosing rationally among different design alternatives.

After almost four decades of practice the overall benefits of state-of-the-art base isolation systems are now well known [1, 2, 7, 15, 24, 23, 25]. Still, the underlying mechanism of protection remains simple, and there is mounting evidence that base isolation may not always provide adequate protection [29]. A key concern, as pointed out by Johnson et al. [11] and Spencer et al. [22], is the inability of base isolation to protect structures against near-source, high-velocity, long-period pulse earthquakes, such as recorded during the Kobe and Northridge earthquakes. Recent revisions to the Uniform Building Code have made design requirements more stringent compared to previous

versions [9, 10]. Not only do the additional design complexities and costs associated with the new procedures make base isolation a less attractive design option than in the past, but the code-mandated accommodation of larger base displacements and the requirement to consider stronger maximum credible earthquakes point to a strong need for supplementing base isolation with passive damping devices (e.g., mechanical damping, viscous damping, friction damping) and/or active control devices.

Passive isolation devices are designed to have force-displacement characteristics that can survive large lateral displacements and hysteretic loadings without a loss in strength occurring. Some of the earliest isolation devices (i.e., dating back to the late 1960s) were low damping natural rubber and synthetic rubber bearings, providing 2-3% of critical damping in the isolation mode [25]. An effective way of increasing damping is to use high damping natural rubber and other fillers (e.g., reinforcing steel plates) that can provide up to 20% isolation mode damping [16]. These isolation devices are very stiff in the vertical direction, and can easily carry the vertical loads of the building, but are flexible in the horizontal direction, thereby allowing the structure to move laterally under ground motion loadings. A second common approach is to supplement low damping natural bearings with some form of mechanical damper. In the United States, Japan, and New Zealand, the most commonly used isolation device is the lead plug rubber bearing. Lead plug rubber bearings are laminated rubber bearings (similar to low damping rubber bearings), plus one or more lead plugs that are inserted into holes [16, 19]. The steel plate laminates force the bearing to deform in shear. Together the laminated rubber bearings plus lead plugs increase the energy dissipation through hysteretic damping. One concern is the possibility of localized buckling of the isolator devices and/or collapse of the structure caused by truly excessive lateral displacements of isolator elements (details on the appropriate analysis procedures can be found in Naeim and Kelly [16]).

Supplemental passive damping devices have been found to be effective in reducing both displacements and base shears for structures that have moderately long periods. Studies [12, 17] indicate that adding a moderate amount of damping to low damping systems will reduce key response values. However, if too much damping is added peak floor accelerations and inter-story drifts will go back up again. In a first step toward addressing these issues, researchers have proposed systems where the main isolation devices are supplemented by active control mechanisms [8, 18]. A natural choice for the implementation of these hybrid systems is bang-bang control mechanisms. While numerical algorithms exist for solving the Lyapunov matrix equation, systematic procedures

for modeling and operating base isolated structures, supplemented by bang-bang active control are still lacking [8]. Bridging these gaps will require a better understanding of the extent to which active control mechanisms can supplement and improve the performance of base isolated structures. For design purposes, we seek an analysis methods that use performance-based metrics (e.g., displacements, velocities, energy) to capture the benefits of active control and base isolation, but are not overly complicated – indeed, as already noted, we need to keep in mind that the complexity of the design method must be balanced against the uncertainty in ground motion prediction and in modeling of actual structural performance.

## 1.1 Scope and Objectives

Traditional metrics of performance assessment include time-history plots of displacement, velocity and acceleration. Time-series plots are conducive to conveying the range and regularity of motion over the capture period. Here, in contrast, we are interested in coordination of the actuator force direction with respect to displacements and velocities, the underlying parameters of system state. By showing that the direction of actuator force application is strongly correlated with an aspect of the system state, we hope to create a pathway toward: (1) Simplified interpretations of behavior, and (2) Development of active control strategies based upon simplified principles.

Starting with simplified models of displacement response for a base isolated structure supplemented by sub-optimal bang-bang control, we formulate models of phase analysis of actuator force direction in relation to system displacements and velocities. For the case of steady state displacement response, we prove that the direction of actuator application can neither be perfectly in phase with displacements, nor perfectly in phase with velocities. In practice, however, the actuator force direction is “almost in phase” with velocities and “almost orthogonal” to sign changes in displacements. This observation suggests that a very simple velocity cancellation control might be effective in adding value to base isolation system responses. Numerical experiments are conducted to assess improvements in performance due to sub-optimal bang-bang control and velocity cancellation control, and to validate the extent to which the phase analysis predictions hold in linearly elastic and nonlinear time-domain settings.

## 1.2 Equation of Motion

The well known general equation of motion for a multi-degree of freedom system subject to an earthquake load and external active controlling forces is as follows:

$$\mathbf{M}\ddot{x}(t) + \mathbf{C}\dot{x}(t) + \mathbf{K}x(t) = \mathbf{H}u(t) - \mathbf{M}r\ddot{x}_g(t). \quad (1)$$

In equation 1,  $x(t)$  is a  $n$ -dimensional vector representing the relative displacements of the  $n$  degrees of freedom.  $\mathbf{M}$ ,  $\mathbf{C}$ , and  $\mathbf{K}$  are the mass, damping, and stiffness  $n \times n$  matrices, respectively.  $\ddot{x}_g(t)$  represents the earthquake ground acceleration,  $\mathbf{H}$  is an  $n \times p$  matrix that designates the location of the controller(s), while  $u(t)$  is a  $p$ -dimensional vector that represents the control force of  $p$ -number of controllers. The first-order state-space form of equation 1 is as follows:

$$\dot{z}(t) = \mathbf{A}z(t) + \mathbf{B}u(t) - \mathbf{W}\ddot{x}_g(t). \quad (2)$$

In equation 2,  $z(t) = [x(t), \dot{x}(t)]^T$  and

$$\mathbf{A} = \begin{bmatrix} \mathbf{0} & \mathbf{1} \\ -\mathbf{M}^{-1}\mathbf{K} & -\mathbf{M}^{-1}\mathbf{C} \end{bmatrix}, \quad \mathbf{B} = \begin{bmatrix} \mathbf{0} \\ \mathbf{M}^{-1}\mathbf{H} \end{bmatrix} \quad \text{and} \quad \mathbf{W} = \begin{bmatrix} 0 \\ r \end{bmatrix}. \quad (3)$$

With respect to the active control, several strategies for implementation seem possible: (1) use a linear control theory, but iteratively adjust the structural parameters to account for the nonlinear behavior, (2) use a nonlinear control theory, or (3) use a linear control theory that has been shown to provide effective improvements to the system response, even when nonlinearities in behavior are not explicitly captured in the system model. Moreover, it is important to understand the sensitivity (and limitations) of suboptimal bang-bang control to nonlinearities in the base isolated system because, for design purposes, it is a prerequisite to selection of an appropriate active control strategy.

### 1.3 Bang-Bang Control Law

One of the well-known control laws in optimal control theory is the bang-bang control law [5, 26, 27]. The key characteristic of optimal bang-bang control is a control force,  $u(t)$ , that switches from one extreme to another (i.e., the control force is always exerting its maximum force in either the positive or negative direction). Since the control force always takes on maximum values, the full capabilities of the actuators can be exploited. Numerical simulation studies have shown that bang-bang control can provide better control efficiency than the well-known Linear Quadratic Regulator (LQR) Control Law [27].

**Control Objective.** The control objective for bang-bang control is to minimize:

$$J(t_f) = \frac{1}{2} \int_0^{t_f} \left( z^T(\tau) \mathbf{Q} z(\tau) \right) d\tau. \quad (4)$$

where  $z(\tau)$  is a  $2n \times 1$  state vector of system displacements and velocities (for structural control, the state variables represent the displacements and velocities at the  $n$ -degrees of freedom), and  $\mathbf{Q}$  is a positive semi-definite matrix whose content is left for the designer to choose. The well known optimal control solution [5, 26, 27] for a system in the form of equation 2 and which minimizes equation 4 is:

$$u(t) = -u_{max} \text{sgn} \left[ \mathbf{B}^T \lambda(t) \right]; \quad (5)$$

where  $\lambda(t)$  is known as the costate vector that is obtained by solving the following differential equation:

$$\dot{\lambda}(t) = -\mathbf{A}^T \lambda(t) - \mathbf{Q} z(t); \quad (6)$$

and  $u_{max}$  is a scalar that represents the maximum actuator control force.

**Suboptimal Bang-Bang Control Law.** To avoid solving equation 6 at each time step for the entire time history response, a suboptimal bang-bang control law is proposed by Wu and Soong [27].



Instead of minimizing equation 4, the objective of suboptimal bang-bang control is to minimize the derivative of the following generalized energy function:

$$V[z(t)] = z^T(t)\mathbf{S}z(t). \quad (7)$$

Equation 7 is also referred to as the Lyapunov function, where the  $\mathbf{S}$  matrix is the solution to the following Lyapunov matrix equation:

$$\mathbf{A}^T\mathbf{S} + \mathbf{S}\mathbf{A} = -\mathbf{Q}. \quad (8)$$

Taking the time derivative of equation 7 and substituting in the closed-loop state equation leads to the following equation results [13, 27]:

$$\dot{V}[z(t)] = -z^T(t)\mathbf{Q}z(t) + 2u^T(t)\mathbf{B}^T\mathbf{S}z(t). \quad (9)$$

Close inspection of equation 9 indicates that in order for this equation to be a minimum for all possible state variables,  $z(t)$ , the second term on the right-hand side of equation 9 should result in a negative scalar for all possible  $z(t)$ , and moreover,  $u(t)$  must be set to a maximum, say  $u_{max}$ . An appropriate choice for  $u(t)$  that fulfills these two criteria is:

$$u(t) = -u_{max}\text{sgn} \left[ \mathbf{B}^T\mathbf{S}z(t) \right]. \quad (10)$$

**Equation of Motion.** The effect of suboptimal bang-bang control on the second-order differential equation of motion for a seismically-resistant structure is obtained by substituting equation ?? into equation 10, and then substituting the resultant equation into equation 1. The equation of motion is as follows:

$$\mathbf{M}\ddot{x}(t) + \mathbf{C}\dot{x}(t) + \mathbf{K}x(t) = -\mathbf{H}u_{max}\text{sgn} \left[ \mathbf{B}^T\mathbf{S} \begin{pmatrix} x(t) \\ \dot{x}(t) \end{pmatrix} \right] - \mathbf{M}r\ddot{x}_g(t); \quad (11)$$

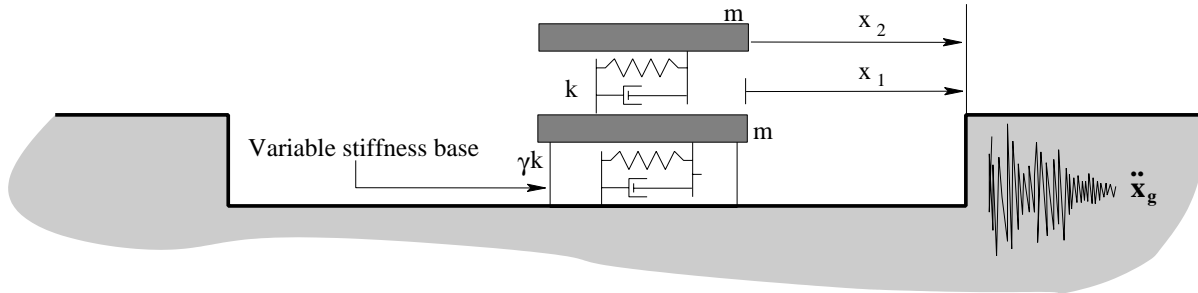


Figure 1: 2-DOF System

where the matrix,  $\mathbf{S}$ , is the  $2n \times 2n$  matrix solution to the Lyapunov matrix equation given in equation 8 and  $\mathbf{B}$  is a  $2n \times p$  matrix as defined by equation 3.

**Energy-Based Bang-Bang Control.** A key tenet of our work is that the terms in  $\mathbf{Q}$  should be selected so that the bang-bang control strategy has a well defined physical meaning. Wu, Soong, Gattulli, and Lin [28] suggest that under the LQR performance criteria, vibratory energy within the structure may be minimized by choosing  $\mathbf{Q}$  to be one of the following options:

$$\mathbf{Q} = \begin{bmatrix} \mathbf{0} & \mathbf{0} \\ \mathbf{0} & \mathbf{M} \end{bmatrix}; \mathbf{Q} = \begin{bmatrix} \mathbf{K} & \mathbf{0} \\ \mathbf{0} & \mathbf{0} \end{bmatrix}; \mathbf{Q} = \begin{bmatrix} \mathbf{K} & \mathbf{0} \\ \mathbf{0} & \mathbf{M} \end{bmatrix}. \quad (12)$$

For the design of base isolated structures supplemented by active control, distributions of structural stiffness, together with system displacements, determine quantities of internal energy present within portions of the structure. Accordingly, the scope of our “phase analysis” study is limited to minimization of internal energy in the superstructure and isolation devices. Assuming that base isolators will be firmly attached to the ground (with full fixity), the integral of internal energy is given by:

$$\mathbf{J}(t) = \frac{k}{2} \int_0^t \begin{pmatrix} x_1(\tau) & x_2(\tau) \end{pmatrix} \begin{bmatrix} 1 + \gamma & -1 \\ -1 & 1 \end{bmatrix} \begin{pmatrix} x_1(\tau) \\ x_2(\tau) \end{pmatrix} d\tau. \quad (13)$$

where  $x_1(\tau)$  and  $x_2(\tau)$  are displacements at the nodal degrees of freedom, and  $k$ , and  $\gamma k$ , are the lateral stiffness in the superstructure and isolation system, respectively. Typically  $\gamma$  will lie in the interval 0.0-0.15. A suitable choice of  $\mathbf{Q}$  is as follows:

$$\mathbf{Q} = \begin{bmatrix} k + \gamma k & -k & 0 & 0 \\ -k & k & 0 & 0 \\ 0 & 0 & 0 & 0 \\ 0 & 0 & 0 & 0 \end{bmatrix}. \quad (14)$$

## 2 Actuator Behavior for Simplified Models of System Response

Consider a 1-DOF system with stiffness,  $k$ , mass,  $m$ , and damping,  $c = \alpha \cdot m + \beta \cdot k$ . Assume that the 1-DOF system has an actuator acting on the DOF. For the following general choice of  $\mathbf{Q}$ ,

$$\mathbf{Q} = \begin{bmatrix} k & 0 \\ 0 & 0 \end{bmatrix}, \quad (15)$$

(i.e., minimize potential energy in the 1-DOF system) the symbolic representation for  $\mathbf{B}^T \mathbf{S}$  is as follows:

$$\mathbf{B}^T \mathbf{S} = \begin{bmatrix} 0 & \frac{1}{m} \end{bmatrix} \begin{bmatrix} \frac{mk}{2(\alpha \cdot m + \beta \cdot k)} + \frac{\alpha \cdot m + \beta \cdot k}{2} & \frac{m}{2} \\ \frac{m}{2} & \frac{m^2}{2(\alpha \cdot m + \beta \cdot k)} \end{bmatrix} = \begin{bmatrix} \frac{1}{2} & \frac{m}{2(\alpha \cdot m + \beta \cdot k)} \end{bmatrix}. \quad (16)$$

The right-hand term in equation 16 states that the displacement coefficient for bang-bang control is always equal to one half. The velocity coefficient is proportional to the system mass and inversely proportional to damping. Beyond the identification of general cause-and-effect relations for bang-bang control, the symbolic representation is incapable of quantifying the extent to which the actuator behavior is coordinated (i.e., in phase) with system displacements and velocities in an actual time-history response. An understanding of the latter issue is complicated by two factors. First, behavior of the structural system is affected by both ground motion displacements and actuator external forces. And second, the system behavior passes through several stages defined by the presence/absence of ground motions and actuator forces. At this point, a rational and well tested framework for simply deciding when to turn an actuator off does not exist.

As a preliminary step toward understanding these issues, in this section we investigate coordination of actuator behavior under two sets of simplifying assumptions for system response. First, we assume that a “periodic ground motion” generates a steady state system response. Then

we look at coordination of actuator behavior with displacements/velocities for a transient damped free vibration. In both cases, the purpose of investigation is to identify the phase angles between system displacements/velocities and the direction of actuator force application.

## 2.1 Steady State Response

Let us assume that the forcing function due to ground accelerations is:

$$p(g, t) = A \sin(gt) \quad (17)$$

where “g” matches the “most dominant” natural circular frequency for ground shaking. For a perfectly isolated structure, displacements of the ground relative to the structure vary with circular frequency “g”. If  $\beta = (g/w)$  then the steady-state displacement and velocity are [6]:

$$x(t) = \left[ \frac{A}{k} \right] \cdot \left[ \frac{(1 - \beta^2) \sin(gt) - 2\xi\beta \cos(gt)}{(1 - \beta^2)^2 + (2\xi\beta)^2} \right] \quad (18)$$

and

$$\dot{x}(t) = \left[ \frac{Ag}{k} \right] \cdot \left[ \frac{(1 - \beta^2) \cos(gt) + 2\xi\beta \sin(gt)}{(1 - \beta^2)^2 + (2\xi\beta)^2} \right]. \quad (19)$$

From the trigonometric identity  $\sin(gt + \phi) = \sin(gt) \cdot \cos(\phi) + \cos(gt) \cdot \sin(\phi)$  it follows that equation 18 can be written,

$$x(t) = \left[ \frac{A}{k} \right] \cdot \left[ \frac{1}{(1 - \beta^2)^2 + (2\xi\beta)^2} \right] \cdot \sin(gt + \phi) \quad (20)$$

where

$$\tan(\phi) = \left[ \frac{-2\xi\beta}{(1 - \beta^2)} \right]. \quad (21)$$

**Bang-Bang Control Strategy.** When the terms in  $\mathbf{Q}$  are selected to minimize potential energy in the 1-DOF system (i.e.,  $k^* = k$ ), the matrix product  $B^T S$  simplifies to:

$$\mathbf{B}^T \mathbf{S} = \begin{bmatrix} 0 & \frac{1}{m} \end{bmatrix} \begin{bmatrix} \frac{mk}{2(\alpha \cdot m + \beta \cdot k)} + \frac{\alpha \cdot m + \beta \cdot k}{2} & \frac{m}{2} \\ \frac{m}{2} & \frac{m^2}{2(\alpha \cdot m + \beta \cdot k)} \end{bmatrix} = \begin{bmatrix} \frac{1}{2} & \frac{m}{2(\alpha \cdot m + \beta \cdot k)} \end{bmatrix}. \quad (22)$$

Substituting equations 18 and 19 into  $\mathbf{Z}(t) = [x(t), \dot{x}(t)]^T$  and pre-multiplying by equation 22 gives:

$$\mathbf{B}^T \mathbf{S} \mathbf{Z} = \begin{bmatrix} \frac{A}{2k} \end{bmatrix} \cdot \begin{bmatrix} \frac{(1 - \beta^2) \sin(gt) - 2\xi\beta \cos(gt) + \frac{mg}{c}(1 - \beta^2) \cos(gt) + \frac{2mg}{c}\xi\beta \sin(gt)}{(1 - \beta^2)^2 + (2\xi\beta)^2} \end{bmatrix} \quad (23)$$

**Strategy for Switching Direction of the Actuator Force.** From the viewpoint of bang-bang control we want to know in which direction the actuator will push as a function of time, and how the strategy varies as a function of the problem parameters. The actuator will switch directions in the force application when:

$$(1 - \beta^2) \sin(gt) - 2\xi\beta \cos(gt) + \frac{mg}{c}(1 - \beta^2) \cos(gt) + \frac{2mg}{c}\xi\beta \sin(gt) = 0. \quad (24)$$

Collecting common terms:

$$\left[ (1 - \beta^2) + \frac{2mg}{c}\xi\beta \right] \sin(gt) = \left[ 2\xi\beta - \frac{mg}{c}(1 - \beta^2) \right] \cos(gt) \quad (25)$$

which gives:

$$\tan(gt) = \left[ \frac{[2\xi\beta - \frac{mg}{c}(1 - \beta^2)]}{[(1 - \beta^2) + \frac{2mg}{c}\xi\beta]} \right] \quad (26)$$

Now recall that  $\xi = c/2mw$  and  $\beta = g/w$ . The expression,  $2mg/c\xi\beta$  simplifies to  $\beta^2$  and

$$\frac{mg}{c}(1 - \beta^2) \quad \text{can be re-written as...} \quad \frac{\beta}{2\xi} \cdot (1 - \beta^2). \quad (27)$$

Hence, equation 26 simplifies to:

$$\tan(gt) = \left[ 2\xi\beta - \frac{\beta}{2\xi} \cdot (1 - \beta^2) \right] \quad (28)$$

**Case 1.** The actuator works perfectly in phase with displacements when a change in actuator force and displacements occurs at the same time. From equation 18,  $\dot{x}(t) = 0$  when:

$$(1 - \beta^2) \sin(gt) - 2\xi\beta \cos(gt) = 0. \quad (29)$$

i.e.,

$$\tan(gt) = \left[ \frac{2\xi\beta}{(1 - \beta^2)} \right] \quad (30)$$

**Case 2.** The actuator works perfectly in phase with velocities – i.e., to oppose the direction of motion – when  $\dot{x}(t) = 0$ . i.e.,

$$(1 - \beta^2) \cos(gt) + 2\xi\beta \sin(gt) = 0. \quad (31)$$

i.e.,

$$\tan(gt) = \left[ \frac{(\beta^2 - 1)}{2\xi\beta} \right] \quad (32)$$

**Theorem 1.** For values of  $\beta \neq 0$ , the actuator works neither perfectly in phase with displacements nor perfectly in phase with velocities.

**Proof.** From equations 28 and 30 it is evident that in order for the actuator to work perfectly in phase with displacements we require:

$$\frac{2\xi\beta}{(1 - \beta^2)} = \left[ 2\xi\beta - \frac{\beta}{2\xi} \cdot (1 - \beta^2) \right] \quad (33)$$

The trivial ... and not very useful ... solution is  $\beta = 0$ . Rearranging the remaining terms gives,

$$\xi^2 = \left[ \frac{-(1 - \beta^2)^2}{4\beta^2} \right]. \quad (34)$$

Physical considerations dictate that  $\xi$  must be greater than zero (i.e., we want the bang-bang control strategy and damping in the physical system to be well defined). From equation 34 it is evident, however, that no value of  $\beta$  exists for which this will occur. The left- and right-hand sides of equation 34 will be closest in value when  $\beta = 1$  and  $\gamma \approx 0$  (i.e., a very lightly damped system is forced near its resonance frequency).

Similarly, in order for the actuator to work perfectly in phase with velocities we require:

$$\frac{(\beta^2 - 1)}{2\xi\beta} = \left[ 2\xi\beta - \frac{\beta}{2\xi} \cdot (1 - \beta^2) \right] \quad (35)$$

Rearranging terms gives,

$$\xi^2 = \left[ \frac{(\beta^2 - 1)(1 - \beta^2)}{4\beta^2} \right] = \left[ \frac{-(1 - \beta^2)^2}{4\beta^2} \right]. \quad (36)$$

There are no values of  $\beta$ , including  $\beta = 0$ , which will make the right-hand side of equation 36 positive. Hence, the theorem is proved.

**Plots of Phase Shift vs Beta.** Figures 2 and ‘3 show the phase shift in displacements, velocities and actuator force change as a function of  $\beta$  for contours of damping,  $\xi = 0.01$  and  $0.10$ , respectively. Small values of  $\beta$  correspond to structures that are stiff (i.e.,  $w = 2\pi/T$  is large compared to the dominant circular natural frequency of ground motion). In contrast, base isolated structures have relatively low values of lateral stiffness and, correspondingly, high values of  $\beta$ . Notice that the contours of displacement and velocity phase shift are separated by  $\pi/2$  radians. Moreover, as predicted by the theorem, phase shift for the bang-bang control is synchronized with displacement phase shift at only two points –  $\beta = 0$  and  $1$ . What the mathematics doesn’t show is that bang-bang control is “almost in phase” with displacements for small values of  $\beta$  (i.e.,  $\beta < 0.1$ ) and “almost in phase” with velocities for  $\beta$  values covering the interval  $0.8$  through  $1.2$ . As  $\beta$  steadily increases from

0 through 2, the rate at which “displacement dominated control” switches to “velocity dominated control” increases with reductions in system damping.



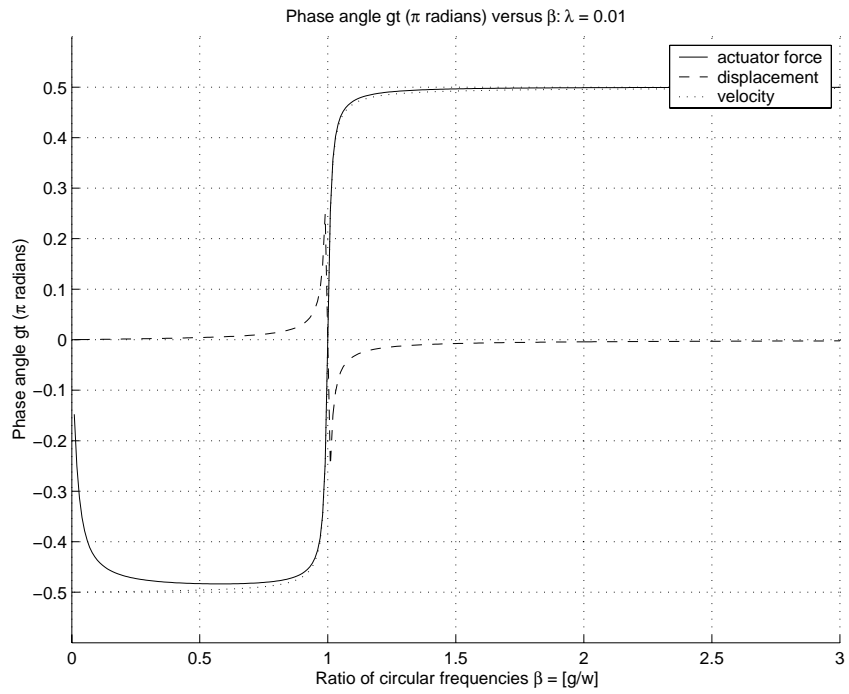


Figure 2: Actuator, Displacement, and Velocity Sign Change for Steady State Response ( $\xi = 0.01$ )

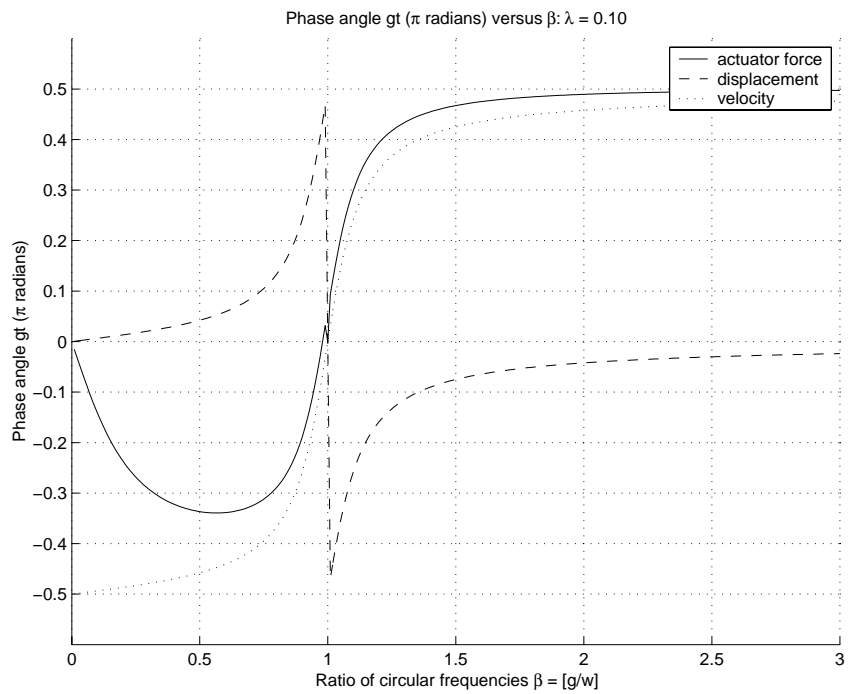


Figure 3: Actuator, Displacement, and Velocity Sign Change for Steady State Response ( $\xi = 0.10$ )

## 2.2 Free Vibration Response

Now let us assume that the structure enters a free vibration response,

$$x(t) = e^{-\xi w_o t} [A \cos(w_d t) + B \sin(w_d t)] \quad (37)$$

with initial displacement and velocity  $x(0)$  and  $\dot{x}(0)$ , respectively. The time history of displacement and velocity are,

$$x(t) = e^{-\xi w_o t} \left[ x(0) \cos(w_d t) + \frac{\dot{x}(0) + x(0)\xi w_o}{w_d} \sin(w_d t) \right] \quad (38)$$

and

$$\dot{x}(t) = e^{-\xi w_o t} \left[ \dot{x}(0) \cos(w_d t) - \frac{1}{\sqrt{1-\xi^2}} (\xi \dot{x}(0) + w_o x(0)) \sin(w_d t) \right]. \quad (39)$$

**Bang-Bang Control Strategy.** Substituting equations 38 and 39 into  $\mathbf{Z}(t) = [x(t), \dot{x}(t)]^T$  and pre-multiplying by equation 22 gives:

$$\mathbf{B}^T \mathbf{S} \mathbf{Z} = \begin{bmatrix} 1 \\ 2 \end{bmatrix} x(t) + \begin{bmatrix} m \\ 2c \end{bmatrix} \dot{x}(t) = \begin{bmatrix} 1 \\ 2 \end{bmatrix} \left[ x(t) + \frac{1}{2\xi w_o} \dot{x}(t) \right]. \quad (40)$$

**Strategy for Switching Direction of the Actuator Force.** The actuator will switch directions in the force application when:

$$C \cos(w_d t) + D \sin(w_d t) = 0, \quad (41)$$

where

$$C = \frac{x(0)}{2} + \frac{\dot{x}(0)}{4\xi w_o} \quad (42)$$

and

$$D = \frac{1}{2w_o\sqrt{1-\xi^2}} \left[ \frac{\dot{x}(0)}{2} + \left[ \xi - \frac{1}{2\xi} \right] w_o x(0) \right]. \quad (43)$$

**Zero Displacements.** The system displacements will change sign when,

$$\tan(w_d t) = \frac{-x(0)w_o\sqrt{1-\xi^2}}{\dot{x}(0) + x(0)w_o\xi}. \quad (44)$$

**Zero Velocities.** The system velocities will be zero when,

$$\tan(w_d t) = \frac{\dot{x}(0)\sqrt{1-\xi^2}}{\xi\dot{x}(0) + w_o x(0)}. \quad (45)$$

**Plots of “Phase of Bang-Bang Control” vs  $\xi$ .**

Because the number of degrees of freedom in the model of free vibration response is one fewer than the corresponding steady state model (i.e.,  $\beta$  is a constant value), it is possible to displace in one plot, a complete picture for how the direction of control force application changes as a function of the remaining problem parameters. We simplify the problem by defining the dimensionless ratio,

$$\rho = \frac{x(0)w_o}{\dot{x}(0)}. \quad (46)$$

Substituting equation 46 into equations 42 and 43 gives:

$$C = \frac{x(0)}{2} + \frac{\dot{x}(0)}{4\xi w_o} = \frac{x(0)}{2} \left[ 1 + \frac{1}{2\rho\xi} \right] \quad (47)$$

and

$$D = \frac{x(0)}{2\sqrt{1-\xi^2}} \left[ \frac{1}{2\rho} + \left[ \xi - \frac{1}{2\xi} \right] \right]. \quad (48)$$

Substituting equations 47 and 48 into 41 and rearranging terms gives:

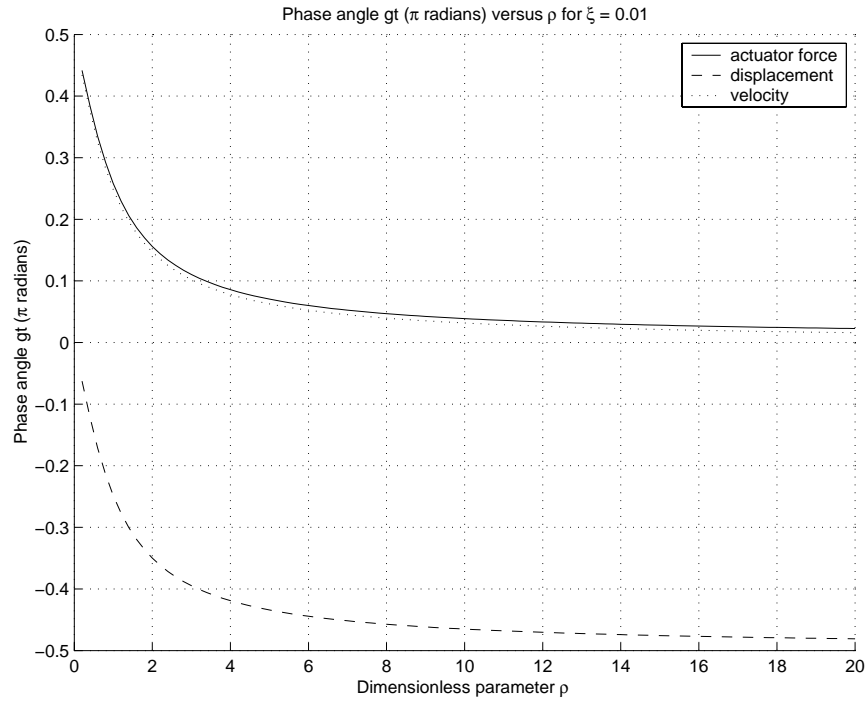


Figure 4: Free Vibration Analysis. Actuator Force, Displacement, and Velocity Sign Change versus Dimensionless Parameter  $\rho$  ( $\xi = 0.01$ )

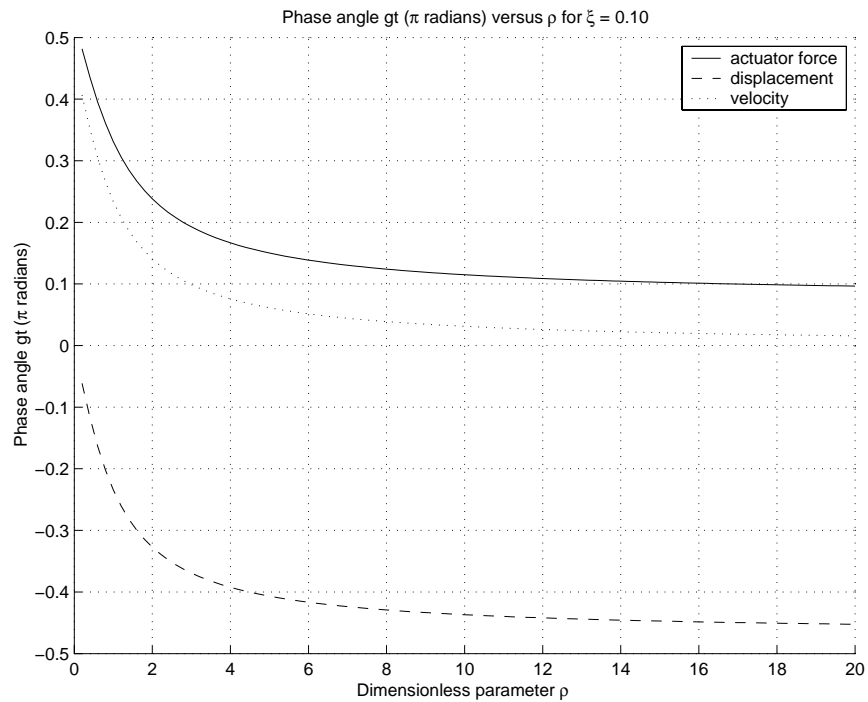


Figure 5: Free Vibration Analysis. Actuator Force, Displacement, and Velocity Sign Change versus Dimensionless Parameter  $\rho$  ( $\xi = 0.10$ )

$$\tan(w_d t) = \frac{-[1 + 2\rho\xi]\sqrt{1 - \xi^2}}{[\xi + 2\rho\xi^2 - \rho]} \quad (49)$$

Similarly, zero displacements and velocities occur at:

$$\tan(w_d t) = \frac{-\sqrt{1 - \xi^2}x(0)w_o}{\dot{x}(0) + x(0)w_o\xi} = \frac{-\rho\sqrt{1 - \xi^2}}{1 + \rho\xi} \quad (50)$$

and

$$\tan(w_d t) = \frac{\dot{x}(0)\sqrt{1 - \xi^2}}{\xi\dot{x}(0) + w_o x(0)} = \frac{\sqrt{1 - \xi^2}}{\xi + \rho}. \quad (51)$$

When  $\xi = 0$ , equations 49, 50 and 51 simplify to  $1/\rho$ ,  $-\rho$ , and  $1/\rho$ , respectively. In other words, for the case of zero damping: (1) the actuator works in perfect phase with velocities, and (2) displacements are orthogonal (i.e., separated by  $\pi/2$  radians) to velocities.

Figures 4 and 5 show phase angles for change in actuator force direction, and sign of system displacements and velocities, versus dimensionless parameter  $\rho$  for critical damping ratios  $\xi = 0.01$  and  $\xi = 0.10$ , respectively. For lightly damped systems in free vibration, switching of the actuator force direction occurs almost in phase with the sign of velocity. This indicates that like the damping model, active control works to oppose changes in system displacement. Finally, we observe that the “steady state” and “free vibration” phase shift models are consistent if latter is viewed as a “steady state response” resulting from a very high forcing frequency (i.e.,  $\beta = g/w \rightarrow \infty$ ).

### 3 Correlation Coefficients for Simplified Response

Analytic expressions for relative behavior (i.e., correlation of displacements versus actuator force direction and velocities versus actuator force direction) are of the form (see Clough and Penzien, pg. 452):

$$\sigma_x^2 = \lim_{T \rightarrow \infty} \frac{1}{T} \cdot \int_0^T [\text{sign}(x(\tau)) - \bar{x}]^2 d\tau \quad (52)$$

and

$$\mu(x, f) = \lim_{T \rightarrow \infty} \frac{1}{T} \cdot \int_0^T [\text{sign}(x(\tau)) - \bar{x}] \cdot [\text{sign}(f(\tau)) - \bar{f}] d\tau \quad (53)$$

and so forth. Fortunately, evaluation of equations 52 and 53 can be simplified by observing that for the steady state response, displacements and velocities are of the form:

$$x(t) = A_x^* \cdot \sin(gt + \phi_x) \quad \text{and} \quad \dot{x}(t) = A_{\dot{x}}^* \cdot \sin(gt + \phi_{\dot{x}}). \quad (54)$$

and for the free vibration response, of the form:

$$x(t) = B_x^*(t) \cdot \sin(w_d t + \phi_x) \quad \text{and} \quad \dot{x}(t) = B_{\dot{x}}^*(t) \cdot \sin(w_d t + \phi_{\dot{x}}). \quad (55)$$

Here, coefficients  $A_x^*$ ,  $A_{\dot{x}}^*$ ,  $B_x^*(t)$  and  $B_{\dot{x}}^*(t)$  are obtained through rearrangement of equations XX and YY. It is important to note that in this application, only the sign of the displacement/velocity matters (the magnitude of velocities and displacement is irrelevant). Instead of evaluating equations 52 and 53 over an infinite interval, we note that the function repeats over intervals of  $2\pi$  radians. Hence, mean values of displacement, velocity and actuator force are given by,

$$\bar{x} = \frac{1}{2\pi} \cdot \int_0^{2\pi} [\text{sign}(x(\tau))] d\tau = 0, \quad (56)$$

$$\bar{\dot{x}} = \frac{1}{2\pi} \cdot \int_0^{2\pi} [\text{sign}(\dot{x}(\tau))] d\tau = 0, \quad (57)$$

$$\bar{f} = \frac{1}{2\pi} \cdot \int_0^{2\pi} [\text{sign}(f(\tau))] d\tau = 0, \quad (58)$$

The measures of variance are given by:

$$\sigma_x^2 = \frac{1}{2\pi} \cdot \int_0^{2\pi} [\text{sign}(x(\tau)) - \bar{x}]^2 d\tau = \frac{1}{2\pi} \cdot \int_0^{2\pi} \text{sign}(x(\tau))^2 d\tau = 1. \quad (59)$$

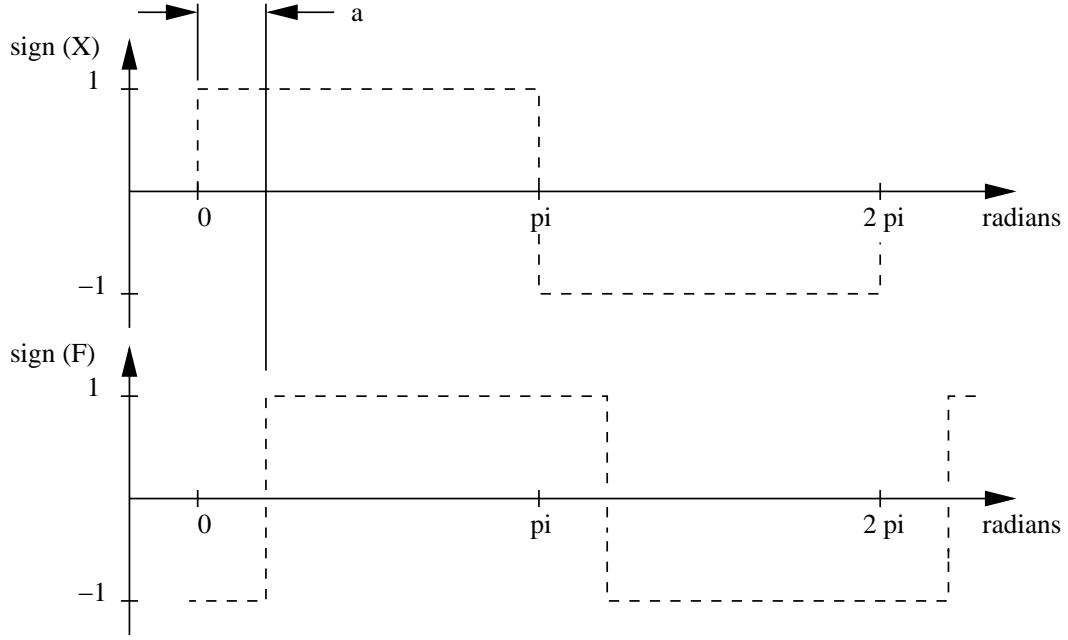


Figure 6: Schematic of Relative Phase between displacements(x)/velocities(v) and Direction of Actuator Force

$$\sigma_x^2 = \frac{1}{2\pi} \cdot \int_0^{2\pi} [\text{sign}(\dot{x}(\tau)) - \bar{\dot{x}}]^2 d\tau = \frac{1}{2\pi} \cdot \int_0^{2\pi} \text{sign}(\dot{x}(\tau))^2 d\tau = 1. \quad (60)$$

$$\sigma_f^2 = \frac{1}{2\pi} \cdot \int_0^{2\pi} [\text{sign}(f(\tau)) - \bar{f}]^2 d\tau = \frac{1}{2\pi} \cdot \int_0^{2\pi} \text{sign}(f(\tau))^2 d\tau = 1. \quad (61)$$

Measures of co-variance for “force and displacement” and “force and velocity” are as follows:

$$\mu(x, f) = \frac{1}{2\pi} \cdot \int_0^{2\pi} \text{sign}(x(\tau)) \cdot \text{sign}(f(\tau)) d\tau. \quad (62)$$

and

$$\mu(\dot{x}, f) = \frac{1}{2\pi} \cdot \int_0^{2\pi} \text{sign}(\dot{x}(\tau)) \cdot \text{sign}(f(\tau)) d\tau. \quad (63)$$

With equations 52 through 63 in place, the correlation coefficients for “force and displacement” and “force and velocity” are as follows:

$$\rho(x, f) = \rho(F, X) = \frac{\mu(x, f)}{\sigma_x \sigma_f} \quad \text{and} \quad \rho(\dot{x}, f) = \rho(F, V) = \frac{\mu(\dot{x}, f)}{\sigma_{\dot{x}} \sigma_f}. \quad (64)$$

Because the mean square values are always positive, the correlation coefficient will always lie in the interval  $[-1, 1]$  (i.e.,  $-1 < \rho(x, f) < 1$  and  $-1 < \rho(\dot{x}, f) < 1$ ). One special case occurs when the variables  $x$  and  $f$  are statistically independent;  $\mu(x, f) = 0$  and, hence,  $\rho(x, f)$  also equals 0.

Based on our phase analysis of a simplified system response, we expect, however, that the velocity and force will be strongly correlated – hence,  $\rho(\dot{x}, f)$  should evaluate to a numerical value close to 1. Moreover, because the velocity and displacement are  $\pi/2$  radians out of phase,  $\rho(x, f)$  should evaluate to a number close to zero. Now let “ $a$ ” be the phase angle between the system displacements and actuator force and/or system velocities and actuator force. Evaluation of equation 64 simplifies to:

$$\text{co-variance } \rho(a) = \begin{cases} \left(1 - \frac{2a}{\pi}\right) & a \in [0, \pi] \quad \text{radians} \\ \left(-1 + \frac{2a}{\pi}\right) & a \in [\pi, 2\pi] \quad \text{radians} \end{cases} \quad (65)$$

Notice that when  $\rho(0)$  evaluates to 1,  $\rho(\pi/2)$  evaluates to 0, and  $\rho(\pi)$  evaluates to -1.

### Steady State and Free Vibration Response

Figures 7 and 8 shows contours of  $\rho(F, X)$  and  $\rho(F, V)$  for steady state response at damping ratios  $\xi = 0.01$  and  $\xi = 0.10$ , respectively. Counterpart contour diagrams for free vibration response are shown in Figures 8 and 9. Given that: (1) the base isolation system design will move the fundamental periods of structural vibration to a region where  $\beta = g/w$  will be greater than one (perhaps in the range 3 to 5), and (2) a realistic time history response will be a combination of forced and free vibration components, we predict that correlation coefficients for actuator force direction and displacements will lie in the interval  $[0.0, 0.15]$ . For very lightly damped systems, actuator force direction and velocities should have a correlation coefficient close to one (i.e.,  $[0.98, 1.0]$ ). As damping increase to  $\xi = 0.10$ , the actuator force/velocity correlation coefficient should decrease to a number close to 0.85 (i.e., cover the interval  $[0.80, 0.85]$ ).



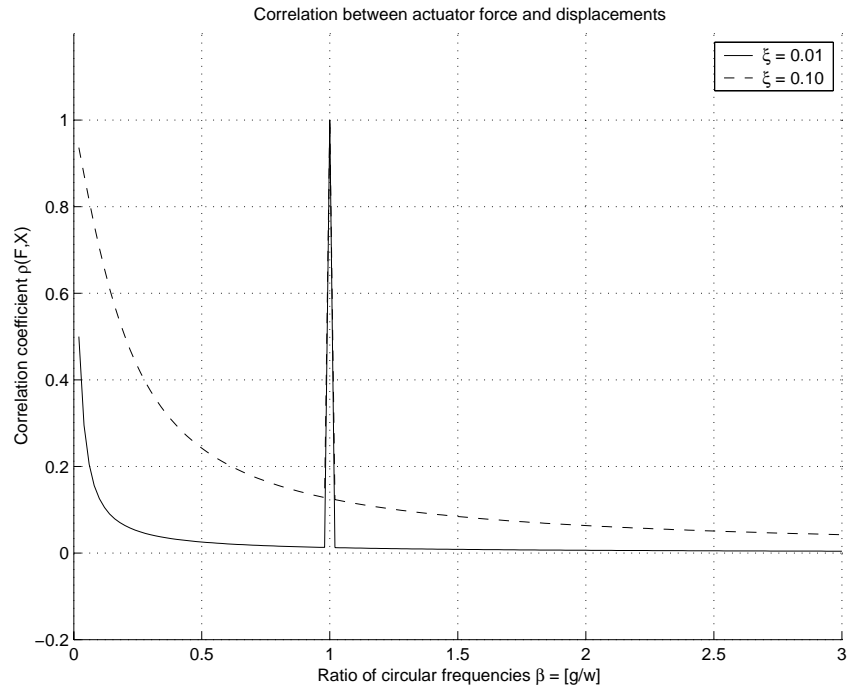


Figure 7: Steady state response. Correlation of actuator force direction to displacements  $\rho(F, X)$  at damping ratios  $\xi = 0.01$  and  $0.10$ .

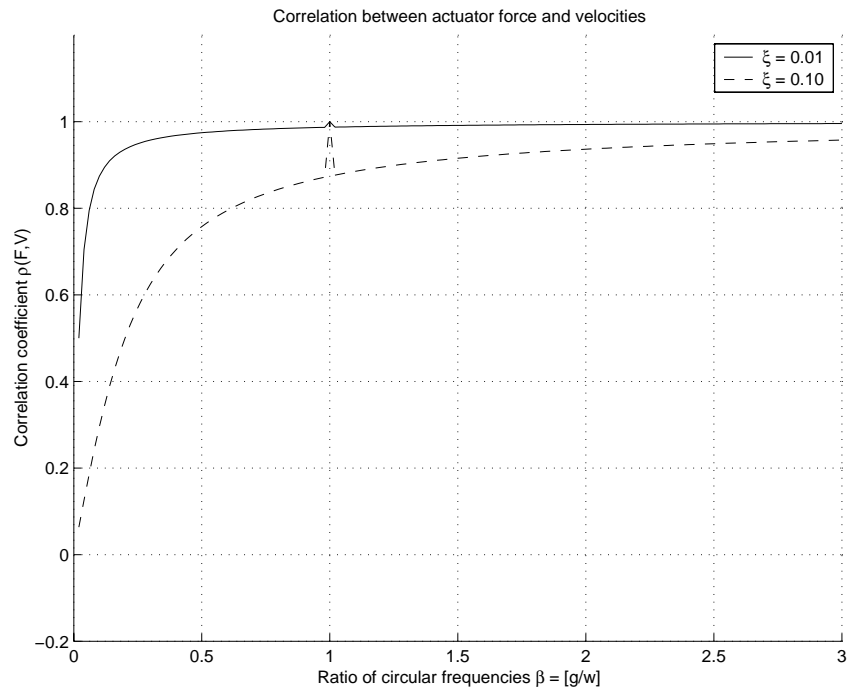


Figure 8: Steady state response. Correlation of actuator force direction to velocities  $\rho(F, V)$  at damping ratios  $\xi = 0.01$  and  $0.10$ .

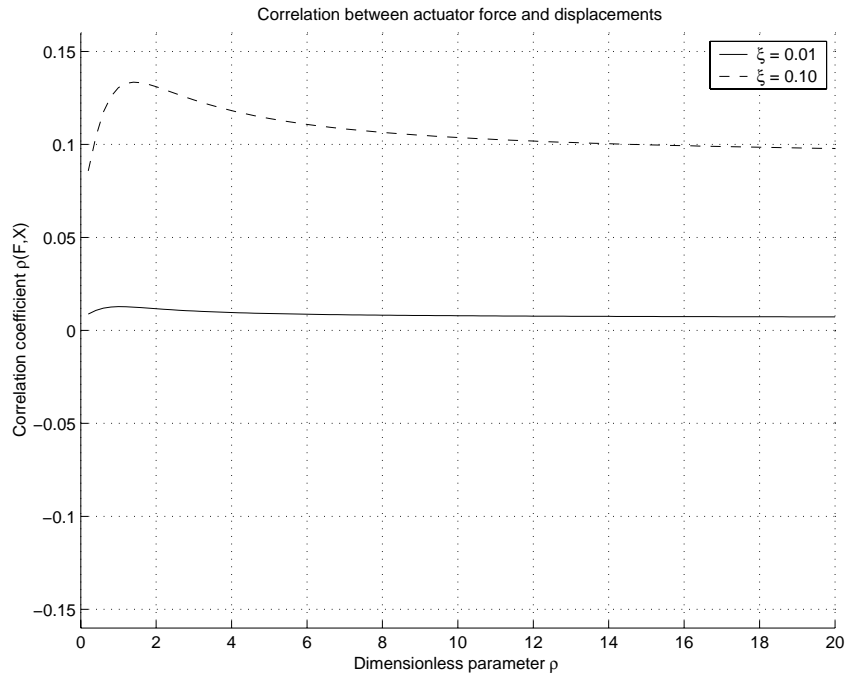


Figure 9: Free Vibration Response. Correlation of actuator force direction to displacements  $\rho(F, X)$  at damping ratios  $\xi = 0.01$  and  $0.10$ .

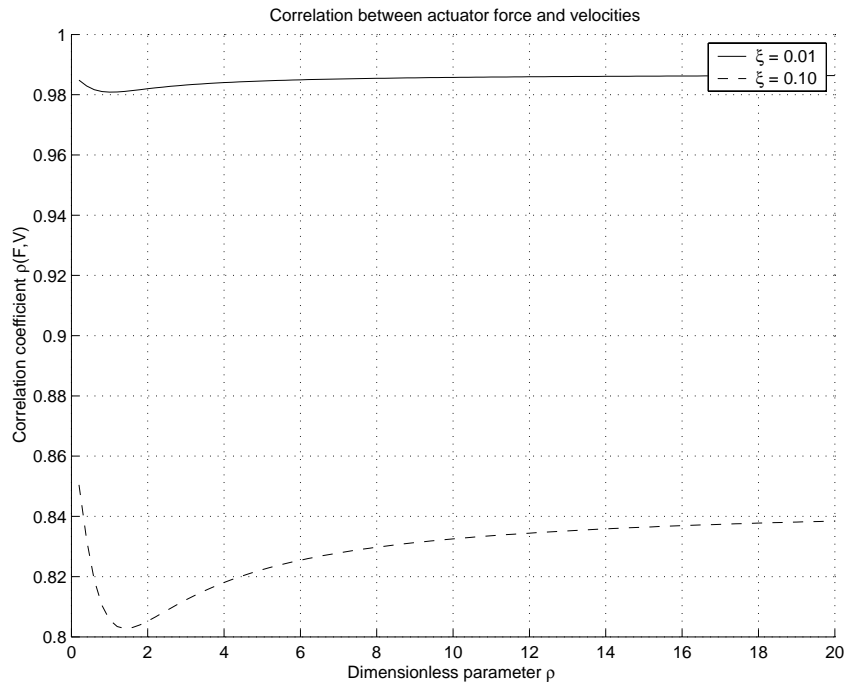


Figure 10: Free Vibration Response. Correlation of actuator force direction to velocities  $\rho(F, V)$  at damping ratios  $\xi = 0.01$  and  $0.10$ .

## 4 Numerical Experiments

Using models of steady state and damped free vibration system response, we have shown that the direction of actuator force application in bang-bang control of base isolated structures is: (1) Almost in phase (but acts in the opposite direction) with system velocities; and (2) Almost orthogonal (i.e., 90 degrees out of phase) to system displacements. Together, these observations suggest that for practical purposes, the following “velocity cancellation” control strategy,

$$\mathbf{U}(t) = \begin{cases} U_{max} & \text{if } \dot{x}_1(t) < 0 \\ -U_{max} & \text{otherwise} \end{cases} \quad (66)$$

might be very effective? Equation 66 is appealing because it has good physical intuition – like damping mechanisms, the control strategy simply tells the actuator to push in a direction that opposes the change in displacements (i.e., velocity cancellation).

Our phase analyses are based on models of displacement response that are overly simple – the dynamic response of a base isolated structure due to ground motions will be an unknown combination of forced and free vibration components – it is neither purely steady state nor purely free vibration. In this application, behavior is further complicated by a combination of ground motion displacements and actuator forces. The phase analysis does not include the relative contribution of these effects. Moreover, while real structures have multiple degrees of freedom, it is well known that the dynamic response of base isolated systems tends to be dominated by first mode effects. The extent to which each of these simplifying factors contributes to time-history behavior needs to be validated by simulation/experiment.

In this section we use the Aladdin scripting language [3, 4] to compute the time-history response of a two-DOF actively controlled mass-spring-damper system subject to an ensemble of severe earthquake ground motions. Simulations are conducted for linear system behavior and localized nonlinear behavior in the isolation device. Each case study is composed of three parts: (1) system response due to base isolation alone (i.e., with  $U_{max} = 0$  kN); (2) system response due to base isolation plus constant stiffness bang-bang control (i.e., with  $U_{max} = 450$  kN); and (3) system response due to base isolation plus the velocity control described in equation 66 (i.e., with  $U_{max} = 450$  kN). For each design case, system response is evaluated with respect to traditional metrics (i.e., peak values of displacement and velocity) and the phase analysis predictions developed

in the previous sections.

The assumption of linearly elastic behavior implies no permanent offset in displacements after the ground motions have ceased. This assumption is consistent with expected behavior of base isolated structures under moderate earthquake loadings. However, for severe ground motion attacks, the isolation system will be expected to deform well into the nonlinear regime, possibly resulting in permanent displacement offsets. Numerical studies are needed to investigate the extent to which permanent offsets in displacement degrade phase analysis predictions.

#### 4.1 Actively Controlled Mass-Spring-Damper System

Figure 11 shows an elevation view of an idealized mass-spring-damper base isolated system.

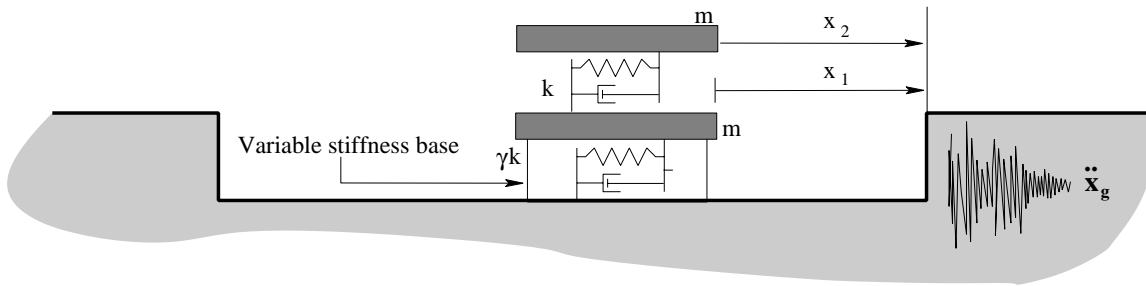


Figure 11: Elevation View of 2 DOF Linear/Nonlinear Mass-Spring-Damper System

Within the superstructure (i.e., element 2), two lumped masses are connected via one linearly elastic spring. Element 1 is modeled with a bi-linear, force-displacement relationship that follows the kinematic hardening rule. Element 1 is used by Lin [14] and is a model of a laminated rubber base-isolator with a lead core. The purpose of element 1 is to isolate the superstructure from the inertia forces generated by the ground displacements. The left-hand side of Table 1 contains a summary of mass and stiffness properties for the structural model.

The yield force and displacement for element 1 are 454 kN and 34.3 mm, respectively. Damping effects are accounted for through linear viscous damping. In the equation  $\mathbf{C} = \alpha\mathbf{M} + \beta\mathbf{K}$ , the coefficients  $\alpha$  and  $\beta$  are chosen so that there is 10% critical damping in the first two modes. Boundary conditions for our model are full-fixity at the base, and full-fixity against vertical displacements and rotations at nodes 2 and 3.

DOF/Mode	Floor	Stiffness (kN/m)		Period (secs)		Part. Factor ( $\Gamma$ )	
	Mass (kg)	Pre-yield	Post-yield	Pre-yield	Post-yield	Pre-yield	Post-yield
1	160,055	13,247	13	0.98	30.86	1.02	1.00
2	160,055	150,000	150,000	0.14	0.14	0.02	0.00

Table 1: Properties of Two DOF Mass-Spring-Damper System

Table 1 shows that prior to yielding, the first and second natural periods of vibration are 0.98 and 0.14 seconds, respectively. We assume that the post-yield stiffness of the isolator is only one thousandth of its initial value. After the base isolator has yielded the first and second natural periods of vibration increase to 30.86 and 0.14 seconds. The modal participation factors are given by

$$\text{Participation Factor( Mode } i \text{ )} = \left[ \frac{\phi_i^T M r}{\phi_i^T M \phi_i} \right] \quad (67)$$

In both the pre- and post-yield states, the modal participation factors indicate that the overall system response is dominated by first mode displacements – this is particularly the case for post-yield displacements. Thus, even though our model contains multiple degrees of freedom, there is a good likelihood that “phase analysis of a single DOF system” will accurately predict more general behavior.

## Actuator Placement and Performance

For the purposes of illustrating the potential benefits of active control, an actuator is located at the top of the lead-rubber base isolator (degree of freedom 1). Unfortunately, at this time there is a complete lack of guidance in the literature on the selection of appropriate max/min forces in the actuator. Hence, in this study, we proceed under the assumption that the hybrid system will not add value to the overall system performance unless the passive and active components of control can work in concert. For the passive control system, stiffness and yield force design parameters are selected so that the structure will have appropriate natural periods of vibration and yield before excessive forces occur within the main structural system. We observe that since the actuators will not affect the natural periods of vibration (i.e., be large enough to change the tangent stiffness of the structure), as a first cut, peak actuator forces should be balanced against the yield capacity of the isolators. Therefore, this study covers two levels of actuator force application:

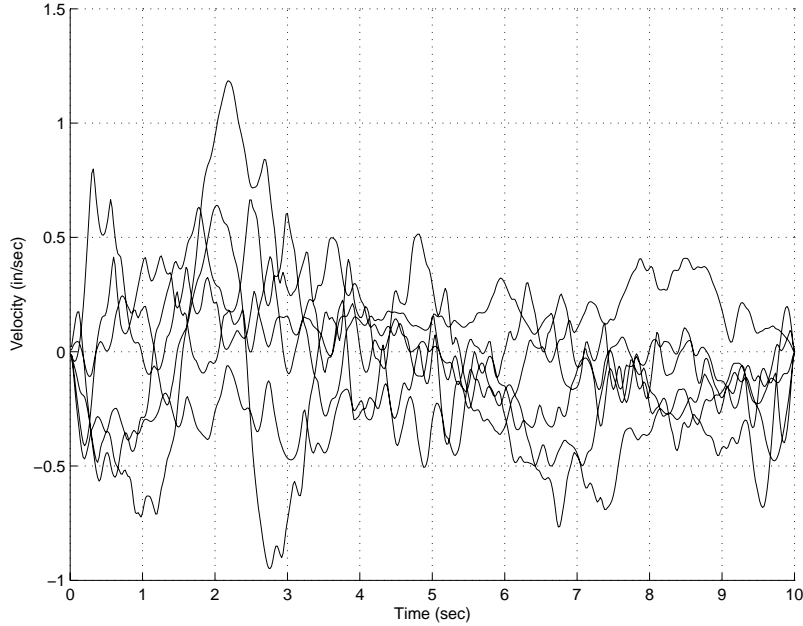


Figure 12: Ground Motion Velocities (in/sec) versus Time (sec) for the six El Centro Ground Motion Records used in this study

1. **Minimum Actuator Force.** The minimum actuator force that can be applied is 0 kN. The ensuing system response is due to base isolation alone.
2. **Maximum Actuator Force.** The maximum force that may be generated is a little less than the yield force of the base isolator (i.e.,  $u_{max} = 0.991 \cdot f_y = 450$  kN).

## 4.2 Library of Ground Motions

This study is based on six ground motions recorded at El Centro, digitized at intervals of 0.02 seconds. Scaled design ground motions were obtained by first isolating the worst ten-second sample of each record. Each record was then translated along the y-axis to remove residual velocity effects. A family of severe earthquake lateral loadings was obtained by constraining the Arias Intensity (Arias 1970) – Arias Intensity is a measure of energy in the accelerogram – for each record to be identical, and scaling the family of records so that the average peak ground acceleration is 0.5g (i.e., 490.5 cm/sec/sec). In other words, if the  $i$ -th ground motion acceleration is denoted by  $\ddot{x}_{ig}(t)$ , then this procedure scales the  $i$ -th ground motion by  $k_i$  so that:

$$\frac{\pi}{2g} \int_0^{10} k_1^2 \ddot{x}_{1g}^2(\tau) d\tau = \frac{\pi}{2g} \int_0^{10} k_2^2 \ddot{x}_{2g}^2(\tau) d\tau = \dots = \frac{\pi}{2g} \int_0^{10} k_6^2 \ddot{x}_{6g}^2(\tau) d\tau = \text{constant}. \quad (68)$$

Table 2 summarizes the six components of scaled ground motion, the peak ground accelerations, minimum and maximum ground velocities, Arias Intensity and ground motion scale factors. Fig's 5 and 6 show the time variation in Arias intensity and ground velocity for the six scaled ground motion records, respectively.

### Dominant Frequencies of Ground Motion

The Fourier transform is a frequency domain analysis technique that is used to determine dominant frequency. Figures 13 through 18 show the frequency content of ground motion for the ten second segments of ground motion extracted from the six El Centro records used in this study. We assume that the centroid of the Fourier Spectrum,

$$\text{Centroid of Fourier Spectrum}(g) = \left[ \frac{\int_0^{25 \text{ Hz}} w \dot{F}(w) dw}{\int_0^{25 \text{ Hz}} F(w) dw} \right]. \quad (69)$$

is a good estimate of the dominant period of ground motion. Assuming that the system response is dominated by the first mode of vibration, then a good estimate of  $\beta = g/w = [T_s/T_g]$  is given by the first period of vibration in the structure divided by the dominant period of ground motion.

Table 3 summarizes the centroid of frequency content, corresponding dominant period of ground motion shaking, and pre- and post-yield beta values for the six El Centro ground motions. By design, the base isolation system separates the natural periods of vibration for the structure from the dominant frequencies of vibration in the ground motions. The isolation system will be expected to remain essentially elastic during small-to-moderate sized ground motions. Corresponding values of pre-yield  $\beta$  cover the interval [2.64, 4.08]. However, during severe ground motion attacks, isolation systems are designed to deform well into the nonlinear range. To accentuate potential nonlinear effects, we have deliberately selected low values of post-yield stiffness. Corresponding values of post-yield  $\beta$  cover the interval [83.4, 128].

```

=====
Record/Location      Ground Motion      Peak Accn      Velocity (m/sec)  Arias Intensity
                    Scale Factor (cm/sec/sec)      Min      Max      (m/sec)
=====
El Centro Site Imperial Valley Irrigation District, May 18, 1940.
-----
1940 EL CENTRO S00E RECORD :   1.690      573.9      -0.47      0.80      6.485
1940 EL CENTRO S90W RECORD :   2.135      441.8      -0.77      0.63      6.485

El Centro Site Imperial Valley Irrigation District, December 30, 1934.
-----
1934 EL CENTRO S00W RECORD :   2.821      444.9      -0.41      0.42      6.485
1934 EL CENTRO S90W RECORD :   3.056      545.6      -0.47      0.07      6.485

El Centro Community Hospital on Keystone Rd., October 15, 1979.
-----
1979 EL CENTRO N50E RECORD :   2.562      437.4      -0.72      1.18      6.485
1979 EL CENTRO N40W RECORD :   2.269      500.4      -0.94      0.64      6.485
=====

```

Table 2: Library of earthquake ground motions recorded at El Centro, California

```

=====
Record/Location      Area      First      Centroid      Tg      Pre-Yield      Post-Yield
                    Area      Moment      (Hz)      (sec)      beta      beta
=====
El Centro Site Imperial Valley Irrigation District, May 18, 1940.
-----
1940 EL CENTRO S00E RECORD :   506.5  1862.8      3.68  0.27      3.62      114.3
1940 EL CENTRO S90W RECORD :   506.5  1497.5      2.95  0.33      2.96      93.5

El Centro Site Imperial Valley Irrigation District, December 30, 1934.
-----
1934 EL CENTRO S00W RECORD :   506.5  2082.0      4.11  0.24      4.08      128.6
1934 EL CENTRO S90W RECORD :   506.5  2001.3      3.95  0.25      3.92      123.4

El Centro Community Hospital on Keystone Rd., October 15, 1979.
-----
1979 EL CENTRO N50E RECORD :   506.5  1497.5      2.95  0.33      2.96      93.5
1979 EL CENTRO N40W RECORD :   506.5  1368.0      2.70  0.37      2.64      83.4
=====

```

Table 3: Ratio  $\beta = (g/w)$  of Forcing Frequencies



## **Time History Analyses**

Time history analyses are computed for 15 seconds, using an integration timestep of 0.02 seconds. For the time interval  $t \in [0, 10]$  seconds, the system response is affected by both ground motions and active control. The ground motions cease at  $t = 10$  seconds. Thus, for the time interval  $t \in [10, 15]$  seconds, the only external actions are due to active control.

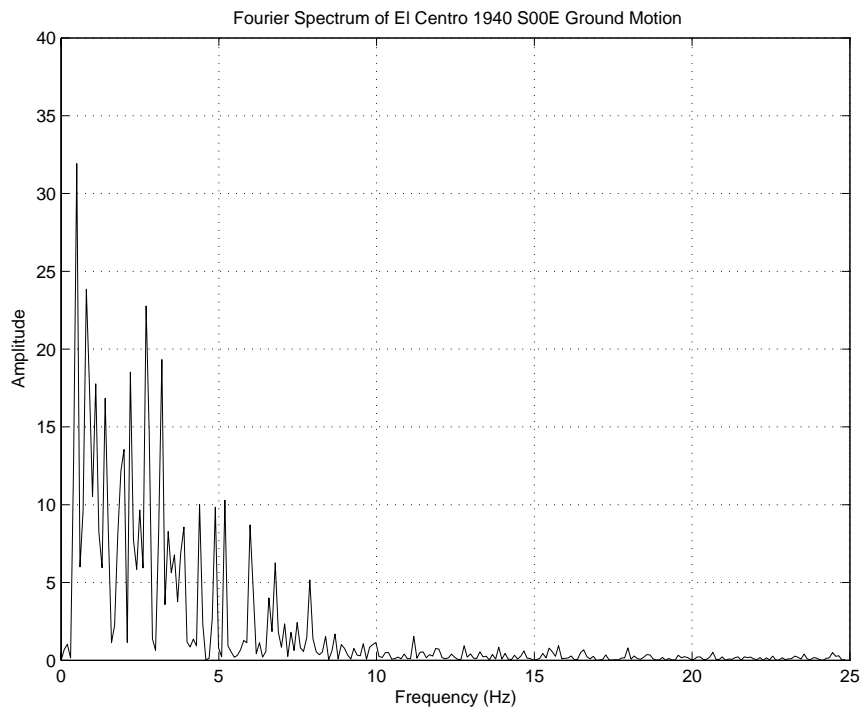


Figure 13: Fourier Spectra for El Centro 1940 S00E Record

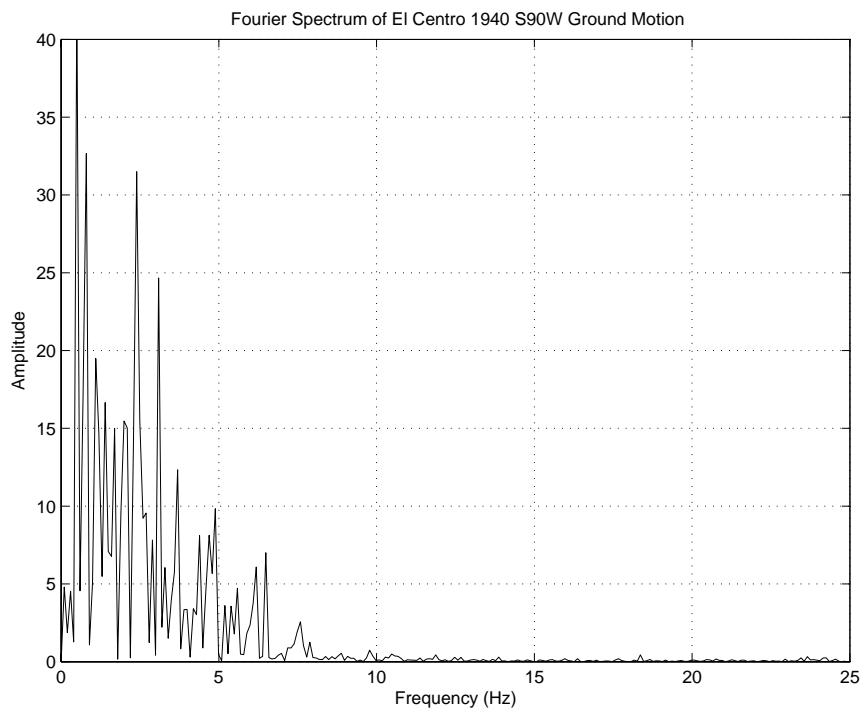


Figure 14: Fourier Spectra for El Centro 1940 S90W Record

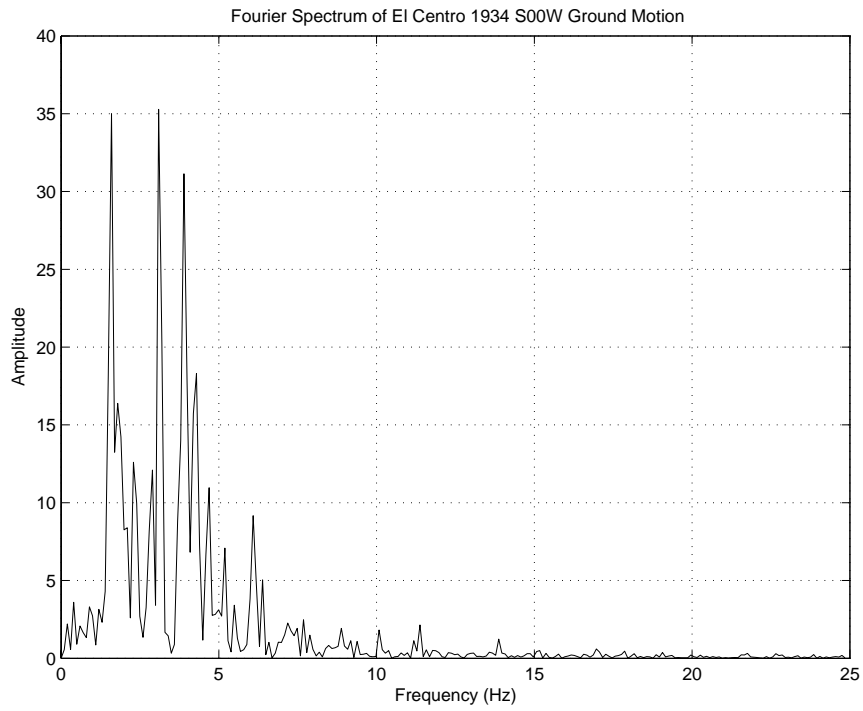


Figure 15: Fourier Spectra for El Centro 1934 S00W Record

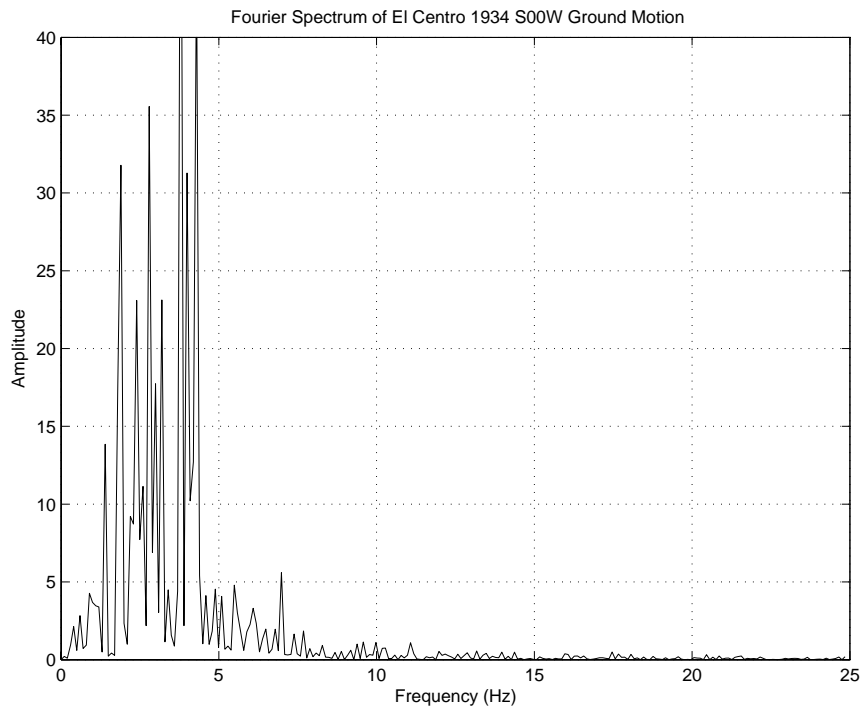


Figure 16: Fourier Spectra for El Centro 1934 S90W Record

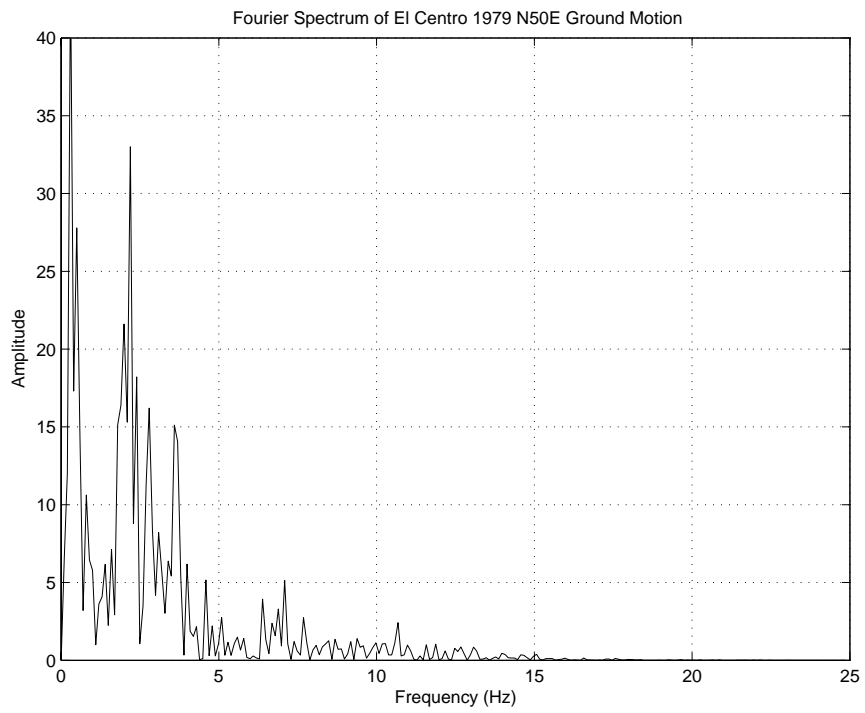


Figure 17: Fourier Spectra for El Centro 1979 N50E Record

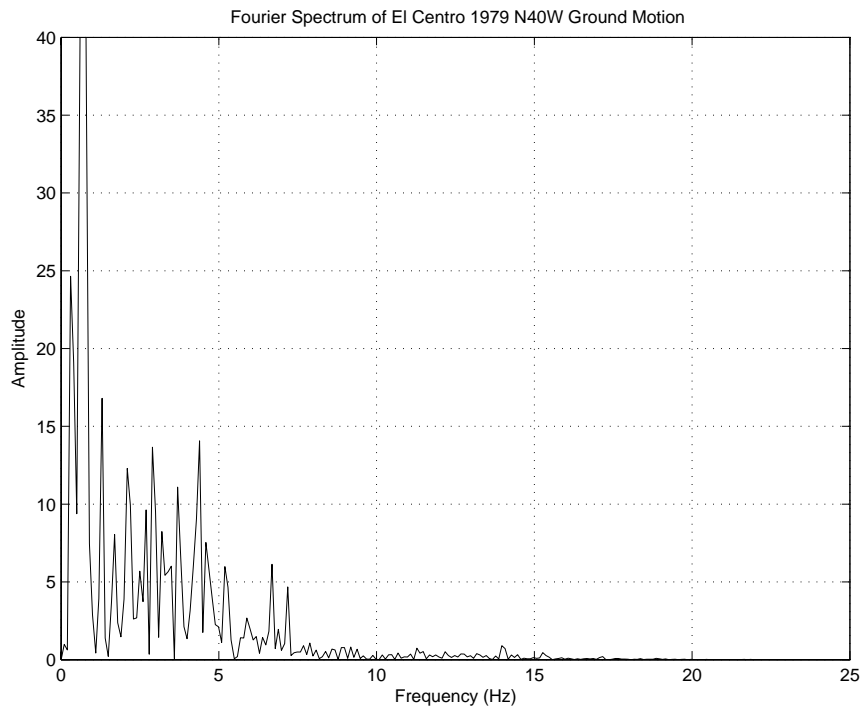


Figure 18: Fourier Spectra for El Centro 1979 N40W Record

### 4.3 Scatter Diagram/Correlation Analysis

The numerical experiment employs discrete counterparts of equations 56 through 64. Figure 19 is a symbolic representation of the direction of actuator force together with its relationship to the system state variables (i.e., various aspects of displacement or velocity).

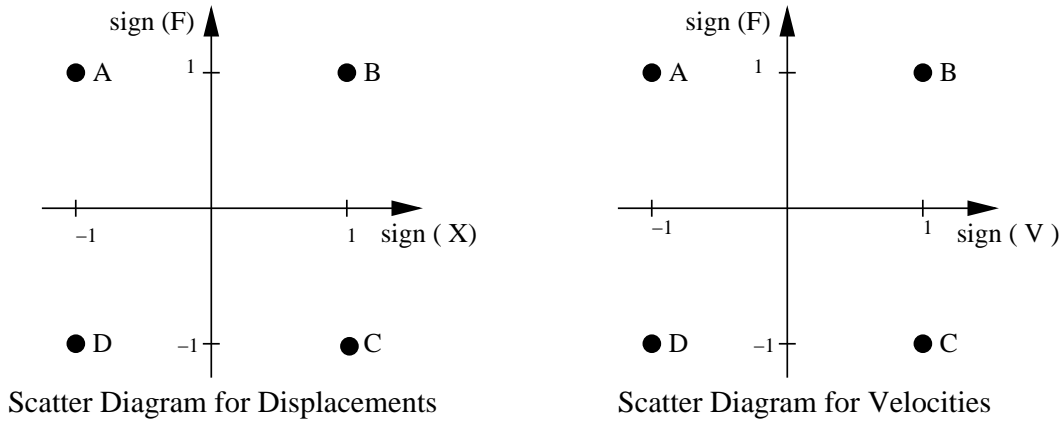


Figure 19: Scatter Diagram for Displacement/Velocity Phase vs Direction of Actuator Force

The probability mass density of  $(\text{sign}(x), \text{sign}(F))$  response coordinates can be represented:

```

=====
Coordinate:      A(-1,1) | B(1,1) | C(1,-1) | D(-1,-1)
=====
No Points :
-----

```

The sum of observations at points A, B, C and D will equal the total number of data points covering the interval of interest in the simulation. The average values of the displacement, velocity, and force sign values are given by:

$$\bar{x} = \frac{1}{N} \sum_{i=1}^{i=N} \text{sign}(x_i), \quad \bar{\dot{x}} = \frac{1}{N} \sum_{i=1}^{i=N} \text{sign}(\dot{x}_i) \quad \text{and} \quad \bar{f} = \frac{1}{N} \sum_{i=1}^{i=N} \text{sign}(F_i). \quad (70)$$

The measures of variance are given by:

$$\sigma_x^2 = \frac{1}{N} \sum_{i=1}^{i=N} (\text{sign}(x_i) - \bar{x})^2. \quad (71)$$

$$\sigma_{\dot{x}}^2 = \frac{1}{N} \sum_{i=1}^{i=N} (\text{sign}(\dot{x}_i) - \bar{\dot{x}})^2. \quad (72)$$

$$\sigma_f^2 = \frac{1}{N} \sum_{i=1}^{i=N} (\text{sign}(f_i) - \bar{f})^2. \quad (73)$$

Measures of co-variance for “force and displacement” and “force and velocity” are as follows:

$$\mu(x, f) = \mu(F, X) = \frac{1}{N} \sum_{i=1}^{i=N} (\text{sign}(x_i) - \bar{x}) \cdot (\text{sign}(f_i) - \bar{f}) \quad (74)$$

and

$$\mu(\dot{x}, f) = \mu(F, V) = \frac{1}{N} \sum_{i=1}^{i=N} (\text{sign}(\dot{x}_i) - \bar{\dot{x}}) \cdot (\text{sign}(f_i) - \bar{f}). \quad (75)$$

With equations 70 through 75 in place, the correlation coefficients for “force and displacement” and “force and velocity” are as follows:

$$\rho(x, f) = \rho(F, X) = \frac{\mu(x, f)}{\sigma_x \sigma_f} \quad \text{and} \quad \rho(\dot{x}, f) = \rho(F, V) = \frac{\mu(\dot{x}, f)}{\sigma_{\dot{x}} \sigma_f}. \quad (76)$$

## 4.4 Case Study 1. Linear Time-History Behavior

This case study examines the time-history responses of a 2-dof linearly elastic base isolated system protected by active (i.e., bang-bang and velocity) control. Simulations are conducted for the ensemble of El Centro records described in Tables 2 and 3. The analyses are divided into three parts: (1) Linear system protected by base isolation alone (peak values from this study act as a benchmark for measuring improvements due to control), (2) Linear system protected by base isolation plus constant stiffness bang-bang control, and (3) Linear system protected by base isolation plus simplified velocity cancellation control. Performance metrics include peak values of displacement and velocity, and statistics of phase analysis. Each simulation has a force vibration segment (i.e.,  $T = [0, 10]$  sec) followed by damped free vibration (i.e.,  $T = [10, 15]$  sec). In all cases, simulations are computed for 1% damping and 10% damping.

**Part 1.** Linear System protected by Base Isolation Alone ( $U_{max} = 0$  kN)

**Displacements and Velocities.** Figures 20 and 22 show, for example, time history responses of displacement at  $\xi = 0.01$  and  $\xi = 0.10$ , as generated by the the 1940 El Centro S00E Record. Figures 21 and 23 show the corresponding Fast Fourier transforms of system response. The lightly damped system response is dominated by frequencies that are very close to the structure's fundamental period (i.e.,  $T = 0.98$  seconds). As expected, peak displacements are reduced when the system damping is increase from  $\xi = 0.01$  to  $\xi = 0.10$ . This trend is accompanied by an increase in the range of ground motion frequencies affecting the displacement response. Indeed, the spectrum response of system displacements at  $\xi = 0.10$  is considerably broader than at  $\xi = 0.01$ .

Part A: 1% Critical Damping

Ground Motion	Displacement at Node 1		Force in Element 1	
	Minimum (cm)	Maximum (cm)	Minimum (kN)	Maximum (kN)
1940 EL CENTRO S00E:	-25.54 cm	28.11 cm	-3384 kN	3724 kN
1940 EL CENTRO S90W:	-12.64 cm	13.49 cm	-1675 kN	1787 kN
1934 EL CENTRO S00W:	-11.23 cm	9.013 cm	-1488 kN	1194 kN
1934 EL CENTRO S90W:	-13.37 cm	12.04 cm	-1771 kN	1596 kN
1979 EL CENTRO N50E:	-17.69 cm	15.56 cm	-2344 kN	2061 kN
1979 EL CENTRO N40W:	-16.94 cm	17.79 cm	-2244 kN	2357 kN
Average Value:	-16.23 cm	16.00 cm	-2234 kN	2119 kN

```

=====
Part B: 10% Critical Damping
=====

```

Ground Motion	Displacement at Node 1		Force in Element 1	
	Minimum (cm)	Maximum (cm)	Minimum (kN)	Maximum (kN)
1940 EL CENTRO S00E:	-13.03 cm	12.21 cm	-1726 kN	1617 kN
1940 EL CENTRO S90W:	-8.49 cm	8.37 cm	-1125 kN	1109 kN
1934 EL CENTRO S00W:	-9.25 cm	4.55 cm	-1225 kN	603 kN
1934 EL CENTRO S90W:	-5.25 cm	6.29 cm	-695 kN	833 kN
1979 EL CENTRO N50E:	-10.44 cm	8.04 cm	-1382 kN	1066 kN
1979 EL CENTRO N40W:	-13.25 cm	14.17 cm	-1755 kN	1877 kN
Average Value:	-9.95 cm	8.93 cm	-1318 kN	1184 kN

```

=====

```

Notice that in all cases, the min/max values of element force are considerably higher than the design yield force (450 kN) for the isolator. As a result, high lateral forces can be transferred from the ground to the superstructure, which in turn, will generate higher values of column shear forces and inter-story drift.

**Phase Analysis.** Tables 4 and 5 show the scatter diagram data and phase analysis results for the linear time-history response generated by the El Centro 1940 S00E ground motion record. Tables 6 and 7 summarize the statistics of response and  $\rho(X, F)$  and  $\rho(V, F)$  values for the ensemble of El Centro Ground motion inputs. Simulations are computed for 1% and 10% critical damping,

For the most part, the theoretical predictions for  $\rho(X, F)$  and  $\rho(V, F)$  are validated by the time-history analyses. On average,  $\rho(X, F)$  is a little greater than zero and  $\rho(V, F) \approx 1$  when damping is 1%,  $\rho(X, F)$ . When the damping increases from 1% to 10%,  $\rho(X, F)$  increases to about 0.2 (average) and  $\rho(V, F)$  decreases to about 0.75 (average). As expected, the ensemble of scaled El Centro record generates a wide range of peak displacements and element level forces – in comparison,  $\rho(X, F)$  and  $\rho(V, F)$  statistics are remarkably consistent. We also note – see the following table – that

```

Correlation coefficient corr(X,V)
=====

```

Time Interval/Damping	1% damping	10% damping
[ 0 sec, 10 sec]:	0.0239	0.0408

```

=====

```



[10 sec, 15 sec]:	0.0475	0.0254
[ 0 sec, 15 sec]:	0.0318	0.0165

=====

displacements and velocities remain orthogonal, even for damping ratios significantly greater than zero.

---

**Part 2.** Linear System protected by Base Isolation plus Bang-Bang Control ( $U_{max} = 450$  kN)

In this simulation we apply an actuator force of  $U_{max} = 450$  kN, which is just below the design yield force (454 kN) of the base isolator.

**Displacements and Velocities.** The insert below shows min/max values of displacements at node 1 and corresponding min/max values of forces in the base isolator element.

Part A: 1% Critical Damping

=====

Ground Motion	Displacement at Node 1		Force in Element 1	
	Minimum (cm)	Maximum (cm)	Minimum (kN)	Maximum (kN)
1940 EL CENTRO S00E:	-6.28 cm	5.40 cm	-832 kN	716 kN
1940 EL CENTRO S90W:	-7.66 cm	5.77 cm	-1015 kN	764 kN
1934 EL CENTRO S00W:	-5.00 cm	2.01 cm	-663 kN	266 kN
1934 EL CENTRO S90W:	-2.09 cm	2.82 cm	-276.8 kN	373.5 kN
1979 EL CENTRO N50E:	-5.13 cm	3.68 cm	-679.7 kN	487.1 kN
1979 EL CENTRO N40W:	-8.25 cm	10.46 cm	-1093 kN	1386 kN
Average Value:	-5.73 cm	5.02 cm	-760 kN	655 kN

=====

Part B: 10% Critical Damping

=====

Ground Motion	Displacement at Node 1		Force in Element 1	
	Minimum (cm)	Maximum (cm)	Minimum (kN)	Maximum (kN)
1940 EL CENTRO S00E:	-5.61 cm	3.66 cm	-743 kN	485 kN
1940 EL CENTRO S90W:	-6.90 cm	5.00 cm	-914 kN	662 kN
1934 EL CENTRO S00W:	-4.77 cm	2.10 cm	-631 kN	278 kN
1934 EL CENTRO S90W:	-1.64 cm	2.56 cm	-217 kN	339 kN
1979 EL CENTRO N50E:	-4.04 cm	3.19 cm	-535 kN	422 kN

=====

1979 EL CENTRO N40W:	-5.30 cm	8.51 cm	-702 kN	1128 kN
Average Value:	-4.71 cm	4.17 cm	-623 kN	555 kN

Notice that peak values of system response are now less than one half of their counterpart values in Part 1. We conclude that the bang-bang control works!

**Phase Analysis.** Tables 8 and 9 show the scatter diagram data and phase analysis results for the linear time history response corresponding to base isolation plus bang-bang active control and an actuator force of 450 kN. The ground motion input is El Centro 1940 S00E. Tables 10 and 11 summarize the statistics of response on  $\rho(X, F)$  and  $\rho(V, F)$  values for responses generated by the ensemble of scaled El Centro ground motions.

The phase analysis predictions are based on simplified models of steady-state and free vibration displacement response. The time history responses in this case study are complicated by two factors: (1) ground motion inputs, and (2) significant actuator forces for active control. In comparing Tables 6 and 7 with 10 and 11, it is evident that in addition to reducing peak values of system response, the actuator forces affect the phase characteristics of response. During the time interval  $t = [0, 10]$  seconds, displacements are almost orthogonal to the direction of actuator force application. However, the direction of actuator force application is only marginally correlated to velocities (c.f., average value of 0.997 in Table 7, but only 0.553 in Table 11).

---

**Part 3.** Linear System protected by Base Isolation plus Velocity Control ( $U_{max} = 450$  kN)

The appeal of the proposed “velocity cancellation” control strategy is its simplicity – the algorithm simply works to oppose the direction of movement (i.e. cancel out velocities). In this section, we are interested in comparing performance of the “velocity control” and “sub-optimal bang-bang control” strategies.

**Displacements and Velocities.** The insert below shows min/max values of displacements at node 1 and corresponding min/max values of forces in the base isolator element.

Part A: 1% Critical Damping

Displacement at Node 1	Force in Element 1
------------------------	--------------------

Ground Motion	Minimum (cm)	Maximum (cm)	Minimum (kN)	Maximum (kN)
1940 EL CENTRO S00E:	-7.06 cm	6.22 cm	-936 kN	825 kN
1940 EL CENTRO S90W:	-7.45 cm	5.77 cm	-987 kN	765 kN
1934 EL CENTRO S00W:	-5.00 cm	2.01 cm	-663 kN	265 kN
1934 EL CENTRO S90W:	-2.35 cm	2.82 cm	-312 kN	373 kN
1979 EL CENTRO N50E:	-5.20 cm	4.13 cm	-689 kN	547 kN
1979 EL CENTRO N40W:	-8.44 cm	10.41 cm	-1119 kN	1380 kN
Average Value:	-5.91 cm	5.22 cm	-784 kN	692 kN

Part B: 10% Critical Damping

Ground Motion	Displacement at Node 1		Force in Element 1	
	Minimum (cm)	Maximum (cm)	Minimum (kN)	Maximum (kN)
1940 EL CENTRO S00E:	-6.32 cm	4.24 cm	-837 kN	562 kN
1940 EL CENTRO S90W:	-6.39 cm	5.00 cm	-846 kN	663 kN
1934 EL CENTRO S00W:	-4.16 cm	1.83 cm	-551 kN	243 kN
1934 EL CENTRO S90W:	-1.83 cm	2.56 cm	-242 kN	339 kN
1979 EL CENTRO N50E:	-4.25 cm	3.23 cm	-563 kN	427 kN
1979 EL CENTRO N40W:	-4.88 cm	8.38 cm	-647 kN	1110 kN
Average Value:	-4.63 cm	4.20 cm	-615 kN	557 kN

Clearly, peak values of displacement and element force are only marginally higher than in Part 2 (the sub-optimal bang-bang control simulation).

**Phase Analysis.** Tables 12 and 13 show the scatter diagram data and phase analysis results for the linear time history response corresponding to base isolation plus “velocity cancellation” control and an actuator force of 450 kN. The ground motion input is El Centro 1940 S00E. Tables 14 and 15 summarize the statistics of response on  $\rho(X, F)$  and  $\rho(V, F)$  values for responses generated by the ensemble of scaled El Centro ground motions.

By design, the “velocity cancellation” control strategy works perfectly in phase with the system velocity measurements at node 1. Accordingly,  $\rho(V, F) = 1$  across the ensemble of responses. For system responses at both 1% and 10% critical damping, average values of  $\rho(X, F)$  computed over the time interval  $[0, 10]$  seconds are -0.017 and 0.000, respectively. We can interpret these

results by first noting that the actuator works to increase the effective damping – extreme values of system response are reduced, accordingly. What is less evident, however, is that the control strategy accomplishes this task in a way that, on average, favors neither positive nor negative displacements.

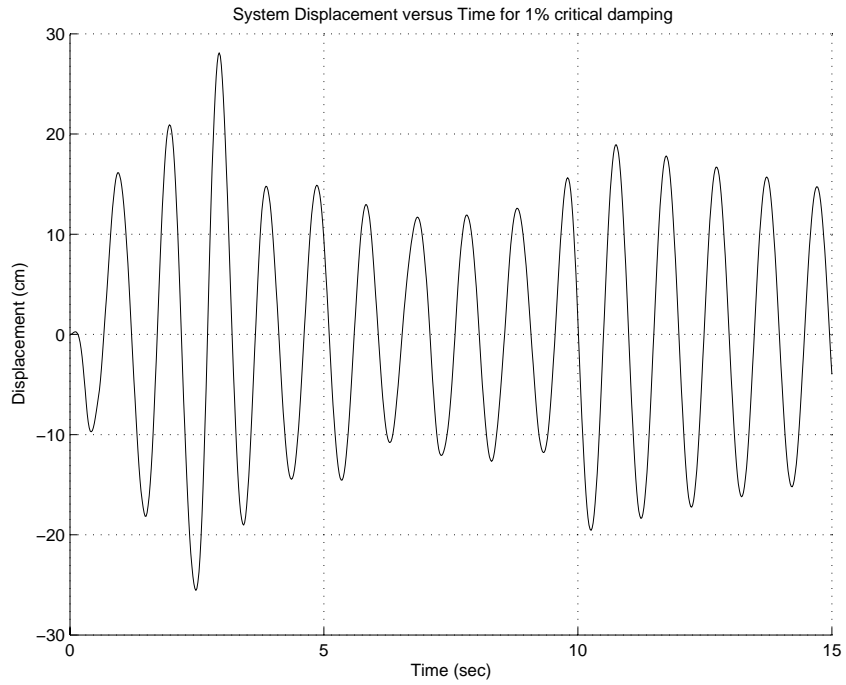


Figure 20: 2DOF System Displacement Response (cm) versus Time (sec) for 1940 El Centro S00E Ground Motion Record and 1% Critical Damping

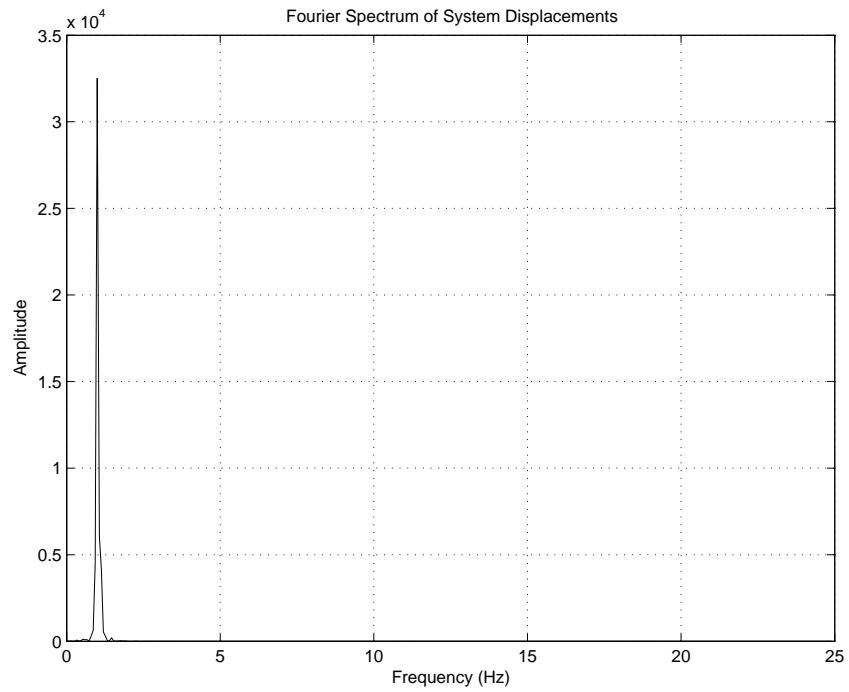


Figure 21: Fourier Transform for System Displacement Response due to 1940 El Centro S00E Ground Motion Record and 1% Critical Damping

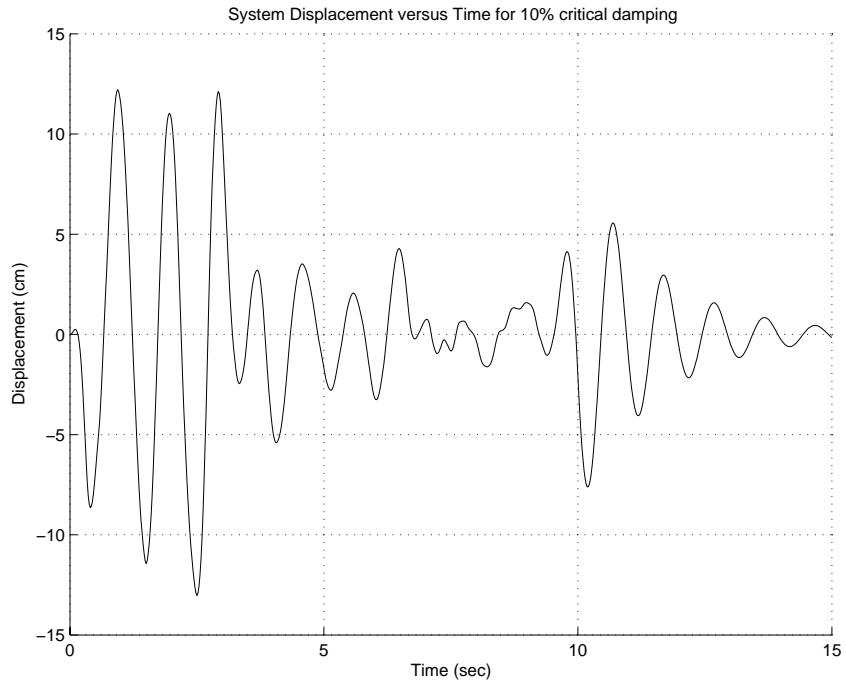


Figure 22: 2DOF System Displacement Response (cm) versus Time (sec) for 1940 El Centro S00E Ground Motion Record and 10% Critical Damping

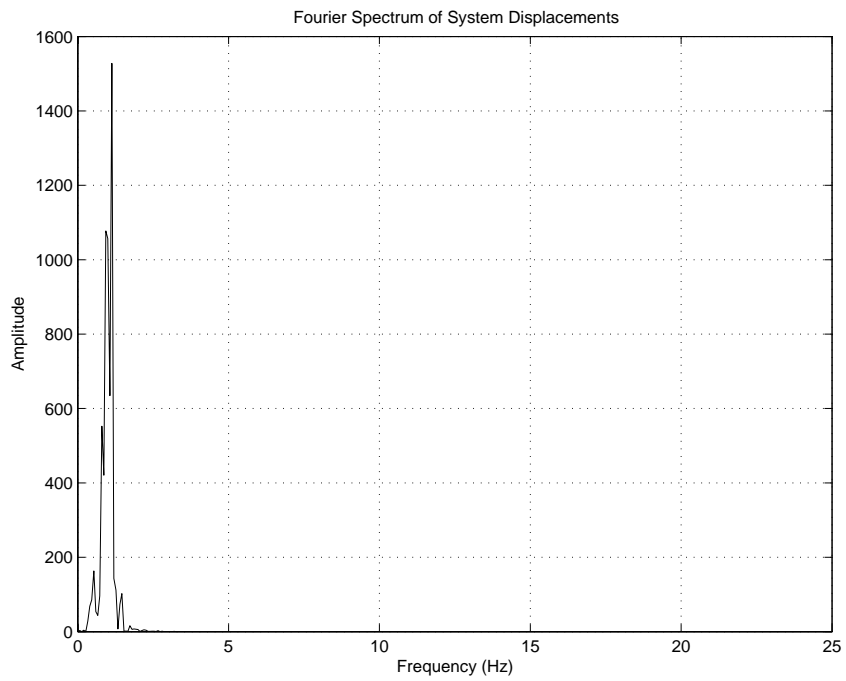


Figure 23: Fourier Transform for System Displacement Response due to 1940 El Centro S00E Ground Motion Record and 10% Critical Damping

Part A: 1% Critical Damping

```

=====
Period/Scatter Plot:  A(-1,1)      B(1,1)  C(1,-1)  D(-1,-1)  Total
=====
[ 0 sec, 10 sec]:    118        132     121      129       500
[10 sec, 15 sec]:     61         62      60       67       250
[ 0 sec, 15 sec]:    179        194     181      196       750
=====

```

```

=====
Range/Statistics:    average(X)  std(X)   std(F)   cov(X,F)  corr(X,F)
=====
[ 0 sec, 10 sec]:    0.3134 cm  0.9999      1      0.044     0.044
[10 sec, 15 sec]:   -0.1957 cm  1.002     1.002   0.03174   0.032
[ 0 sec, 15 sec]:    0.1439 cm   1         1       0.04     0.040
=====

```

Part B: 10% Critical Damping

```

=====
Period/Scatter Plot:  A(-1,1)      B(1,1)  C(1,-1)  D(-1,-1)  Total
=====
[ 0 sec, 10 sec]:     91        168     97      144       500
[10 sec, 15 sec]:     51         74      50       75       250
[ 0 sec, 15 sec]:    142        242    147      219       750
=====

```

```

=====
Range/Statistics:    average(X)  std(X)   std(F)   cov(X,F)  corr(X,F)
=====
[ 0 sec, 10 sec]:    0.1332 cm  0.9982     0.9994   0.2458   0.246
[10 sec, 15 sec]:   -0.2561 cm  1.002     1.002   0.1928   0.192
[ 0 sec, 15 sec]:    0.0037 cm  0.9993     0.9997   0.2284   0.229
=====

```

Table 4: Part 1. Linear Elastic System Response due to Base Isolation Alone ( $U_{max} = 0$  kN). “Displacement/actuator force” scatter diagram data and phase analysis generated by 1940 El Centro S00E Record. Part(a): 1% critical damping, Part(b): 10% critical damping.

Part A: 1% Critical Damping

```

=====
Period/Scatter Plot:  A(-1,1)      B(1,1)   C(1,-1)  D(-1,-1)  Total
=====
[ 0 sec, 10 sec]:    2         248      3         247        500
[10 sec, 15 sec]:    1         122      2         125        250
[ 0 sec, 15 sec]:    3         370      5         372        750
=====

```

```

=====
Range/Statistics:    average(V)  std(V)   std(F)   cov(V,F)  corr(V,F)
=====
[ 0 sec, 10 sec]:  0.011 cm/sec  1        1        0.98      0.980
[10 sec, 15 sec]: -1.001 cm/sec 1.002    1.002    0.9716    0.968
[ 0 sec, 15 sec]: -0.325 cm/sec 1        1        0.976     0.976
=====

```

Part B: 10% Critical Damping

```

=====
Period/Scatter Plot:  A         B         C         D         Total
=====
[ 0 sec, 10 sec]:    32        227       20        221        500
[10 sec, 15 sec]:    16        109       15        110        250
[ 0 sec, 15 sec]:    48        336       35        331        750
=====

```

```

=====
Range/Statistics:    average(V)  std(V)   std(F)   cov(V,F)  corr(V,F)
=====
[ 0 sec, 10 sec]:  -0.259 cm/sec  0.999    0.999    0.792     0.793
[10 sec, 15 sec]:  0.487 cm/sec  1.002    1.002    0.755     0.752
[ 0 sec, 15 sec]: -0.011 cm/sec  0.999    0.999    0.779     0.779
=====

```

Table 5: Part 1. Linear Elastic System Response due to Base Isolation Alone ( $U_{max} = 0$  kN). “Velocity/actuator force” scatter diagram data and phase analysis generated by 1940 El Centro S00E Record. Part(a): 1% critical damping, Part(b): 10% critical damping.



Part A: 1% Critical Damping

Ground Motion	Simulation		average(X)	std(X)	std(F)	Statistics	
	Interval					cov(X,F)	corr(X,F)
1940 EL CENTRO S00E:	[ 0, 10 ]	sec:	0.313 cm	0.999	1	0.044	0.044
	[ 10, 15 ]	sec:	-0.196 cm	1.002	1.002	0.03174	0.032
1940 EL CENTRO S90W:	[ 0, 10 ]	sec:	-0.132 cm	0.999	1	-0.00377	-0.004
	[ 10, 15 ]	sec:	0.060 cm	1.002	1.002	0.01619	0.016
1934 EL CENTRO S00W:	[ 0, 10 ]	sec:	-0.030 cm	0.999	0.9979	0.0497	0.049
	[ 10, 15 ]	sec:	0.075 cm	1.002	1.002	0.02403	0.024
1934 EL CENTRO S90W:	[ 0, 10 ]	sec:	-0.127 cm	0.999	0.9997	0.05638	0.056
	[ 10, 15 ]	sec:	0.072 cm	1.002	1.002	0.02384	0.024
1979 EL CENTRO N50E:	[ 0, 10 ]	sec:	-0.150 cm	0.998	0.9984	0.07686	0.077
	[ 10, 15 ]	sec:	0.075 cm	1.002	1.002	0.007968	0.008
1979 EL CENTRO N40W:	[ 0, 10 ]	sec:	-0.116 cm	0.999	0.9997	0.03962	0.040
	[ 10, 15 ]	sec:	0.039 cm	1.002	1.002	0.008289	0.008
=====							
Average Value:		[ 0, 10 ] sec:	-0.040 cm				0.043
		[ 10, 15 ] sec:	0.021 cm				0.019

Part B: 10% Critical Damping

Ground Motion	Simulation		average(X)	std(X)	std(F)	Statistics	
	Interval					cov(X,F)	corr(X,F)
1940 EL CENTRO S00E:	[ 0, 10 ]	sec:	0.133 cm	0.998	0.9994	0.2458	0.246
	[ 10, 15 ]	sec:	-0.256 cm	1.002	1.002	0.1928	0.192
1940 EL CENTRO S90W:	[ 0, 10 ]	sec:	-0.021 cm	0.999	0.9995	0.2844	0.285
	[ 10, 15 ]	sec:	0.037 cm	1.002	1.002	0.1928	0.192
1934 EL CENTRO S00W:	[ 0, 10 ]	sec:	-0.016 cm	0.998	0.999	0.1654	0.166
	[ 10, 15 ]	sec:	0.031 cm	1.002	1.002	0.1928	0.192
1934 EL CENTRO S90W:	[ 0, 10 ]	sec:	0.028 cm	0.998	1	0.172	0.172
	[ 10, 15 ]	sec:	-0.054 cm	1.002	1.002	0.1926	0.192
1979 EL CENTRO N50E:	[ 0, 10 ]	sec:	0.027 cm	0.997	0.9984	0.2553	0.257
	[ 10, 15 ]	sec:	-0.051 cm	1.002	1.002	0.1928	0.192
1979 EL CENTRO N40W:	[ 0, 10 ]	sec:	-0.039 cm	0.995	0.9965	0.2876	0.290
	[ 10, 15 ]	sec:	0.076 cm	1.002	1.002	0.2007	0.200
=====							
Average Value:		[ 0, 10 ] sec:	0.019 cm				0.236
		[ 10, 15 ] sec:	-0.036 cm				0.193

Table 6: Part 1. “Displacement/actuator force” scatter diagram data and phase analysis of time history responses for a linear system protected by base isolation alone ( $U_{max} = 0$  kN). Part(a): 1% critical damping, Part(b): 10% critical damping.

Part A: 1% Critical Damping

Ground Motion	Simulation			Statistics		
	Interval	average(V)	std(V)	std(F)	cov(V,F)	corr(V,F)
1940 EL CENTRO S00E:	[ 0, 10 ] sec:	0.010 cm/sec	1	1	0.98	0.980
	[ 10, 15 ] sec:	-1.001 cm/sec	1.002	1.002	0.9716	0.968
1940 EL CENTRO S90W:	[ 0, 10 ] sec:	-0.285 cm/sec	0.999	1	0.9679	0.968
	[ 10, 15 ] sec:	0.601 cm/sec	1.002	1.002	0.9798	0.976
1934 EL CENTRO S00W:	[ 0, 10 ] sec:	0.717 cm/sec	0.998	0.9979	0.9682	0.972
	[ 10, 15 ] sec:	-0.363 cm/sec	1.002	1.002	0.9799	0.976
1934 EL CENTRO S90W:	[ 0, 10 ] sec:	-0.109 cm/sec	0.999	0.9997	0.9912	0.992
	[ 10, 15 ] sec:	0.475 cm/sec	1.002	1.002	0.9798	0.976
1979 EL CENTRO N50E:	[ 0, 10 ] sec:	-0.246 cm/sec	0.999	0.9984	0.9691	0.972
	[ 10, 15 ] sec:	0.635 cm/sec	1.002	1.002	0.9798	0.976
1979 EL CENTRO N40W:	[ 0, 10 ] sec:	-0.444 cm/sec	0.999	0.9997	0.9832	0.984
	[ 10, 15 ] sec:	0.655 cm/sec	1.002	1.002	0.9798	0.976
=====						
Average Value:	[ 0, 10 ] sec:	-0.059 cm/sec				0.977
	[ 10, 15 ] sec:	0.167 cm/sec				0.975

Part B: 10% Critical Damping

Ground Motion	Simulation			Statistics		
	Interval	average(V)	std(V)	std(F)	cov(V,F)	corr(V,F)
1940 EL CENTRO S00E:	[ 0, 10 ] sec:	-0.259 cm/sec	0.9999	0.9994	0.792	0.793
	[ 10, 15 ] sec:	0.487 cm/sec	1.002	1.002	0.755	0.752
1940 EL CENTRO S90W:	[ 0, 10 ] sec:	-0.813 cm/sec	1	0.9995	0.728	0.729
	[ 10, 15 ] sec:	1.569 cm/sec	1.002	1.002	0.755	0.752
1934 EL CENTRO S00W:	[ 0, 10 ] sec:	0.001 cm/sec	0.9995	0.999	0.771	0.772
	[ 10, 15 ] sec:	-0.002 cm/sec	1.002	1.002	0.747	0.744
1934 EL CENTRO S90W:	[ 0, 10 ] sec:	-0.023 cm/sec	1	1	0.796	0.796
	[ 10, 15 ] sec:	0.042 cm/sec	1.002	1.002	0.747	0.744
1979 EL CENTRO N50E:	[ 0, 10 ] sec:	-0.277 cm/sec	0.999	0.9984	0.814	0.816
	[ 10, 15 ] sec:	0.532 cm/sec	1.002	1.002	0.755	0.752
1979 EL CENTRO N40W:	[ 0, 10 ] sec:	0.167 cm/sec	1	0.9965	0.732	0.735
	[ 10, 15 ] sec:	-0.318 cm/sec	1.002	1.002	0.746	0.744
=====						
Average Value:	[ 0, 10 ] sec:	-0.201 cm/sec				0.774
	[ 10, 15 ] sec:	0.385 cm/sec				0.748

Table 7: Part 1. “Velocity/actuator force” scatter diagram data and phase analysis of time history responses for a linear system protected by base isolation alone ( $U_{max} = 0$  kN). Part(a): 1% critical damping, Part(b): 10% critical damping.

Part A: 1% Critical Damping

```

=====
Period/Scatter Plot:  A(-1,1)      B(1,1)    C(1,-1)   D(-1,-1)   Total
=====
[ 0 sec, 10 sec]:    161        88        111        140        500
[10 sec, 15 sec]:     99        36         37         78        250
[ 0 sec, 15 sec]:    260       124        148        218        750
=====

```

```

=====
Range/Statistics:    average(X)  std(X)    std(F)    cov(X,F)   corr(X,F)
=====
[ 0 sec, 10 sec]:    0.048 cm   0.979      1          -0.08882   -0.090
[10 sec, 15 sec]:   -0.336 cm  0.9075    0.9988     -0.0302    -0.033
[ 0 sec, 15 sec]:   -0.079 cm  0.9608    0.9997     -0.07334   -0.076
=====

```

Part B: 10% Critical Damping

```

=====
Period/Scatter Plot:  A          B          C          D          Total
=====
[ 0 sec, 10 sec]:    104        141        133        122        500
[10 sec, 15 sec]:     74         53         51         72        250
[ 0 sec, 15 sec]:    178        194        184        194        750
=====

```

```

=====
Range/Statistics:    average(X)  std(X)    std(F)    cov(X,F)   corr(X,F)
=====
[ 0 sec, 10 sec]:    0.098 cm   0.9954    0.9998     0.05392    0.054
[10 sec, 15 sec]:   -0.114 cm  0.9849    1.002     -0.01311   -0.013
[ 0 sec, 15 sec]:    0.027 cm   1          1          0.02935    0.029
=====

```

Table 8: Part 2. Linear Elastic System Response due to Base Isolation plus Bang-Bang Control ( $U_{max} = 450$  kN). “Displacement/actuator force” scatter diagram data and phase analysis generated by 1940 El Centro S00E Record. Part(a): 1% critical damping, Part(b): 10% critical damping.

Part A: 1% Critical Damping

```

=====
Period/Scatter Plot:  A(-1,1)      B(1,1)      C(1,-1)      D(-1,-1)      Total
=====
[ 0 sec, 10 sec]:    57         192         52         199         500
[10 sec, 15 sec]:    0         135         6          109         250
[ 0 sec, 15 sec]:    57         327         58         308         750
=====

```

```

=====
Range/Statistics:    average(V)    std(V)      std(F)      cov(V,F)     corr(V,F)
=====
[ 0 sec, 10 sec]:  -0.140 cm/sec  0.9997      1           0.5639      0.564
[10 sec, 15 sec]:  0.283 cm/sec   1           0.9988     0.8308      0.831
[ 0 sec, 15 sec]:  0.000 cm/sec   1           0.9997     0.6533      0.653
=====

```

Part B: 10% Critical Damping

```

=====
Period/Scatter Plot:  A          B          C          D          Total
=====
[ 0 sec, 10 sec]:    38         207         41         214         500
[10 sec, 15 sec]:    0         127         9          114         250
[ 0 sec, 15 sec]:    38         334         50         328         750
=====

```

```

=====
Range/Statistics:    average(V)    std(V)      std(F)      cov(V,F)     corr(V,F)
=====
[ 0 sec, 10 sec]:  -0.133 cm/sec   1           0.9998     0.6838      0.684
[10 sec, 15 sec]:  0.266 cm/sec   1.001      1.002     0.939       0.936
[ 0 sec, 15 sec]:  -0.000 cm/sec   0.999      1           0.7681      0.768
=====

```

Table 9: Part 2. Linear Elastic System Response due to Base Isolation plus Bang-Bang Control ( $U_{max} = 450$  kN). “Velocity/actuator force” scatter diagram data and phase analysis generated by 1940 El Centro S00E Record. Part(a): 1% critical damping, Part(b): 10% critical damping.

Part A: 1% Critical Damping

Ground Motion	Simulation		average(X)	std(X)	std(F)	Statistics	
	Interval					cov(X,F)	corr(X,F)
1940 EL CENTRO S00E:	[ 0, 10 ]	sec:	0.048 cm	0.979	1	-0.08882	-0.090
	[ 10, 15 ]	sec:	-0.336 cm	0.9075	0.9988	-0.0302	-0.033
1940 EL CENTRO S90W:	[ 0, 10 ]	sec:	-0.005 cm	0.9974	0.9998	0.02144	0.021
	[ 10, 15 ]	sec:	0.237 cm	0.9379	1.002	-0.0879	-0.094
1934 EL CENTRO S00W:	[ 0, 10 ]	sec:	0.088 cm	0.9746	0.9996	-0.04573	-0.047
	[ 10, 15 ]	sec:	-0.010 cm	1.002	1.002	-0.02403	-0.024
1934 EL CENTRO S90W:	[ 0, 10 ]	sec:	0.120 cm	0.9968	0.9999	-0.09472	-0.095
	[ 10, 15 ]	sec:	-0.306 cm	0.9596	1.001	-0.04235	-0.044
1979 EL CENTRO N50E:	[ 0, 10 ]	sec:	0.060 cm	0.9988	0.9998	-0.05104	-0.051
	[ 10, 15 ]	sec:	-0.022 cm	0.9981	1.002	-0.007325	-0.007
1979 EL CENTRO N40W:	[ 0, 10 ]	sec:	-0.177 cm	0.9718	0.9986	-0.05973	-0.061
	[ 10, 15 ]	sec:	0.056 cm	0.9784	1.002	-0.01259	-0.013
=====							
Average Value:		[ 0, 10 ]	sec:	0.134 cm			-0.054
		[ 10, 15 ]	sec:	-0.063 cm			-0.036

Part B: 10% Critical Damping

Ground Motion	Simulation		average(X)	std(X)	std(F)	Statistics	
	Interval					cov(X,F)	corr(X,F)
1940 EL CENTRO S00E:	[ 0, 10 ]	sec:	0.098 cm	0.9954	0.9998	0.05392	0.054
	[ 10, 15 ]	sec:	-0.114 cm	0.9849	1.002	-0.01311	-0.013
1940 EL CENTRO S90W:	[ 0, 10 ]	sec:	0.005 cm	0.9884	0.9998	0.167	0.169
	[ 10, 15 ]	sec:	0.003 cm	0.9927	1.001	-0.02043	-0.020
1934 EL CENTRO S00W:	[ 0, 10 ]	sec:	-0.029 cm	0.9990	1	0.06382	0.064
	[ 10, 15 ]	sec:	0.017 cm	0.9974	1.002	0.01529	0.015
1934 EL CENTRO S90W:	[ 0, 10 ]	sec:	0.086 cm	1	1	0.06406	0.064
	[ 10, 15 ]	sec:	-0.117 cm	0.9891	1.002	0.0241	0.024
1979 EL CENTRO N50E:	[ 0, 10 ]	sec:	0.014 cm	0.9851	1	0.09669	0.098
	[ 10, 15 ]	sec:	-0.012 cm	1	1.002	-8.917e-19	-0.000
1979 EL CENTRO N40W:	[ 0, 10 ]	sec:	-0.019 cm	1	1	0.168	0.168
	[ 10, 15 ]	sec:	-0.001 cm	1.001	1.002	0.03187	0.031
=====							
Average Value:		[ 0, 10 ]	sec:	0.025 cm			0.101
		[ 10, 15 ]	sec:	-0.037 cm			0.006

Table 10: Part 2. “Displacement/actuator force” scatter diagram data and phase analysis of time history responses for a linear system protected by isolation plus bang-bang active control ( $U_{max} = 450$  kN). Part(a): 1% critical damping, Part(b): 10% critical damping.

Part A: 1% Critical Damping

Ground Motion	Simulation		average(V)	std(V)	std(F)	Statistics	
	Interval					cov(V,F)	corr(V,F)
1940 EL CENTRO S00E:	[ 0, 10 ]	sec:	-0.140 cm/sec	0.9997	1	0.5639	0.564
	[ 10, 15 ]	sec:	0.283 cm/sec	1	0.9988	0.8308	0.831
1940 EL CENTRO S90W:	[ 0, 10 ]	sec:	-0.640 cm/sec	0.9997	0.9998	0.4995	0.500
	[ 10, 15 ]	sec:	1.296 cm/sec	1.002	1.002	0.8432	0.840
1934 EL CENTRO S00W:	[ 0, 10 ]	sec:	-0.042 cm/sec	0.999	0.9996	0.5128	0.513
	[ 10, 15 ]	sec:	0.077 cm/sec	1.001	1.002	0.9234	0.920
1934 EL CENTRO S90W:	[ 0, 10 ]	sec:	0.027 cm/sec	1	0.9999	0.4961	0.496
	[ 10, 15 ]	sec:	-0.035 cm/sec	1	1.001	0.8403	0.840
1979 EL CENTRO N50E:	[ 0, 10 ]	sec:	-0.050 cm/sec	0.999	0.9998	0.5991	0.599
	[ 10, 15 ]	sec:	0.109 cm/sec	1.002	1.002	0.9959	0.992
1979 EL CENTRO N40W:	[ 0, 10 ]	sec:	0.046 cm/sec	0.999	0.9986	0.6457	0.647
	[ 10, 15 ]	sec:	-0.061 cm/sec	1.002	1.002	0.9637	0.960
=====							
Average Value:	[ 0, 10 ]	sec:	-0.133 cm/sec				0.553
	[ 10, 15 ]	sec:	0.278 cm/sec				0.897

Part B: 10% Critical Damping

Ground Motion	Simulation		average(V)	std(V)	std(F)	Statistics	
	Interval					cov(V,F)	corr(V,F)
1940 EL CENTRO S00E:	[ 0, 10 ]	sec:	-0.133 cm/sec	1	0.9998	0.6838	0.684
	[ 10, 15 ]	sec:	0.266 cm/sec	1.001	1.002	0.939	0.936
1940 EL CENTRO S90W:	[ 0, 10 ]	sec:	-0.526 cm/sec	0.9996	0.9998	0.5526	0.553
	[ 10, 15 ]	sec:	1.045 cm/sec	1.002	1.001	0.947	0.944
1934 EL CENTRO S00W:	[ 0, 10 ]	sec:	0.002 cm/sec	0.9998	1	0.6001	0.600
	[ 10, 15 ]	sec:	0.006 cm/sec	1.002	1.002	0.9798	0.976
1934 EL CENTRO S90W:	[ 0, 10 ]	sec:	0.018 cm/sec	1	1	0.532	0.532
	[ 10, 15 ]	sec:	-0.035 cm/sec	1.002	1.002	0.9558	0.952
1979 EL CENTRO N50E:	[ 0, 10 ]	sec:	-0.024 cm/sec	0.9997	1	0.6439	0.644
	[ 10, 15 ]	sec:	0.035 cm/sec	1.002	1.002	0.988	0.984
1979 EL CENTRO N40W:	[ 0, 10 ]	sec:	0.010 cm/sec	0.993	1	0.575	0.579
	[ 10, 15 ]	sec:	-0.032 cm/sec	1.002	1.002	0.9798	0.976
=====							
Average Value:	[ 0, 10 ]	sec:	-0.109 cm/sec				0.599
	[ 10, 15 ]	sec:	0.213 cm/sec				0.961

Table 11: Part 2. “Velocity/actuator force” scatter diagram data and phase analysis of time history responses for a linear system protected by base isolation plus bang-bang control ( $U_{max} = 450$  kN). Part(a): 1% critical damping, Part(b): 10% critical damping.

Part A: 1% Critical Damping

```

=====
Period/Scatter Plot:  A(-1,1)      B(1,1)  C(1,-1)  D(-1,-1)  Total
=====
[ 0 sec, 10 sec]:    115       130     150      105       500
[10 sec, 15 sec]:     81       49      49       71       250
[ 0 sec, 15 sec]:    196       179     199      176       750
=====

```

```

=====
Range/Statistics:    average(X)  std(X)   std(F)   cov(X,F)  corr(X,F)
=====
[ 0 sec, 10 sec]:    0.100 cm  0.9928   0.9998   -0.0576   -0.058
[10 sec, 15 sec]:   -0.200 cm 0.9747   1.001    -0.03084  -0.032
[ 0 sec, 15 sec]:    0.000 cm   1        1        -0.05333  -0.053
=====

```

Part B: 10% Critical Damping

```

=====
Period/Scatter Plot:  A         B         C         D         Total
=====
[ 0 sec, 10 sec]:    115       124       149       112       500
[10 sec, 15 sec]:     74       54        54        68       250
[ 0 sec, 15 sec]:    189       178       203       180       750
=====

```

```

=====
Range/Statistics:    average(X)  std(X)   std(F)   cov(X,F)  corr(X,F)
=====
[ 0 sec, 10 sec]:    0.188 cm  0.9958   0.999    -0.05195  -0.052
[10 sec, 15 sec]:   -0.172 cm 0.9916   1.002    -0.01259  -0.013
[ 0 sec, 15 sec]:    0.068 cm  0.9999   0.9998   -0.04238  -0.042
=====

```

Table 12: Part 3. “Displacement/actuator force” scatter diagram data and phase analysis of time history responses for a linear system protected by isolation plus velocity control ( $U_{max} = 450$  kN). Part(a): 1% critical damping, Part(b): 10% critical damping.

Part A: 1% Critical Damping

```

=====
Period/Scatter Plot:  A(-1,1)      B(1,1)  C(1,-1)  D(-1,-1)  Total
=====
[ 0 sec, 10 sec]:    0          245      0         255        500
[10 sec, 15 sec]:   19          111     23         97         250
[ 0 sec, 15 sec]:   19          356     23        352        750
=====

```

```

=====
Range/Statistics:    average(V)  std(V)   std(F)   cov(V,F)  corr(V,F)
=====
[ 0 sec, 10 sec]:  -0.134 cm/sec  0.9998  0.9998   0.9996    1
[10 sec, 15 sec]:  0.216 cm/sec  1.001   1.001    1.002    1
[ 0 sec, 15 sec]: -0.018 cm/sec    1       1         1         1
=====

```

Part B: 10% Critical Damping

```

=====
Period/Scatter Plot:  A          B          C          D          Total
=====
[ 0 sec, 10 sec]:    0          239         0          261         500
[10 sec, 15 sec]:    0          128         7          115         250
[ 0 sec, 15 sec]:    0          367         7          376         750
=====

```

```

=====
Range/Statistics:    average(V)  std(V)   std(F)   cov(V,F)  corr(V,F)
=====
[ 0 sec, 10 sec]:  -0.136 cm/sec  0.999   0.999   0.9981    1
[10 sec, 15 sec]:  0.262 cm/sec  1.002   1.002   1.003    1
[ 0 sec, 15 sec]: -0.004 cm/sec  0.999   0.999   0.9995    1
=====

```

Table 13: Part 3. “Velocity/actuator force” scatter diagram data and phase analysis for a linear system protected by base isolation plus velocity control ( $U_{max} = 450$  kN). Ground motion is 1940 El Centro S00E Record. Part(a): 1% critical damping, Part(b): 10% critical damping.



Part A: 1% Critical Damping

Ground Motion	Simulation		average(X)	std(X)	std(F)	Statistics	
	Interval					cov(X,F)	corr(X,F)
1940 EL CENTRO S00E:	[ 0, 10 ]	sec:	0.100 cm	0.9928	0.999	-0.0576	-0.058
	[ 10, 15 ]	sec:	-0.200 cm	0.9747	1.001	-0.03084	-0.032
1940 EL CENTRO S90W:	[ 0, 10 ]	sec:	-0.006 cm	0.9844	0.999	0.04282	0.043
	[ 10, 15 ]	sec:	0.093 cm	0.9818	1.002	-0.08996	-0.091
1934 EL CENTRO S00W:	[ 0, 10 ]	sec:	-0.052 cm	0.9958	0.999	-0.0411	-0.041
	[ 10, 15 ]	sec:	0.017 cm	0.9938	1.002	-0.0171	-0.017
1934 EL CENTRO S90W:	[ 0, 10 ]	sec:	0.063 cm	0.9999	1.000	0.024	0.024
	[ 10, 15 ]	sec:	-0.236 cm	0.9818	1.001	-0.0096	-0.010
1979 EL CENTRO N50E:	[ 0, 10 ]	sec:	-0.022 cm	0.9998	1.000	-0.0362	-0.036
	[ 10, 15 ]	sec:	-0.071 cm	0.9801	1.002	-0.02076	-0.021
1979 EL CENTRO N40W:	[ 0, 10 ]	sec:	-0.354 cm	0.9612	0.994	-0.0313	-0.033
	[ 10, 15 ]	sec:	0.069 cm	0.9904	1.002	0.0024	0.002
=====							
Average Value:	[ 0, 10 ]	sec:	-0.045 cm				-0.017
	[ 10, 15 ]	sec:	-0.054 cm				-0.028

Part B: 10% Critical Damping

Ground Motion	Simulation		average(X)	std(X)	std(F)	Statistics	
	Interval					cov(X,F)	corr(X,F)
1940 EL CENTRO S00E:	[ 0, 10 ]	sec:	0.188 cm	0.9958	0.999	-0.05195	-0.052
	[ 10, 15 ]	sec:	-0.172 cm	0.9916	1.002	-0.01259	-0.013
1940 EL CENTRO S90W:	[ 0, 10 ]	sec:	0.096 cm	0.9514	0.999	0.02432	0.025
	[ 10, 15 ]	sec:	-0.111 cm	1.002	1.000	-0.02545	-0.025
1934 EL CENTRO S00W:	[ 0, 10 ]	sec:	0.552 cm	0.9912	1.000	-0.02347	-0.024
	[ 10, 15 ]	sec:	-0.591 cm	1.002	1.002	0.02403	0.024
1934 EL CENTRO S90W:	[ 0, 10 ]	sec:	0.172 cm	0.995	0.999	-0.00825	-0.008
	[ 10, 15 ]	sec:	-0.180 cm	0.978	1.002	-0.01889	-0.019
1979 EL CENTRO N50E:	[ 0, 10 ]	sec:	0.078 cm	0.9998	0.999	-0.0076	-0.008
	[ 10, 15 ]	sec:	-0.018 cm	1.001	1.002	0.0000	0.000
1979 EL CENTRO N40W:	[ 0, 10 ]	sec:	-0.098 cm	0.9737	0.999	0.06238	0.064
	[ 10, 15 ]	sec:	0.006 cm	1.002	1.002	0.03213	0.032
=====							
Average Value:	[ 0, 10 ]	sec:	0.165 cm				-0.000
	[ 10, 15 ]	sec:	-0.173 cm				-0.000

Table 14: Part 3. “Displacement/actuator force” scatter diagram data and phase analysis of time history responses for a linear system protected by isolation plus velocity control ( $U_{max} = 450$  kN). Part(a): 1% critical damping, Part(b): 10% critical damping.

Part A: 1% Critical Damping

Ground Motion	Simulation		average(V)	std(V)	std(F)	Statistics	
	Interval					cov(V,F)	corr(V,F)
1940 EL CENTRO S00E:	[ 0, 10 ]	sec:	-0.134 cm/sec	0.999	0.9998	0.9996	1
	[ 10, 15 ]	sec:	0.216 cm/sec	1.001	1.001	1.002	1
1940 EL CENTRO S90W:	[ 0, 10 ]	sec:	-0.639 cm/sec	0.999	0.9999	0.9997	1
	[ 10, 15 ]	sec:	1.239 cm/sec	1.002	1.002	1.004	1
1934 EL CENTRO S00W:	[ 0, 10 ]	sec:	-0.053 cm/sec	0.999	0.9999	0.9999	1
	[ 10, 15 ]	sec:	0.124 cm/sec	1.002	1.002	1.004	1
1934 EL CENTRO S90W:	[ 0, 10 ]	sec:	-0.035 cm/sec	1	1	1	1
	[ 10, 15 ]	sec:	0.034 cm/sec	1.001	1.001	1.003	1
1979 EL CENTRO N50E:	[ 0, 10 ]	sec:	-0.087 cm/sec	1	1	0.999	1
	[ 10, 15 ]	sec:	0.182 cm/sec	1.002	1.002	1.004	1
1979 EL CENTRO N40W:	[ 0, 10 ]	sec:	0.061 cm/sec	0.9946	0.9946	0.9892	1
	[ 10, 15 ]	sec:	-0.101 cm/sec	1.002	1.002	1.004	1
Average Value:		[ 0, 10 ] sec:	-0.148 cm/sec				1.000
		[ 10, 15 ] sec:	0.282 cm/sec				1.000

Part B: 10% Critical Damping

Ground Motion	Simulation		average(V)	std(V)	std(F)	Statistics	
	Interval					cov(V,F)	corr(V,F)
1940 EL CENTRO S00E:	[ 0, 10 ]	sec:	-0.136 cm/sec	0.999	0.999	0.9981	1
	[ 10, 15 ]	sec:	0.262 cm/sec	1.002	1.002	1.003	1
1940 EL CENTRO S90W:	[ 0, 10 ]	sec:	-0.545 cm/sec	0.999	0.999	0.998	1
	[ 10, 15 ]	sec:	1.092 cm/sec	1.000	1.000	1.001	1
1934 EL CENTRO S00W:	[ 0, 10 ]	sec:	-0.545 cm/sec	0.999	0.999	0.998	1
	[ 10, 15 ]	sec:	1.092 cm/sec	1	1	1.001	1
1934 EL CENTRO S90W:	[ 0, 10 ]	sec:	-31.33 cm/sec	0.9994	0.999	0.999	1
	[ 10, 15 ]	sec:	30.41 cm/sec	1.002	1.002	1.003	1
1979 EL CENTRO N50E:	[ 0, 10 ]	sec:	-0.036 cm/sec	0.999	0.9998	0.999	1
	[ 10, 15 ]	sec:	0.069 cm/sec	1.002	1.002	1.004	1
1979 EL CENTRO N40W:	[ 0, 10 ]	sec:	0.030 cm/sec	0.9996	0.9996	0.9992	1
	[ 10, 15 ]	sec:	-0.058 cm/sec	1.002	1.002	1.004	1
Average Value:		[ 0, 10 ] sec:	-5.42 cm/sec				1.000
		[ 10, 15 ] sec:	5.47 cm/sec				1.000

Table 15: Part 3. “Velocity/actuator force” scatter diagram data and phase analysis of time history responses for a linear system protected by base isolation plus velocity control ( $U_{max} = 450$  kN). Part(a): 1% critical damping, Part(b): 10% critical damping.

## 4.5 Case Study 2. Nonlinear Time-History Response

The second case study examines nonlinear time-history behavior generated by the ensemble of El Centro records described in Tables 2 and 3. The analyses are divided into three parts: (1) Nonlinear system response due to base isolation alone (peak values from this study act as a benchmark for measuring improvements due to control), (2) Nonlinear system response due to base isolation plus constant stiffness bang-bang control, and (3) Nonlinear system response due to base isolation plus velocity cancellation control. Performance metrics include peak values of displacement and velocity, and statistics of phase analysis.

A distinguishing feature of this case study is evolution of nonlinear time-history displacements which may no longer be orthogonal to velocities. phase angle predictions cannot be expected to correlate well with the statistics of simulation. For this class of problems, however, it is important to keep in mind that nonlinear behavior is confined to the isolation devices. Thus, while nonlinearities exist (and, in fact, are relied upon to protect the structure and its contents), their influence on the overall system-level behavior could be minor. To this end, Sebastianelli and Austin [20, 21] have shown via numerical experiment that sub-optimal bang-bang control can be effective even in situations of localized nonlinearities in the isolation devices. Hence, the primary purpose of this experiment is to see if these benefits also hold for “velocity cancellation” control in a nonlinear setting.

The nonlinear analyses assume an isolator yield force = 454 kN. Simulations are computed for 1% and 10% critical damping. All remaining simulation control parameters are as previously described.

---

### Part 1. Base Isolation Alone ( $U_{max} = 0$ kN)

**Displacements and Velocities.** Figures 24 and 25, and 26 and 27 show the nonlinear displacement response (cm) versus time (sec) and corresponding Fourier Transform for system responses at 1% and 10% critical damping, generated by 1940 El Centro S00E Ground Motion Record. Unlike linear system behavior, nonlinear behavior is characterized by permanent plastic deformations. In the Fourier Transform analyses, the latter is represented by large coefficient values for frequencies approaching 0 Hz. The insert below shows min/max values of displacements at node 1 and

corresponding min/max values of forces in the base isolator element.

Part A: 1% Critical Damping

Ground Motion	Displacement at Node 1		Force in Element 1	
	Minimum (cm)	Maximum (cm)	Minimum (kN)	Maximum (kN)
1940 EL CENTRO S00E:	-14.52 cm	10.10 cm	-524 kN	523 kN
1940 EL CENTRO S90W:	-9.74 cm	11.80 cm	-523 kN	524 kN
1934 EL CENTRO S00W:	-12.86 cm	5.17 cm	-524 kN	523 kN
1934 EL CENTRO S90W:	-2.53 cm	13.05 cm	-522 kN	524 kN
1979 EL CENTRO N50E:	-48.20 cm	5.70 cm	-528 kN	523 kN
1979 EL CENTRO N40W:	-10.20 cm	50.50 cm	-523 kN	529 kN
Average Value:	-16.34 cm	16.05 cm	-524 kN	524 kN

Part B: 10% Critical Damping

Ground Motion	Displacement at Node 1		Force in Element 1	
	Minimum (cm)	Maximum (cm)	Minimum (kN)	Maximum (kN)
1940 EL CENTRO S00E:	-15.07 cm	8.15 cm	-524 kN	523 kN
1940 EL CENTRO S90W:	-10.72 cm	8.91 cm	-523 kN	523 kN
1934 EL CENTRO S00W:	-9.56 cm	4.58 cm	-523 kN	523 kN
1934 EL CENTRO S90W:	-2.24 cm	8.80 cm	-522 kN	523 kN
1979 EL CENTRO N50E:	-30.25 cm	4.91 cm	-526 kN	523 kN
1979 EL CENTRO N40W:	-8.71 cm	32.30 cm	-523 kN	526 kN
Average Value:	-12.75 cm	11.27 cm	-523 kN	523 kN

At 1% critical damping, average min/max values of nonlinear displacement are virtually identical to their linear counterparts. At 10% critical damping, average min/max values of nonlinear as slightly higher than those for linear system behavior. In both cases, the min/max nonlinear behavior forces imparted to the superstructure are significantly smaller than those occurring for linear behavior (i.e., the base isolation system works!).

**Phase Analysis.** Tables 16 and 17 show the scatter diagram data and phase analysis results for the nonlinear time-history response generated by the El Centro 1940 S00E ground motion record. Tables 18 and 19 summarize the statistics of response and  $\rho(X, F)$  and  $\rho(V, F)$  values for the ensemble of El Centro Ground motion inputs.

At 1% critical damping, average values for  $\rho(X, F)$  and  $\rho(V, F)$  are close to 0.07 and 0.90 respectively (the same quantities in Case Study 1 are 0.04 and 0.97, respectively). This observation can be explained, in part, through the symbolic analysis of sub-optimal bang-bang control, where the velocity coefficients in the control algorithm are inversely proportional to the damping. For low levels of damping, the velocity coefficients completely dominate the control strategy and displacements play a relatively minor role. In their complementary role, the numerical experiments suggest that even if part of the system displacements is a permanent offset, bang-bang control in a nonlinear setting can still work well.

When critical damping is increased from 1% to 10%, average values for  $\rho(X, F)$  and  $\rho(V, F)$  move to 0.416 and 0.481. Under these circumstances, bang-bang control computes an actuator force direction that is neither in phase with velocities nor displacements.

---

**Part 2.** Base Isolation + Bang-Bang Control ( $U_{max} = 450$  kN)

**Displacements and Velocities.** The insert below shows min/max values of displacements at node 1 and corresponding min/max values of forces in the base isolator element.

Part A: 1% Critical Damping

Ground Motion	Displacement at Node 1		Force in Element 1	
	Minimum (cm)	Maximum (cm)	Minimum (kN)	Maximum (kN)
1940 EL CENTRO S00E:	-6.52 cm	1.80 cm	-523 kN	523 kN
1940 EL CENTRO S90W:	-7.14 cm	5.97 cm	-523 kN	523 kN
1934 EL CENTRO S00W:	-5.13 cm	2.00 cm	-523 kN	265 kN
1934 EL CENTRO S90W:	-2.09 cm	2.82 cm	-277 kN	373 kN
1979 EL CENTRO N50E:	-5.62 cm	2.07 cm	-523 kN	496 kN
1979 EL CENTRO N40W:	-1.90 cm	15.33 cm	-521 kN	524 kN
Average Value:	-3.64 cm	4.99 cm	-481 kN	450 kN

Part B: 10% Critical Damping

Ground Motion	Displacement at Node 1		Force in Element 1	
	Minimum (cm)	Maximum (cm)	Minimum (kN)	Maximum (kN)
1940 EL CENTRO S00E:	-5.77 cm	1.99 cm	-523 kN	504 kN
1940 EL CENTRO S90W:	-6.48 cm	5.11 cm	-523 kN	523 kN
1934 EL CENTRO S00W:	-4.89 cm	1.83 cm	-523 kN	243 kN

1934 EL CENTRO S90W:	-1.64 cm	2.56 cm	-217 kN	339 kN
1979 EL CENTRO N50E:	-4.04 cm	3.23 cm	-523 kN	440 kN
1979 EL CENTRO N40W:	-1.62 cm	11.04 cm	-522 kN	524 kN
=====				
Average Value:	-4.07 cm	4.29 cm	-471 kN	428 kN
=====				

At 1% critical damping, sub-optimal bang-bang control decreases the range of average min/max displacements from  $[-16.34, 16.05]$  cm to  $[-3.64, 4.92]$  cm. At 10% critical damping, average min/max displacements decrease from  $[-12.75, 11.27]$  cm to  $[-4.07, 4.29]$  cm with the addition of sub-optimal bang-bang control. Again we observe that sub-optimal bang-bang control is an effective means for reducing peak displacements.

**Phase Analysis.** Tables 20 and 21 show the scatter diagram data and phase analysis results for the linear time history response corresponding to base isolation plus bang-bang active control and an actuator force of 450 kN. The ground motion input is El Centro 1940 S00E. Tables 22 and 23 summarize the statistics of response on  $\rho(X, F)$  and  $\rho(V, F)$  values for responses generated by the ensemble of scaled El Centro ground motions.

At 1% critical damping,  $\rho(X, F) \approx 0$ , indicating that nonlinear displacements are almost orthogonal to the direction of actuator force application. This observation is not predicted by the phase analysis formulation. At the same time,  $\rho(V, F)$  values cover the range  $[0.42, 0.84]$ , indicating that the actuator works in phase with velocities, but not strongly in phase. When critical damping increases to 10%, the average value of  $\rho(X, F)$  increases to 0.125 and the range of  $\rho(V, F)$  values spreads to  $[0.20, 0.98]$ . It is probably coincidence that the average values of  $\rho(V, F)$  at 1% and 10% critical damping are almost the same.

---

### Part 3. Base Isolation + Velocity Cancellation Control ( $U_{max} = 450$ kN)

The “velocity cancellation” control strategy forces the actuator to work in lockstep with nodal velocities.

**Displacements and Velocities.** The insert below shows min/max values of displacements at node 1 and corresponding min/max values of forces in the base isolator element.

Part A: 1% Critical Damping

Ground Motion	Displacement at Node 1		Force in Element 1	
	Minimum (cm)	Maximum (cm)	Minimum (kN)	Maximum (kN)
1940 EL CENTRO S00E:	-7.47 cm	2.57 cm	-523 kN	523 kN
1940 EL CENTRO S90W:	-7.12 cm	5.97 cm	-523 kN	523 kN
1934 EL CENTRO S00W:	-5.13 cm	2.01 cm	-523 kN	266 kN
1934 EL CENTRO S90W:	-2.35 cm	2.82 cm	-311 kN	373 kN
1979 EL CENTRO N50E:	-5.82 cm	1.74 cm	-523 kN	436 kN
1979 EL CENTRO N40W:	-2.27 cm	15.51 cm	-521 kN	524 kN
Average Value:	-5.02 cm	5.10 cm	-487 kN	440 kN

Part B: 10% Critical Damping

Ground Motion	Displacement at Node 1		Force in Element 1	
	Minimum (cm)	Maximum (cm)	Minimum (kN)	Maximum (kN)
1940 EL CENTRO S00E:	-6.61 cm	1.22 cm	-523 kN	515 kN
1940 EL CENTRO S90W:	-6.38 cm	5.10 cm	-523 kN	523 kN
1934 EL CENTRO S00W:	-4.17 cm	1.84 cm	-523 kN	243 kN
1934 EL CENTRO S90W:	-1.83 cm	2.56 cm	-243 kN	339 kN
1979 EL CENTRO N50E:	-4.26 cm	3.43 cm	-523 kN	496 kN
1979 EL CENTRO N40W:	-1.85 cm	10.82 cm	-480 kN	524 kN
Average Value:	-4.18 cm	4.16 cm	-469 kN	440 kN

In a side-by-side comparison of min/max displacements,

Control Strategy	1% Critical Damping		10% Critical Damping	
	Minimum (cm)	Maximum (cm)	Minimum (cm)	Maximum (cm)
Base Isolation Alone	-16.34 cm	16.05 cm	-12.75 cm	11.27 cm
Sub-optimal Bang-Bang	-3.64 cm	4.99 cm	-4.07 cm	4.29 cm
Velocity Cancellation	-5.02 cm	5.10 cm	-4.18 cm	4.16 cm

it is evident that the sub-optimal bang-bang and velocity cancellation control strategies both lead to significant reductions in peak displacements. Peak displacements under “velocity cancellation”

control are marginally larger than for “sub-optimal bang-bang control,” but this margin is tiny compared to the overall improvements in applying active control in the first place.

**Phase Analysis.** Tables 24 and 25 show the scatter diagram data and phase analysis results for the linear time history response corresponding to base isolation plus “velocity cancellation” control and an actuator force of 450 kN. The ground motion input is El Centro 1940 S00E. Tables 26 and 27 summarize the statistics of response on  $\rho(X, F)$  and  $\rho(V, F)$  values for responses generated by the ensemble of scaled El Centro ground motions.

By design, the “velocity cancellation” control strategy works perfectly in phase with the system velocity measurements at node 1. Accordingly,  $\rho(V, F) = 1$  across the ensemble of responses. For system responses at both 1% and 10% critical damping, average values of  $\rho(X, F)$  computed over the time interval  $[0, 10]$  seconds are 0.013 and 0.023, respectively. We can interpret these results by first noting that the actuator works to increase the effective damping – extreme values of system response are reduced, accordingly. What is less evident, however, is that the control strategy accomplishes this task in a way that, on average, favors neither positive nor negative displacements.



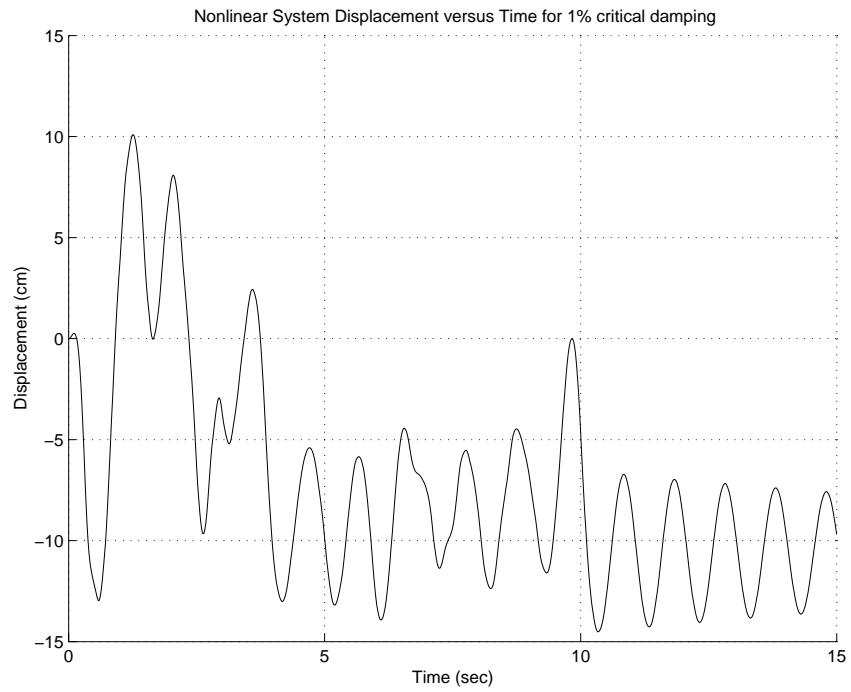


Figure 24: 2DOF Nonlinear Displacement Response (cm) versus Time (sec) for 1940 El Centro S00E Ground Motion Record and 1% Critical Damping

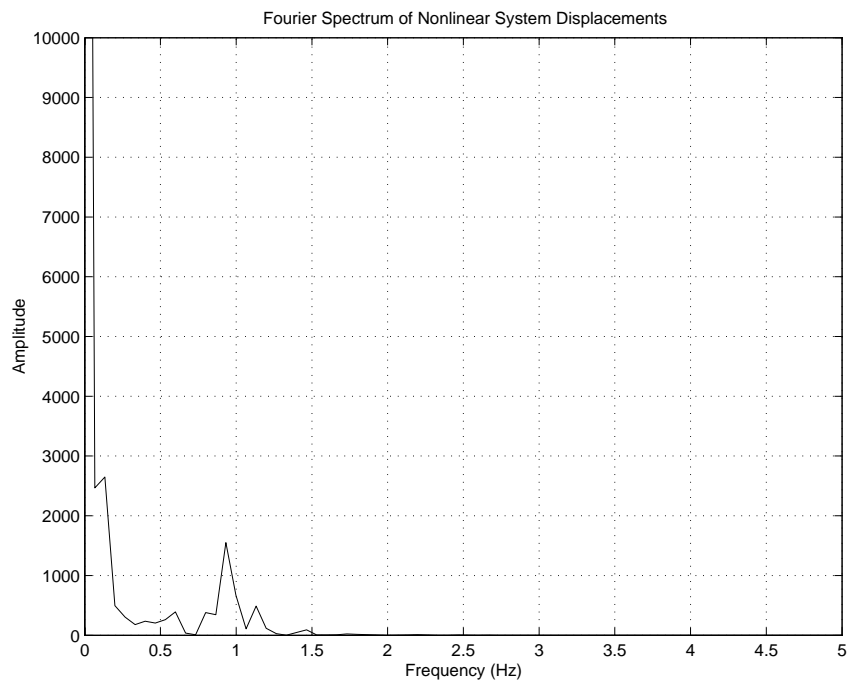


Figure 25: Fourier Transform for Nonlinear Displacement Response due to 1940 El Centro S00E Ground Motion Record and 1% Critical Damping

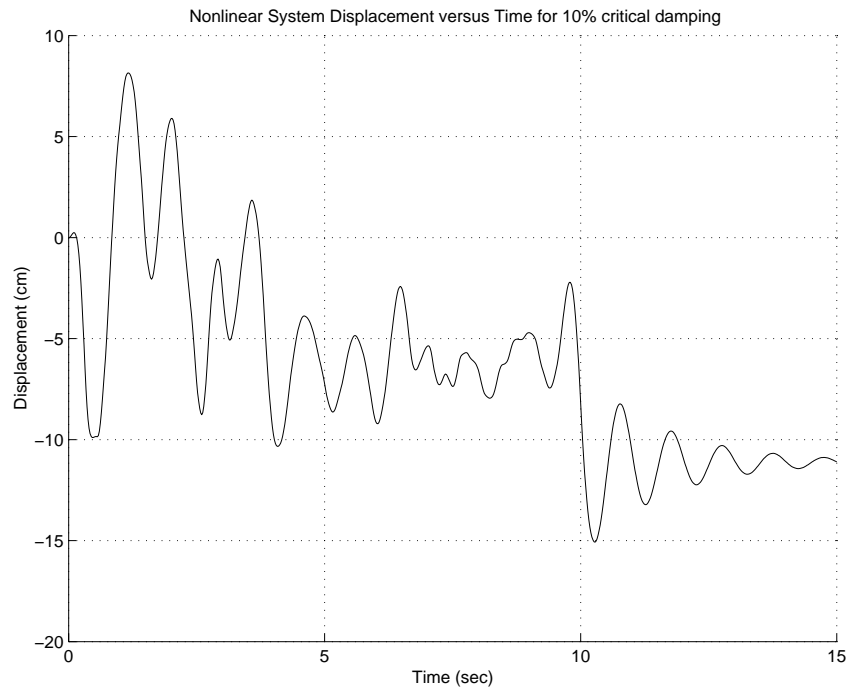


Figure 26: 2DOF System Displacement Response (cm) versus Time (sec) for 1940 El Centro S00E Ground Motion Record and 10% Critical Damping

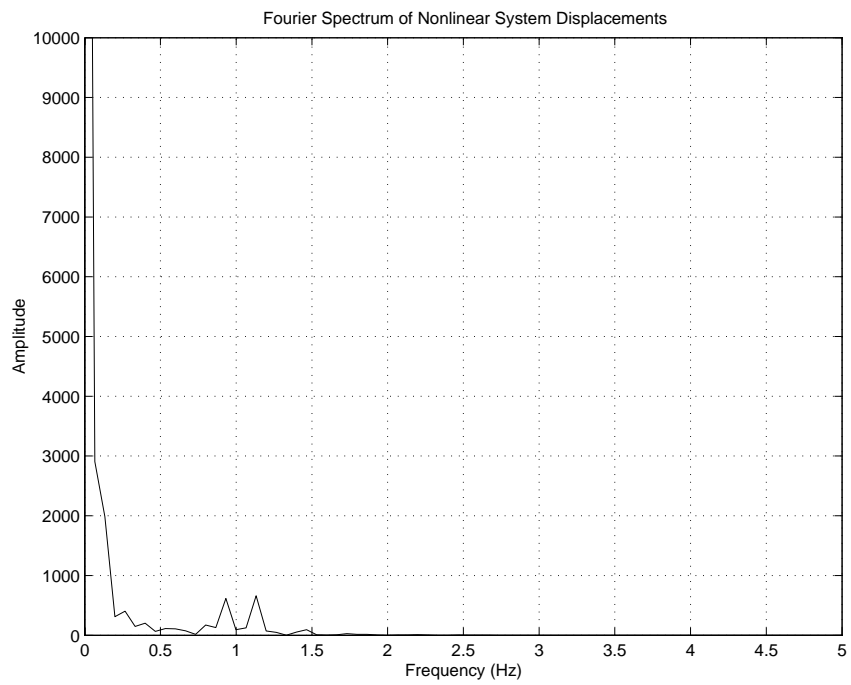


Figure 27: Fourier Transform for Nonlinear Displacement Response due to 1940 El Centro S00E Ground Motion Record and 10% Critical Damping

Part A: 1% Critical Damping

=====

```

=====
Period/Scatter Plot:  A(-1,1)      B(1,1)      C(1,-1)      D(-1,-1)      Total
=====
[ 0 sec, 10 sec]:    187         50          44           219           500
[10 sec, 15 sec]:    113         0           0            137           250
[ 0 sec, 15 sec]:    300         50          44           356           750
=====

```

```

=====
Range/Statistics:    average(X)    std(X)      std(F)      cov(X,F)      corr(X,F)
=====
[ 0 sec, 10 sec]:    -5.50 cm     0.7814      0.9986      0.04355       0.056
[10 sec, 15 sec]:    -10.57 cm    0.0042      0.9974      0.00001       0.000
[ 0 sec, 15 sec]:    -7.18 cm     0.6622      0.9978      0.03271       0.049
=====

```

Part B: 10% Critical Damping

=====

Displacements...

```

=====
Period/Scatter Plot:  A(-1,1)      B(1,1)      C(1,-1)      D(-1,-1)      Total
=====
[ 0 sec, 10 sec]:    75           50          28           347           500
[10 sec, 15 sec]:    0            0           0            250           250
[ 0 sec, 15 sec]:    75           50          28           597           750
=====

```

Displacements...

```

=====
Range/Statistics:    average(X)    std(X)      std(F)      cov(X,F)      corr(X,F)
=====
[ 0 sec, 10 sec]:    -4.23 cm     0.7257      0.8660      0.2440        0.388
[10 sec, 15 sec]:    -11.28 cm    0.0040      0.0040      0.0000        1.000
[ 0 sec, 15 sec]:    -6.56 cm     0.6105      0.7454      0.1973        0.434
=====

```

Table 16: Part 1. Nonlinear Time History Response due to Base Isolation Alone ( $U_{max} = 0$  kN). “Displacement/actuator force” scatter diagram data and phase analysis generated by 1940 El Centro Record. Part(a): 1% critical damping, Part(b): 10% critical damping.

Part A: 1% Critical Damping

```

=====
Period/Scatter Plot:  A(-1,1)      B(1,1)  C(1,-1)  D(-1,-1)  Total
=====
[ 0 sec, 10 sec]:      1         236      8         255        500
[10 sec, 15 sec]:      0         113     10         127         250
[ 0 sec, 15 sec]:      1         349     18         382         750
=====

```

```

=====
Range/Statistics:     average(V)  std(V)   std(F)   cov(V,F)  corr(V,F)
=====
[ 0 sec, 10 sec]: -0.521 cm/sec  0.999   0.9986   0.9628   0.964
[10 sec, 15 sec]: -0.938 cm/sec  1.002   0.9974   0.9294   0.930
[ 0 sec, 15 sec]: -0.659 cm/sec  0.999   0.9978   0.9504   0.953
=====

```

Part B: 10% Critical Damping

Velocities...

```

=====
Period/Scatter Plot:  A(-1,1)      B(1,1)  C(1,-1)  D(-1,-1)  Total
=====
[ 0 sec, 10 sec]:      9         116     132        243         500
[10 sec, 15 sec]:      0           0      124        126         250
[ 0 sec, 15 sec]:      9         116     256        369         750
=====

```

Velocities...

```

=====
Range/Statistics :     average(V)  std(V)   std(F)   cov(V,F)  corr(V,F)
=====
[ 0 sec, 10 sec]: -0.873 cm/sec      1   0.8660   0.432   0.499
[10 sec, 15 sec]: -0.478 cm/sec  1.002  0.0040   0.000   0.000
[ 0 sec, 15 sec]: -0.741 cm/sec      1   0.7454   0.288   0.386
=====

```

Table 17: Part 1. Nonlinear Time History Response due to Base Isolation Alone ( $U_{max} = 0$  kN). “Velocity/actuator force” scatter diagram data and phase analysis generated by 1940 El Centro Record. Part(a): 1% critical damping, Part(b): 10% critical damping.

Part A: 1% Critical Damping

Ground Motion	Simulation		average(X)	std(X)	std(F)	Statistics	
	Interval					cov(X,F)	corr(X,F)
1940 EL CENTRO S00E:	[ 0, 10 ]	sec:	-5.50 cm	0.7814	0.9986	0.0435	0.056
	[ 10, 15 ]	sec:	-10.57 cm	0.0040	0.9974	0.0000	0.000
1940 EL CENTRO S90W:	[ 0, 10 ]	sec:	-0.51 cm	0.9968	0.9984	0.0355	0.036
	[ 10, 15 ]	sec:	-5.72 cm	0.0040	1.001	0.0000	0.000
1934 EL CENTRO S00W:	[ 0, 10 ]	sec:	-7.10 cm	0.4102	0.9998	0.0258	0.063
	[ 10, 15 ]	sec:	-8.91 cm	0.0040	0.9957	0.0000	0.000
1934 EL CENTRO S90W:	[ 0, 10 ]	sec:	4.27 cm	0.5607	0.9979	0.0070	0.012
	[ 10, 15 ]	sec:	7.50 cm	0.0040	0.9994	0.0000	0.000
1979 EL CENTRO N50E:	[ 0, 10 ]	sec:	-28.63 cm	0.6940	0.9755	0.1016	0.150
	[ 10, 15 ]	sec:	-34.28 cm	0.0040	0.9642	0.0000	0.001
1979 EL CENTRO N40W:	[ 0, 10 ]	sec:	19.79 cm	0.6981	0.9896	0.0769	0.111
	[ 10, 15 ]	sec:	24.26 cm	0.0040	0.9818	0.0000	0.000
Average Value:							
	[ 0, 10 ]	sec:	-2.94 cm				0.071
	[ 10, 15 ]	sec:	-4.62 cm				0.000

Part B: 10% Critical Damping

Ground Motion	Simulation		average(X)	std(X)	std(F)	Statistics	
	Interval					cov(X,F)	corr(X,F)
1940 EL CENTRO S00E:	[ 0, 10 ]	sec:	-4.23 cm	0.7257	0.8660	0.2440	0.388
	[ 10, 15 ]	sec:	-11.28 cm	0.0040	0.0040	0.0000	1.000
1940 EL CENTRO S90W:	[ 0, 10 ]	sec:	-0.28 cm	0.9968	0.9968	0.2496	0.251
	[ 10, 15 ]	sec:	-6.84 cm	0.0040	0.3927	0.0000	0.009
1934 EL CENTRO S00W:	[ 0, 10 ]	sec:	-5.27 cm	0.4012	0.6940	0.0965	0.346
	[ 10, 15 ]	sec:	-5.60 cm	0.0040	0.0040	0.0000	1.000
1934 EL CENTRO S90W:	[ 0, 10 ]	sec:	2.64 cm	0.6546	0.9656	0.0834	0.132
	[ 10, 15 ]	sec:	4.14 cm	0.0040	0.3527	0.0000	0.010
1979 EL CENTRO N50E:	[ 0, 10 ]	sec:	-17.44 cm	0.6813	0.5548	0.2910	0.770
	[ 10, 15 ]	sec:	-22.35 cm	0.0040	0.0040	0.0000	1.000
1979 EL CENTRO N40W:	[ 0, 10 ]	sec:	12.41 cm	0.7141	0.7102	0.3112	0.614
	[ 10, 15 ]	sec:	16.50 cm ]:	0.0040	0.0040	0.0000	1.000
Average Value:							
	[ 0, 10 ]	sec:	-2.02 cm				0.416
	[ 10, 15 ]	sec:	-4.24 cm				0.669

Table 18: Part 1. Nonlinear time-history response generated by ensemble of scaled El Centro Records ( $U_{max} = 450$  kN). “Displacement/actuator force” scatter diagram data and phase analysis. Part(a): 1% critical damping, Part(b): 10% critical damping.

Part A: 1% Critical Damping

Ground Motion	Simulation				Statistics	
	Interval	average(V)	std(V)	std(F)	cov(V,F)	corr(V,F)
1940 EL CENTRO S00E:	[ 0, 10 ] sec:	-0.521 cm/sec	0.999	0.9986	0.9628	0.964
	[ 10, 15 ] sec:	-0.938 cm/sec	1.002	0.9974	0.9294	0.930
1940 EL CENTRO S90W:	[ 0, 10 ] sec:	-0.944 cm/sec	0.999	0.9984	0.9431	0.945
	[ 10, 15 ] sec:	0.1803 cm/sec	1.002	1.0010	0.9635	0.961
1934 EL CENTRO S00W:	[ 0, 10 ] sec:	-0.7541 cm/sec	0.998	0.9998	0.9173	0.919
	[ 10, 15 ] sec:	-0.0114 cm/sec	1.002	0.9957	0.8773	0.879
1934 EL CENTRO S90W:	[ 0, 10 ] sec:	0.5873 cm/sec	1.000	0.9979	0.9397	0.942
	[ 10, 15 ] sec:	0.0046 cm/sec	1.002	0.9994	0.9168	0.916
1979 EL CENTRO N50E:	[ 0, 10 ] sec:	-3.637 cm/sec	0.999	0.9755	0.8001	0.821
	[ 10, 15 ] sec:	-0.037 cm/sec	1.002	0.9642	0.7426	0.769
1979 EL CENTRO N40W:	[ 0, 10 ] sec:	2.649 cm/sec	0.999	0.9896	0.8457	0.855
	[ 10, 15 ] sec:	-0.001 cm/sec	1.002	0.9818	0.8096	0.823
=====						
Average Value:	[ 0, 10 ] sec:	-0.438 cm/sec				0.908
	[ 10, 15 ] sec:	-0.133 cm/sec				0.879

Part B: 10% Critical Damping

Ground Motion	Simulation				Statistics	
	Interval	average(V)	std(V)	std(F)	cov(V,F)	corr(V,F)
1940 EL CENTRO S00E:	[ 0, 10 ] sec:	-0.873 cm/sec	1.000	0.8660	0.4320	0.499
	[ 10, 15 ] sec:	-0.478 cm/sec	1.002	0.0040	0.0000	0.000
1940 EL CENTRO S90W:	[ 0, 10 ] sec:	-1.068 cm/sec	0.999	0.9968	0.7538	0.756
	[ 10, 15 ] sec:	0.751 cm/sec	1.002	0.3927	0.0810	0.206
1934 EL CENTRO S00W:	[ 0, 10 ] sec:	-0.560 cm/sec	0.997	0.6940	0.2438	0.352
	[ 10, 15 ] sec:	0.000 cm/sec	1.002	0.0040	0.0000	0.000
1934 EL CENTRO S90W:	[ 0, 10 ] sec:	0.405 cm/sec	0.999	0.9656	0.7118	0.737
	[ 10, 15 ] sec:	0.024 cm/sec	1.002	0.3527	0.0637	0.180
1979 EL CENTRO N50E:	[ 0, 10 ] sec:	-2.523 cm/sec	0.997	0.5548	0.1174	0.212
	[ 10, 15 ] sec:	0.585 cm/sec	1.002	0.0040	0.0000	0.000
1979 EL CENTRO N40W:	[ 0, 10 ] sec:	1.806 cm/sec	0.999	0.7102	0.2353	0.331
	[ 10, 15 ] sec:	-0.324 cm/sec	1.002	0.0040	0.0000	0.000
=====						
Average Value:	[ 0, 10 ] sec:	-0.468 cm/sec				0.481
	[ 10, 15 ] sec:	0.093 cm/sec				0.064

Table 19: Part 1. Nonlinear time-history response generated by ensemble of scaled El Centro Records ( $U_{max} = 450$  kN). “Velocity/actuator force” scatter diagram data and phase analysis. Part(a): 1% critical damping, Part(b): 10% critical damping.

Part A: 1% Critical Damping

```

=====
Period/Scatter Plot:  A(-1,1)      B(1,1)  C(1,-1)  D(-1,-1)  Total
=====
[ 0 sec, 10 sec]:    217         20       35       228       500
[10 sec, 15 sec]:    125         0        0        125       250
[ 0 sec, 15 sec]:    342         20       35       353       750
=====

```

```

=====
Range/Statistics:    average(X)  std(X)   std(F)   cov(X,F)  corr(X,F)
=====
[ 0 sec, 10 sec]:    -1.888 cm  0.6258   0.9986   -0.04856  -0.077
[10 sec, 15 sec]:    -2.226 cm  0.0040   1.002    0          0.000
[ 0 sec, 15 sec]:    -1.998 cm  0.5214   0.9994   -0.03492  -0.067
=====

```

Part B: 10% Critical Damping

```

=====
Period/Scatter Plot:  A(-1,1)      B(1,1)  C(1,-1)  D(-1,-1)  Total
=====
[ 0 sec, 10 sec]:    146         35       46       273       500
[10 sec, 15 sec]:    80          0        0        170       250
[ 0 sec, 15 sec]:    226         35       46       443       750
=====

```

```

=====
Range/Statistics:    average(X)  std(X)   std(F)   cov(X,F)  corr(X,F)
=====
[ 0 sec, 10 sec]:    -0.7779 cm  0.7369   0.9612   0.04542   0.064
[10 sec, 15 sec]:    -0.7128 cm  0.0040   0.9348   5.83e-06  0.001
[ 0 sec, 15 sec]:    -0.7552 cm  0.6208   0.9527   0.03633   0.061
=====

```

Table 20: Part 2. Nonlinear Time History Response due to Base Isolation plus Bang-bang Control ( $U_{max} = 450$  kN). “Displacement/actuator force” scatter diagram data and phase analysis generated by 1940 El Centro Record. Part(a): 1% critical damping, Part(b): 10% critical damping.

Part A: 1% Critical Damping

```

=====
Period/Scatter Plot:  A(-1,1)      B(1,1)      C(1,-1)      D(-1,-1)      Total
=====
[ 0 sec, 10 sec]:    41         196         51          212          500
[10 sec, 15 sec]:    0         125         16          109          250
[ 0 sec, 15 sec]:    41         321         67          321          750
=====

```

```

=====
Range/Statistics:    average(V)    std(V)      std(F)      cov(V,F)     corr(V,F)
=====
[ 0 sec, 10 sec]:   -0.328 cm/sec  0.9999      0.9986      0.6314      0.632
[10 sec, 15 sec]:   0.313 cm/sec  0.9966      1.002       0.755       0.756
[ 0 sec, 15 sec]:   -0.114 cm/sec  0.9996      0.9994      0.6729      0.674
=====

```

Part B: 10% Critical Damping

```

=====
Period/Scatter Plot:  A(-1,1)      B(1,1)      C(1,-1)      D(-1,-1)      Total
=====
[ 0 sec, 10 sec]:    19         162         87          232          500
[10 sec, 15 sec]:    0          80          79          91           250
[ 0 sec, 15 sec]:    19         242        166          323          750
=====

```

```

=====
Range/Statistics:    average(V)    std(V)      std(F)      cov(V,F)     corr(V,F)
=====
[ 0 sec, 10 sec]:   -0.256 cm/sec    1          0.9612      0.5749      0.598
[10 sec, 15 sec]:   0.408 cm/sec    0.9974      0.9348      0.5648      0.606
[ 0 sec, 15 sec]:   -0.035 cm/sec    0.9996      0.9527      0.5689      0.597
=====

```

Table 21: Part 2. Nonlinear Time History Response due to Base Isolation plus Bang-bang Control ( $U_{max} = 450$  kN). “Velocity/actuator force” scatter diagram data and phase analysis generated by 1940 El Centro Record. Part(a): 1% critical damping, Part(b): 10% critical damping.



Part A: 1% Critical Damping

Ground Motion	Simulation		average(X)	std(X)	std(F)	Statistics	
	Interval					cov(X,F)	corr(X,F)
1940 EL CENTRO S00E:	[ 0, 10 ]	sec:	-1.888 cm	0.6258	0.9986	-0.04856	-0.077
	[ 10, 15 ]	sec:	-2.226 cm	0.0040	1.002	0	0.000
1940 EL CENTRO S90W:	[ 0, 10 ]	sec:	1.786 cm	0.5724	0.9999	0.03088	0.054
	[ 10, 15 ]	sec:	-3.054 cm	0.0040	1.002	3.886e-07	0.000
1934 EL CENTRO S00W:	[ 0, 10 ]	sec:	-0.970 cm	0.5892	0.9988	0.009216	0.016
	[ 10, 15 ]	sec:	-0.944 cm	0.0040	1	1.036e-06	0.000
1934 EL CENTRO S90W:	[ 0, 10 ]	sec:	0.120 cm	0.9968	0.9999	-0.09472	-0.095
	[ 10, 15 ]	sec:	-0.306 cm	0.9596	1.001	-0.04235	-0.044
1979 EL CENTRO N50E:	[ 0, 10 ]	sec:	-1.161 cm	0.9038	0.9979	-0.03139	-0.035
	[ 10, 15 ]	sec:	-1.325 cm	0.0040	0.9966	1.684e-06	0.000
1979 EL CENTRO N40W:	[ 0, 10 ]	sec:	7.115 cm	0.765	0.9656	0.08056	0.109
	[ 10, 15 ]	sec:	8.508 cm	0.004024	0.742	1.088e-05	0.004
=====							
Average Value:		[ 0, 10 ]	sec:	0.830 cm			-0.004
		[ 10, 15 ]	sec:	0.108 cm			-0.008

Part B: 10% Critical Damping

Ground Motion	Simulation		average(X)	std(X)	std(F)	Statistics	
	Interval					cov(X,F)	corr(X,F)
1940 EL CENTRO S00E:	[ 0, 10 ]	sec:	-0.778 cm	0.7369	0.9612	0.0454	0.064
	[ 10, 15 ]	sec:	-0.713 cm	0.0040	0.9348	0.0000	0.001
1940 EL CENTRO S90W:	[ 0, 10 ]	sec:	0.551 cm	0.8858	0.9902	0.1790	0.204
	[ 10, 15 ]	sec:	-0.767 cm	0.0040	0.8654	0.0000	0.002
1934 EL CENTRO S00W:	[ 0, 10 ]	sec:	-0.497 cm	0.8146	0.9928	0.0464	0.057
	[ 10, 15 ]	sec:	-0.261 cm	0.1266	0.9834	0.0095	0.077
1934 EL CENTRO S90W:	[ 0, 10 ]	sec:	0.085 cm	1	1	0.0641	0.064
	[ 10, 15 ]	sec:	-0.117 cm	0.9891	1.002	0.0241	0.024
1979 EL CENTRO N50E:	[ 0, 10 ]	sec:	-0.025 cm	0.9994	0.9999	0.0994	0.099
	[ 10, 15 ]	sec:	-0.096 cm	0.1266	1.002	0.0080	0.063
1979 EL CENTRO N40W:	[ 0, 10 ]	sec:	1.734 cm	0.7332	0.9038	0.1770	0.267
	[ 10, 15 ]	sec:	1.001 cm	0.0040	0.4450	0.0000	0.008
=====							
Average Value:		[ 0, 10 ]	sec:	0.178 cm			0.125
		[ 10, 15 ]	sec:	-0.160 cm			0.029

Table 22: Part 2. Nonlinear time-history response generated by ensemble of scaled El Centro Records ( $U_{max} = 450$  kN). “Displacement/actuator force” scatter diagram data and phase analysis. Part(a): 1% critical damping, Part(b): 10% critical damping.

Part A: 1% Critical Damping

Ground Motion	Simulation		average(V)	std(V)	std(F)	Statistics	
	Interval					cov(V,F)	corr(V,F)
1940 EL CENTRO S00E:	[ 0, 10 ]	sec:	-0.328 cm/sec	0.9999	0.9986	0.6314	0.632
	[ 10, 15 ]	sec:	0.313 cm/sec	0.9966	1.002	0.7550	0.756
1940 EL CENTRO S90W:	[ 0, 10 ]	sec:	-0.695 cm/sec	1	0.9999	0.5681	0.568
	[ 10, 15 ]	sec:	0.845 cm/sec	0.9957	1.002	0.7738	0.776
1934 EL CENTRO S00W:	[ 0, 10 ]	sec:	-0.148 cm/sec	1	0.9988	0.5204	0.521
	[ 10, 15 ]	sec:	0.119 cm/sec	1.002	1	0.7224	0.721
1934 EL CENTRO S90W:	[ 0, 10 ]	sec:	0.027 cm/sec	1	0.9999	0.4961	0.496
	[ 10, 15 ]	sec:	-0.035 cm/sec	1	1.001	0.8403	0.841
1979 EL CENTRO N50E:	[ 0, 10 ]	sec:	-0.151 cm/sec	1	0.9979	0.576	0.577
	[ 10, 15 ]	sec:	0.032 cm/sec	0.9994	0.9966	0.8188	0.822
1979 EL CENTRO N40W:	[ 0, 10 ]	sec:	0.911 cm/sec	1	0.9656	0.553	0.573
	[ 10, 15 ]	sec:	-0.114 cm/sec	1.002	0.742	0.3106	0.418
Average Value:		[ 0, 10 ] sec:	-0.064 cm/sec				0.561
		[ 10, 15 ] sec:	0.191 cm/sec				0.722

Part B: 10% Critical Damping

Ground Motion	Simulation		average(V)	std(V)	std(F)	Statistics	
	Interval					cov(V,F)	corr(V,F)
1940 EL CENTRO S00E:	[ 0, 10 ]	sec:	-0.256 cm/sec	1	0.9612	0.5749	0.598
	[ 10, 15 ]	sec:	0.408 cm/sec	0.9974	0.9348	0.5648	0.606
1940 EL CENTRO S90W:	[ 0, 10 ]	sec:	-0.559 cm/sec	0.9999	0.9902	0.5583	0.564
	[ 10, 15 ]	sec:	1.011 cm/sec	1.001	0.8654	0.5179	0.598
1934 EL CENTRO S00W:	[ 0, 10 ]	sec:	-0.031 cm/sec	0.9986	0.9928	0.5942	0.599
	[ 10, 15 ]	sec:	0.015 cm/sec	0.9834	0.9834	0.6394	0.661
1934 EL CENTRO S90W:	[ 0, 10 ]	sec:	0.018 cm/sec	1	1.0000	0.5320	0.532
	[ 10, 15 ]	sec:	-0.034 cm/sec	1.002	1.0020	0.9558	0.952
1979 EL CENTRO N50E:	[ 0, 10 ]	sec:	-0.017 cm/sec	0.999	0.9999	0.6282	0.628
	[ 10, 15 ]	sec:	0.028 cm/sec	1.002	1.0020	0.9878	0.984
1979 EL CENTRO N40W:	[ 0, 10 ]	sec:	0.113 cm/sec	0.9988	0.9038	0.4325	0.479
	[ 10, 15 ]	sec:	-0.014 cm/sec	0.9927	0.4450	0.0902	0.204
Average Value:		[ 0, 10 ] sec:	-0.012 cm/sec				0.566
		[ 10, 15 ] sec:	0.235 cm/sec				0.667

Table 23: Part 2. Nonlinear time-history response generated by ensemble of scaled El Centro Records ( $U_{max} = 450$  kN). “Velocity/actuator force” scatter diagram data and phase analysis. Part(a): 1% critical damping, Part(b): 10% critical damping.

Part A: 1% Critical Damping

```

=====
Period/Scatter Plot:  A(-1,1)      B(1,1)  C(1,-1)  D(-1,-1)  Total
=====
[ 0 sec, 10 sec]:    207         32       43       218       500
[10 sec, 15 sec]:    131         0        0       119       250
[ 0 sec, 15 sec]:    338         32       43       337       750
=====

```

```

=====
Range/Statistics:     average(X)  std(X)   std(F)   cov(X,F)  corr(X,F)
=====
[ 0 sec, 10 sec]:    -1.41 cm   0.7141   0.999    -0.0308   -0.043
[10 sec, 15 sec]:    -1.63 cm   0.0040   1.001    -0.0000   -0.000
[ 0 sec, 15 sec]:    -1.48 cm   0.6000   0.999    -0.0266   -0.044
=====

```

Part B: 10% Critical Damping

```

=====
Period/Scatter Plot:  A(-1,1)      B(1,1)  C(1,-1)  D(-1,-1)  Total
=====
[ 0 sec, 10 sec]:    228         19       17       236       500
[10 sec, 15 sec]:    133         0        0       117       250
[ 0 sec, 15 sec]:    361         19       17       353       750
=====

```

```

=====
Range/Statistics:     average(X)  std(X)   std(F)   cov(X,F)  corr(X,F)
=====
[ 0 sec, 10 sec]:    -2.50 cm   0.517    0.9999   0.0097    0.019
[10 sec, 15 sec]:    -2.95 cm   0.004    1.0000   0.0000   -0.000
[ 0 sec, 15 sec]:    -2.64 cm   0.427    0.9999   0.0040    0.009
=====

```

Table 24: Part 3. Nonlinear Time History Response due to Base Isolation plus Velocity Control ( $U_{max} = 450$  kN). “Displacement/actuator force” scatter diagram data and phase analysis generated by 1940 El Centro Record. Part(a): 1% critical damping, Part(b): 10% critical damping.

Part A: 1% Critical Damping

```

=====
Period/Scatter Plot:  A(-1,1)      B(1,1)  C(1,-1)  D(-1,-1)  Total
=====
[ 0 sec, 10 sec]:    0          239      0         261        500
[10 sec, 15 sec]:    2          129     10         109        250
[ 0 sec, 15 sec]:    2          368     10         370        750
=====

```

```

=====
Range/Statistics:    average(V)  std(V)   std(F)   cov(V,F)  corr(V,F)
=====
[ 0 sec, 10 sec]:  -0.25 cm/sec  0.999    0.999    0.998      1
[10 sec, 15 sec]:  0.21 cm/sec  1.001    1.001    1.002      1
[ 0 sec, 15 sec]:  -0.10 cm/sec  0.999    0.999    0.999      1
=====

```

Part B: 10% Critical Damping

```

=====
Period/Scatter Plot:  A(-1,1)      B(1,1)  C(1,-1)  D(-1,-1)  Total
=====
[ 0 sec, 10 sec]:    0          247      0         253        500
[10 sec, 15 sec]:    1          132      8         109        250
[ 0 sec, 15 sec]:    1          379      8         362        750
=====

```

```

=====
Range/Statistics:    average(V)  std(V)   std(F)   cov(V,F)  corr(V,F)
=====
[ 0 sec, 10 sec]:  -0.43 cm/sec  0.9999   0.9999   0.9999     1
[10 sec, 15 sec]:  0.34 cm/sec  1.0000   1.0000   0.9999     1
[ 0 sec, 15 sec]:  -0.17 cm/sec  0.9999   0.9999   0.9998     1
=====

```

Table 25: Part 3. Nonlinear Time History Response due to Base Isolation plus Velocity Control ( $U_{max} = 450$  kN). “Velocity/actuator force” scatter diagram data and phase analysis generated by 1940 El Centro Record. Part(a): 1% critical damping, Part(b): 10% critical damping.

Part A: 1% Critical Damping

Ground Motion	Simulation		average(X)	std(X)	std(F)	Statistics	
	Interval					cov(X,F)	corr(X,F)
1940 EL CENTRO S00E:	[ 0, 10 ]	sec:	-1.41 cm	0.7141	0.999	-0.0308	-0.043
	[ 10, 15 ]	sec:	-1.63 cm	0.0040	1.001	-0.0000	-0.000
1940 EL CENTRO S90W:	[ 0, 10 ]	sec:	2.03 cm	0.6682	0.998	0.0507	0.075
	[ 10, 15 ]	sec:	-3.38 cm	0.0040	0.999	-0.0000	-0.000
1934 EL CENTRO S00W:	[ 0, 10 ]	sec:	-1.20 cm	0.5426	0.999	0.0048	0.008
	[ 10, 15 ]	sec:	-1.19 cm	0.0040	1.002	0.00007	-0.000
1934 EL CENTRO S90W:	[ 0, 10 ]	sec:	0.06 cm	0.9999	1	0.024	0.024
	[ 10, 15 ]	sec:	-0.23 cm	0.9818	1.001	-0.009639	-0.010
1979 EL CENTRO N50E:	[ 0, 10 ]	sec:	-1.48 cm	0.0040	1.002	-1.295e-07	-0.000
	[ 10, 15 ]	sec:	-1.93 cm	0.7477	1	-0.01421	-0.019
1979 EL CENTRO N40W:	[ 0, 10 ]	sec:	7.54 cm	0.7582	0.999	0.00992	0.013
	[ 10, 15 ]	sec:	10.33 cm	0.0040	1.002	0	0.000
Average Value:			[ 0, 10 ] sec:	0.92 cm			0.013
			[ 10, 15 ] sec:	0.32 cm			0.000

Part B: 10% Critical Damping

Ground Motion	Simulation		average(X)	std(X)	std(F)	Statistics	
	Interval					cov(X,F)	corr(X,F)
1940 EL CENTRO S00E:	[ 0, 10 ]	sec:	-2.50 cm	0.517	0.9999	0.0097	0.019
	[ 10, 15 ]	sec:	-2.95 cm	0.004	1.0000	0.0000	-0.000
1940 EL CENTRO S90W:	[ 0, 10 ]	sec:	1.18 cm	0.775	0.9992	0.0493	0.063
	[ 10, 15 ]	sec:	-2.63 cm	0.004	0.9994	-0.0000	-0.000
1934 EL CENTRO S00W:	[ 0, 10 ]	sec:	-0.25 cm	0.981	1	0.0095	0.009
	[ 10, 15 ]	sec:	-0.22 cm	0.178	1.0020	-0.0001	-0.000
1934 EL CENTRO S90W:	[ 0, 10 ]	sec:	0.17 cm	0.994	0.9994	-0.0082	-0.008
	[ 10, 15 ]	sec:	-0.18 cm	0.978	1.002	-0.0189	-0.019
1979 EL CENTRO N50E:	[ 0, 10 ]	sec:	-0.17 cm	0.984	0.9998	0.0044	0.004
	[ 10, 15 ]	sec:	-0.34 cm	0.004	1.002	-0.000	-0.000
1979 EL CENTRO N40W:	[ 0, 10 ]	sec:	5.06 cm	0.755	1.000	0.024	0.032
	[ 10, 15 ]	sec:	6.95 cm	0.004	1.002	-0.000	0.000
Average Value:			[ 0, 10 ] sec:	0.58 cm			0.023
			[ 10, 15 ] sec:	0.10 cm			-0.003

Table 26: Part 3. Nonlinear time-history response generated by ensemble of scaled El Centro Records ( $U_{max} = 450$  kN). “Displacement/actuator force” scatter diagram data and phase analysis. Part(a): 1% critical damping, Part(b): 10% critical damping.

Part A: 1% Critical Damping

Ground Motion	Simulation				Statistics	
	Interval	average(V)	std(V)	std(F)	cov(V,F)	corr(V,F)
1940 EL CENTRO S00E:	[ 0, 10 ] sec:	-0.25 cm/sec	0.999	0.999	0.998	1
	[ 10, 15 ] sec:	0.21 cm/sec	1.001	1.001	1.002	1
1940 EL CENTRO S90W:	[ 0, 10 ] sec:	-0.67 cm/sec	0.998	0.998	0.997	1
	[ 10, 15 ] sec:	0.68 cm/sec	0.999	0.999	0.998	1
1934 EL CENTRO S00W:	[ 0, 10 ] sec:	-0.14 cm/sec	0.999	0.999	0.999	1
	[ 10, 15 ] sec:	0.10 cm/sec	1.002	1.002	1.004	1
1934 EL CENTRO S90W:	[ 0, 10 ] sec:	-0.03 cm/sec	1	1	1	1
	[ 10, 15 ] sec:	0.03 cm/sec	1.001	1.001	1.003	1
1979 EL CENTRO N50E:	[ 0, 10 ] sec:	-0.25 cm/sec	0.999	0.999	0.999	1
	[ 10, 15 ] sec:	0.15 cm/sec	1.002	1.002	1.004	1
1979 EL CENTRO N40W:	[ 0, 10 ] sec:	1.05 cm/sec	0.999	0.999	0.9984	1
	[ 10, 15 ] sec:	-0.06 cm/sec	1.002	1.002	1.004	1
=====						
Average Value:	[ 0, 10 ] sec:	-0.05 cm/sec				1.000
	[ 10, 15 ] sec:	0.18 cm/sec				1.000

Part B: 10% Critical Damping

Ground Motion	Simulation				Statistics	
	Interval	average(V)	std(V)	std(F)	cov(V,F)	corr(V,F)
1940 EL CENTRO S00E:	[ 0, 10 ] sec:	-0.43 cm/sec	0.9999	0.9999	0.9999	1
	[ 10, 15 ] sec:	0.34 cm/sec	1.0000	1.0000	0.9999	1
1940 EL CENTRO S90W:	[ 0, 10 ] sec:	-0.59 cm/sec	0.9992	0.9992	0.9984	1
	[ 10, 15 ] sec:	0.70 cm/sec	0.9994	0.9994	0.9988	1
1934 EL CENTRO S00W:	[ 0, 10 ] sec:	-0.03 cm/sec	1	1	0.9999	1
	[ 10, 15 ] sec:	0.02 cm/sec	1.002	1.002	1.004	1
1934 EL CENTRO S90W:	[ 0, 10 ] sec:	-0.06 cm/sec	0.999	0.9994	0.9987	1
	[ 10, 15 ] sec:	0.12 cm/sec	1.002	1.002	1.003	1
1979 EL CENTRO N50E:	[ 0, 10 ] sec:	-0.07 cm/sec	0.999	0.9998	0.9996	1
	[ 10, 15 ] sec:	0.09 cm/sec	1.002	1.002	1.004	1
1979 EL CENTRO N40W:	[ 0, 10 ] sec:	0.77 cm/sec	1	1	1	1
	[ 10, 15 ] sec:	-0.15 cm/sec	1.002	1.002	1.004	1
=====						
Average Value:	[ 0, 10 ] sec:	-0.07 cm/sec				1.000
	[ 10, 15 ] sec:	0.19 cm/sec				1.000

Table 27: Part 3. Nonlinear time-history response generated by ensemble of scaled El Centro Records ( $U_{max} = 450$  kN). “Velocity/actuator force” scatter diagram data and phase analysis. Part(a): 1% critical damping, Part(b): 10% critical damping.

## 5 Summary and Conclusions

The design of base isolated structures supplemented by active control mechanisms is complicated by large uncertainties in future ground motions, and the need to design control strategies that will protect large-scale structural systems for a wide range of ground motion inputs. Traditional metrics of performance assessment include time-history plots of displacement, velocity and acceleration. Time-series plots are conducive to conveying the range and regularity of motion over the simulation period. Here, in contrast, we have focused our attention on understanding the coordination of the actuator force direction with respect to displacements and velocities, the underlying parameters of system state. The research goal has been to show that the direction of actuator force application is strongly correlated with an aspect of the system state, thereby creating a pathway toward: (1) Simplified interpretations of behavior, and (2) Development of active control strategies based upon simplified principles. The conclusions of this study are as follows:

1. Starting with simplified models of displacement response for a base isolated structure, we have formulated models of phase analysis of actuator force direction in relation to system displacements and velocities. For the case of steady state displacement response of a single degree of freedom system, we have proved that the direction of actuator application can neither be perfectly in phase with displacements, nor perfectly in phase with velocities. In practice, however, the actuator force direction is “almost in phase” with velocities and “almost orthogonal” to sign changes in displacements. In other words, for the active control of lightly damped base isolated structures, the bang-bang control strategy works like an active damping mechanism.
2. The theoretical results suggest that a very simple velocity cancellation control strategy – certainly, pushing in a direction that opposes the change in displacements is easy to understand – might be effective in adding value to base isolation system responses. To validate the theoretical predictions, numerical experiments have been conducted to assess improvements in performance due to sub-optimal bang-bang control and velocity cancellation control, and to explore the extent to which the phase analysis predictions hold in linearly elastic and nonlinear time-domain settings.
3. Table 28 summarizes the average values of peak displacement and internal force in element 1 for each of the three case study problems. Simulations have been conducted at 1% and 10% critical damping, and for linearly elastic and nonlinear system behavior. As expected,

peak displacements at 10% critical damping are smaller than at 1% critical damping. The case study 1 simulations (i.e., base isolation alone) serve as a benchmark against which improvements in system response due to various strategies of active control can be measured. The case study 2 simulations correspond to base isolation plus sub-optimal bang-bang control ( $U_{max} = 450$  kN). For linear system responses, peak values of actively controlled displacements are a little less than 50% of peak displacement values occurring for base isolation alone. For nonlinear system responses, improvements in peak displacements due to active control are even better! The case study 3 simulations (i.e., velocity cancellation control with  $U_{max} = 450$  kN) are inspired by the phase analyses of simplified linearly elastic system behavior. Velocity cancellation control has the distinguishing feature of forcing the actuator to work in lockstep (i.e., perfect phase) with system velocities. The simulations indicate that in both the linear and nonlinear domains, this strategy is very effective – on average, peak values of displacement are only slightly larger (i.e., less than 10%) those occurring in case study 2. However, the real beauty of case study 3 is its simplicity – the actuator simply works to oppose the direction of motion.

4. The phase analysis computations are based on the assumption of regular periodic patterns of displacement and velocity, as might be generated by a linearly elastic single degree of freedom system. The theoretical analyses predict that: (1) The direction of actuator force will be “almost in phase” with velocities, particularly when the underlying system is lightly damped, and (2) The actuator/velocity correlation will degrade as damping increases. Moreover, because the underlying system behavior is assumed to be linear-elastic, velocities will be orthogonal to displacements. It follows that the actuator/displacement correlation will be close to zero. Nonlinear system behavior will be characterized by velocities and displacements that are no longer orthogonal and, therefore, we postulate that the phase analysis predictions will break down. Nonetheless, as noted above, nonlinear studies are important because they can assess the effectiveness of sub-optimal and velocity cancellation control strategies, even when the system response contains localized nonlinear excursions in the isolation devices.

Table 29 summarizes average values of phase angle between the direction of actuator force and system velocities and displacements. Parts A and B cover phase analysis for linear and nonlinear system response, respectively. Once again, the case study 1 simulations serve as a benchmark against which the effects of active control can be assessed. When the structural system is lightly damped (i.e., 1% damping), the time-history response of displacements oscillates back and forth in a regular pattern – for details, see Figure 20. The actuator/velocity



correlation coefficient is about 0.97, which is very close to values predicted by the theoretical analysis. Figure 22 shows the same time-history response at 10% critical damping. Now, the system response is much less regular, and the actuator/velocity correlation coefficients decrease to about 0.77. When the actuator force is increased to  $U_{max} = 450$  kN, the displacement response becomes even less regular and the actuator/velocity correlation coefficients drop to 0.55 and 0.59 at 1% and 10% damping. After the ground motions cease (i.e., at  $t = 10$  seconds), the system response becomes more regular and the actuator/velocity correlation coefficients increase to 0.89 and 0.96 at 1% and 10% damping, respectively. And finally, by design, velocity cancellation control works in perfect phase with the system velocities. Throughout these analyses, velocities remain orthogonal to displacements, and this is reflected in the actuator/displacement correlation coefficients.

From a phase analysis perspective, the key point to note in Part B is that velocities are no longer always orthogonal to displacements; loss of this property is reflected in the scatter of actuator/velocity and actuator/displacement correlation coefficients.

Part A: Average values of Peak Displacements and Forces in Element 1 at 1% and 10% Critical Damping, and Linear System Response.

1% Critical Damping

Case Study	Displacement at Node 1		Force in Element 1	
	Min (cm)	Max (cm)	Min (kN)	Max (kN)
Case Study 1:	-16.23 cm	16.00 cm	-2,234 kN	2,119 kN
Case Study 2:	-5.73 cm	5.02 cm	-760 kN	655 kN
Case Study 3:	-5.91 cm	5.22 cm	-784 kN	692 kN

10% Critical Damping

Case Study 1:	-9.95 cm	8.93 cm	-1,318 kN	1,184 kN
Case Study 2:	-4.71 cm	4.17 cm	-623 kN	555 kN
Case Study 3:	-4.63 cm	4.20 cm	-615 kN	557 kN

Part B: Average values of Peak Displacements and Forces in Element 1 at 1% and 10% Critical Damping, and Nonlinear System Response.

1% Critical Damping

Case Study 1:	-16.34 cm	16.05 cm	-524 kN	524 kN
Case Study 2:	-3.64 cm	4.99 cm	-481 kN	450 kN
Case Study 3:	-5.02 cm	5.10 cm	-487 kN	440 kN

10% Critical Damping

Case Study 1:	-12.75 cm	11.27 cm	-523 kN	523 kN
Case Study 2:	-4.07 cm	4.29 cm	-471 kN	428 kN
Case Study 3:	-4.18 cm	4.16 cm	-469 kN	440 kN

Legend

Case Study 1 = Base Isolation Alone.  
Case Study 2 = Base Isolation + Sub-Optimal Bang-Bang Control.  
Case Study 3 = Base Isolation + Velocity Cancellation Control.

Table 28: Average Values of Peak Displacement and Forces in Element 1. Simulations are conducted at 1% and 10% critical damping. Part A: Linear System Response. Part B: Nonlinear System Response.

Part A: Average values of phase angle between the actuator, and system velocities and displacements at 1% and 10% critical damping, and linear system response.

1% Critical Damping

Case Study	Actuator/Velocities		Actuator/Displacements	
	[ 0-10 ] sec	[ 10-15 ] sec	[ 0-10 ] sec	[ 10-15 ] sec
Case Study 1:	0.977	0.975	0.043	0.019
Case Study 2:	0.553	0.897	-0.054	-0.036
Case Study 3:	1.000	1.000	-0.017	-0.028

10% Critical Damping

Case Study 1:	0.774	0.748	0.236	0.193
Case Study 2:	0.599	0.961	0.101	0.006
Case Study 3:	1.000	1.000	0.000	0.000

Part B: Average values of phase angle between the actuator, and system velocities and displacements at 1% and 10% critical damping, and nonlinear system response.

1% Critical Damping

Case Study 1:	0.908	0.879	0.031	0.000
Case Study 2:	0.561	0.772	-0.004	-0.008
Case Study 3:	1.000	1.000	0.013	0.000

10% Critical Damping

Case Study 1:	0.481	0.064	0.416	0.669
Case Study 2:	0.566	0.667	0.125	0.029
Case Study 3:	1.000	1.000	0.023	-0.003

Legend

-----  
Case Study 1 = Base Isolation Alone.  
Case Study 2 = Base Isolation + Sub-Optimal Bang-Bang Control.  
Case Study 3 = Base Isolation + Velocity Cancellation Control.  
=====

Table 29: Average Values of Phase Angle between the Actuator and System Velocities and Displacements. Simulations are conducted at 1% and 10% critical damping. Part A: Linear System Response. Part B: Nonlinear System Response.

## References

- [1] Andriono T., Carr A.J. A Simplified Earthquake Resistant Design Method for Base Isolated MultiStorey Buildings. *Bulletin of the New Zealand National Society for Earthquake Engineering*, 24(3):238–250, September 1991.
- [2] Andriono T., Carr A.J. Reduction and Distribution of Lateral Seismic Forces on Base Isolated Mutli-Storey Structures. *Bulletin of the New Zealand National Society for Earthquake Engineering*, 24(3):225–237, September 1991.
- [3] Austin M. A., Lin W. J., and Chen X. G. Structural Matrix Computations with Units. *Journal of Computing in Civil Engineering, ASCE*, 14(3):174–182, 2000.
- [4] Austin M. A., Chen X. G., Lin W.-J. ALADDIN: A Computational Toolkit for Interactive Engineering Matrix and Finite Element Analysis. Technical Report TR95-74, Institute for Systems Research, University of Maryland, College Park, December 1995.
- [5] Bellman R., Glicksberg I., and Gross O. On the Bang-Bang Control Problem. *Quarterly of Applied Mathematics*, 14(1):11–18, 1956.
- [6] Chopra A. K. *Dynamics of Structures: Theory and Applications to Earthquake Engineering*. Prentice Hall, 1995.
- [7] Ghobarah A., Ali H.M. Seismic Design of Base-Isolated Highway Bridges utilizing Lead-Rubber Bearings. *Canadian Journal of Civil Engineering*, 17:413–422, 1990.
- [8] Housner G. W., Bergman L. A., et al. Structural Control: Past, Present, and Future. *Journal of Engineering Mechanics, ASCE*, 123(9):897–971, 1997.
- [9] International Conference of Building Officials (ICBO). Uniform Building Code Regulation for Seismic-Isolated Structures, 1994. Volume 2, Appendix Chapter 16.
- [10] International Conference of Building Officials (ICBO). Uniform Building Code Regulation for Seismic-Isolated Structures, 1997. Volume 2, Appendix Chapter 16.
- [11] Johnson E. A., Ramallo J. C., Spencer B. F., and Sain M. K. Intelligent Base Isolation Systems. In *Proceedings of the Second World Conference on Structural Control*, 1998.
- [12] Johnson E.A., Ramallo J.C., Spencer B.F., and Sain M.F. Intelligent Base Isolation Systems. In *Proceedings of Second World Conference on Structural Control*, Kyoto, Japan, 1998.

- [13] Kailath T. *Linear Systems*. Prentice-Hall, London, England, 1980.
- [14] Lin W. J. Modern Computational Environments for Seismic Analysis of Highway Bridge Structures, 1997. Doctoral Dissertation.
- [15] Mayes R.L., Buckle I.G., Kelly T.R., Jones L. AASHTO Seismic Isolation Design Requirements for Highway Bridges. *Journal of the Structural Division, ASCE*, 118(1):284–304, January 1992.
- [16] Naeim F. and Kelly J. *Design of Seismic Isolated Structures*. John Wiley and Sons, 1998.
- [17] Ramallo J.C., Johnson E.A. a,d Spencer B.F. Smart Base Isolation Systems. *Journal of Engineering Mechanics, ASCE*, 128(10), October 2002.
- [18] Reinhorn A. M., Soong T. T., and Wen C. Y. Base-isolated Structures with Active Control. In *Proceedings of Pressure Vessels and Piping (PVP) Conference*, volume PVP-127, pages 413–420, 1987.
- [19] Robinson W.H. Lead-Rubber Hysteretic Bearings Suitable for Protecting Structures During an Earthquake. *Earthquake Engineering and Structural Dynamics*, 10:593–602, 1982.
- [20] Sebastianelli R., and Austin M.A. Computational Assessment of Suboptimal Bang-Bang Control Strategies for Performance-Based Design of Base Isolated Structures. ISR Technical Report 2005-89, Institute for Systems Research, University of Maryland, College Park, MD. 20742, June 2005.
- [21] Sebastianelli R., and Austin M.A. Energy- and Power-Balance Assessment of Base Isolated Structures Supplemented with Modified Bang-Bang Control. ISR Technical Report 2005-90, Institute for Systems Research, University of Maryland, College Park, MD. 20742, June 2005.
- [22] Spencer B. F. and Nagarajaiah S. State of the Art of Structural Control. *Journal of Structural Engineering, ASCE*, pages 845–856, July 2003.
- [23] Turkington D.H., Carr A.J., Cooke N., and Moss P.J. Design Method for Bridges on Lead-Rubber Bearings. *Journal of the Structural Division, ASCE*, 115(12):3017–3030, December 1989.
- [24] Turkington D.H., Carr A.J., Cooke N., and Moss P.J. Seismic Design of Bridges on Lead-Rubber Bearings. *Journal of the Structural Division, ASCE*, 115(12):3000–3016, December 1989.

- [25] Tyler R.G. Rubber Bearings in Base Isolated Structures : A Summary Paper. *Bulletin of the New Zealand National Society of Earthquake Engineering*, 24(3), September 1991.
- [26] Wonham W. M. and Johnson C. D. Optimal Bang-Bang Control with Quadratic Performance Index. *Journal of Basic Engineering*, 86:107–115, 1964.
- [27] Wu Z., and Soong T. T. Modified Bang-Bang Control Law for Structural Control Implementation. *Journal of Engineering Mechanics, ASCE*, 122(8):771–777, 1996.
- [28] Wu Z., Soong T. T., Gattulli V., and Lin R. C. Nonlinear Control Algorithms for Peak Response Reduction. Technical Report NCEER-95-0004, National Center for Earthquake Engineering Research, State University of New York at Buffalo, Buffalo, NY. 14261, February 1995.
- [29] Yoshioka H., Ramallo J. C., and Spencer B. F. Smart Base Isolation Strategies Employing Magnetorheological Dampers. *Journal of Engineering Mechanics, ASCE*, 128(5):540–551, 2002.